NUMERICAL SIMULATION AND ANALYTICAL OPTIMIZATION OF MICROCHANNEL
HEAT SINKS

A THESIS SUBMITTED TO
THE GRADUATE SCHOOL OF NATURAL AND APPLIED SCIENCES
OF
MIDDLE EAST TECHNICAL UNIVERSITY

BY

GÖKER TÜRKAKAR

IN PARTIAL FULFILMENT OF THE REQUIREMENTS
FOR
THE DEGREE OF MASTER OF SCIENCE
IN
MECHANICAL ENGINEERING

AUGUST 2010

Approval of the thesis:

NUMERICAL SIMULATION AND ANALYTICAL OPTIMIZATION OF MICROCHANNEL HEAT SINKS

submitted by **GÖKER TÜRKAKAR** in partial fulfillment of the requirements for the degree of **Master of Science in Mechanical Engineering Department, Middle East Technical University** by,

Prof. Dr. Canan Özgen   _____
Dean, Graduate School of **Natural and Applied Sciences**

Prof. Dr. Suha Oral   _____
Head of Department, **Mechanical Engineering**

Assist. Prof. Dr. Tuba Okutucu Özyurt   _____
Supervisor, **Mechanical Engineering Dept., METU**

Examining Committee Members:

Prof. Dr. Faruk Arınç   _____
Mechanical Engineering Dept., METU

Assist. Prof. Dr. Tuba Okutucu Özyurt   _____
Mechanical Engineering Dept., METU

Assist. Prof. Dr. Almıla Güvenç Yazıcıoğlu   _____
Mechanical Engineering Dept., METU

Assist. Prof. Dr.Cüneyt Sert   _____
Mechanical Engineering Dept., METU

Assoc. Prof. Dr.Haluk Külah   _____
Electrical and Electronics Engineering Dept., METU

                                               Date: 31.08.2010

I hereby declare that all information in this document has been obtained and presented in accordance with academic rules and ethical conduct. I also declare that, as required by these rules and conduct, I have fully cited and referenced all material and results that are not original to this work.

Name, Last Name : Göker Türkakar

Signature :

ABSTRACT

NUMERICAL SIMULATION AND ANALYTICAL OPTIMIZATION OF

MICROCHANNEL HEAT SINKS

Türkakar, Göker

M.Sc., Department of Mechanical Engineering

Supervisor: Assist. Prof. Dr. Tuba Okutucu

August 2010, 133 pages

This study has two main objectives: The performance evaluation of existing microchannel heat sinks using a CFD model, and the dimensional optimization of various heat sinks by minimizing the total thermal resistance.

For the analyses, the geometric modeling is performed using the software GAMBIT while the thermal analysis is performed with FLUENT. The developed model compares very well with those available in the literature. Eight different metal-polymer microchannel heat sinks are analyzed using the model to find out how much heat could be provided to the systems while keeping the substrate temperatures below 85°C under a constant pumping power requirement.

Taking the objective function as the total thermal resistance, the optimum geometries have been obtained for the mentioned metal-polymer heat sinks as well as more conventional silicon ones. The results of the optimization code agreed very well with available ones in the literature.

In the optimization study, the Intel Core i7-900 Desktop Processor Extreme Edition Series is considered as a reference processor which is reported to dissipate 130 W of heat and to have chip core dimensions of 1.891 cm × 1.44

cm. A dimensional optimization study has been performed for various copper and silicon microchannel heat sinks to cool down this processor.

To the best of the author's knowledge, this study contributes to the literature in that, as opposed to the available analytical microchannel optimization studies considering constant thermophysical properties at the fluid inlet temperature, the properties are evaluated at the area weighted average of the fluid inlet and iteratively calculated outlet temperatures. Moreover, the effects of the thermal and hydrodynamic entrance regions on heat transfer and flow are also investigated.

Keywords: Microchannel Heat Sinks, Optimization, Electronics Cooling, Thermal Modeling.

ÖZ

MİKROKANAL ISI ALICILARIN SAYISAL BENZETİMİ VE ANALİTİK OPTİMİZASYONU

Türkakar, Göker

Yüksek Lisans. Makina Mühendisliği Bölümü

Tez Yöneticisi: Yrd. Doç. Dr. Tuba Okutucu

Ağustos 2010, 133 sayfa

Bu çalışmanın iki ana amacı vardır: Bir Hesaplamalı Akışkanlar Dinamiği modeli kullanılarak var olan mikrokanal ısı alıcılarının performans değerlendirmesi; toplam ısıl direnci en aza indirerek çeşitli ısı alıcılarının boyutsal optimizasyonu.

Analizler geometrik modelleme GAMBIT yazılımı ile yapılır iken ısıl analiz FLUENT ile gerçekleştirilmiştir. Geliştirilen model literatürdeki benzer çalışmalar ile çok iyi bir uyum göstermiştir. Bu model ile, sabit pompa gücünde, alt tabaka sıcaklığını 85°C nin altında tutarak sisteme ne kadar ısı verilebileceğini anlamak için sekiz farklı metal-polimer ısı alıcı incelenmiştir.

Hedef fonksiyon, toplam ısıl direnç olarak alınmış, bahsedilen metal-polimer ve daha geleneksel silikon ısı alıcılar için optimum geometriler elde edilmiştir. Optimizasyon sonuçları literatürdekiler ile çok iyi örtüşmüştür.

Optimizasyon çalışmasında, referans işlemci olarak 130 W ısı yaydığı tespit edilen ve 1.891 cm × 1.44 cm çekirdek ölçülerine sahip "Intel Core i7-900 Masaüstü Bilgisayar işlemcisi ele alınmıştır. Bu işlemciyi soğutma amacıyla, çeşitli bakır ve silikon mikrokanal ısı alıcılar üzerinde boyutsal optimizasyon çalışması gerçekleştirilmiştir.

Bu çalışma, kullanılan akışkanın ısıl özelliklerini, şu ana kadar rastlanan analitik optimizasyon çalışmalarının aksine akışkan giriş sıcaklığında değil, giriş ve iterasyonla hesaplanan çıkış sıcaklıklarının alan ağırlıklı ortalamasında

hesaplayarak literatüre bir katkıda bulunmuştur. Bunun yanında, ısıl ve hidrodinamik giriş bölgelerinin ısı transferi ve akışa etkileri de incelenerek literatürdeki benzer analitik optimizasyon çalışmalarından farklı özellikte bir çalışma ortaya konmuştur.

Anahtar kelimeler: Mikrokanal Isı Alıcılar, Optimizasyon, Elektronik Soğutma, İşlemci Soğutma, Isıl Modelleme.

To my family…

ACKNOWLEDGEMENTS

TABLE OF CONTENTS

LIST OF TABLES

LIST OF FIGURES

FIGURES

LIST OF SYMBOLS

SYMBOLS

a: unheated edge

A: Area [cm^2]

c: Specific heat [kJ/kg K]

D: smallest dimension in the channels

D_h: hydraulic diameter [μm]

f: Fanning friction factor

f_{app}: apparent friction factor

g: gravitational acceleration [m/s^2]

h: heat transfer coefficient [W/m^{2}K]

H_c: Channel Height [μm]

$incw_w$: step size in the w_w interval

$incw_c$: step size in the w_c interval

k: thermal conductivity [W/m K]

$K(x)$: incremental pressure defect

L: length of the channel [μm]

$\dot{m}$: mass flow rate [kg/s]

n: number of channels

Nu: Nusselt number

P: pumping power [W]

ΔP: pressure drop [Pa]

Pr: Prandtl number

Po: Poiseuille number

$\dot{Q}$: volumetric flow rate [m^3/s]

Re: Reynolds number

R: thermal resistance [$°C/W$]

t: substrate thickness [μm]

T_o: outlet temperature of the fluid [°C]

T_i: inlet temperature of the fluid [°C]

u_m: mean velocity of the fluid [m/s]

w_c: channel width [μm]

w_c: channel wall thickness [μm]

W: total channel width [cm]

x^+: dimensionless hydrodynamic length

x^*: dimensionless thermal length

Greek Letters:

α_c : aspect ratio, w_c/H_c

η: fin efficiency

μ: dynamic viscosity [Pa.s]

v: kinematic viscosity [m^2/s]

ρ: density (kg/m^3)

Subscripts:

fd: fully developed

num: numerical

exp: experimental

av: average

m: mean

CHAPTER 1

INTRODUCTION

1.1 Motivation

There has been increasing demand of heat dissipation from electronic components for nearly thirty years. Because of the tendency to be smaller, dissipating heat from electronic components gets difficult day by day. At the same time, rapidly developing technology and increasing functionality of electronic components bring about more consumption of energy, this means higher necessity of heat removal from electronic devices. Therefore, classical air cooling and natural convection with extended surfaces, two primitive cooling methods, are not sufficient anymore. For this reason, new ways of cooling applications are sought. For example, mini and micro refrigeration cycles are implemented on electronic devices. Microchannels are thought to be a solution for high heat fluxes for small areas by Tuckerman and Pease, 1981 firstly [1]. They proved that high heat fluxes can be removed from the system in a limited space. Despite high pressure drop due to small hydraulic diameter and huge temperature difference between inlet and outlet, having high heat transfer coefficients and occupying small volumes, microchannels offer a reasonable way of cooling. In the design and manufacturing of microchannels, optimization takes an important role. It is crucial that an engineering design should be made in the most efficient way to reduce the manufacturing and operational

costs while meeting some design constraints. A microchannel should be designed in such a way that the pressure drop should be kept low, thermal performance should be maximized thereby thermal resistance is desired to be low. After the study of Tuckerman and Pease, many other studies have been presented but most do not cover dimensional optimization. These randomly designed geometries have resulted in inefficient thermal design and high temperature rise in the substrate. Li and Peterson [2] claimed that under the same conditions, the optimized geometry performed 20% better. Hence, the dimensional optimization of the microchannels is essential for the upcoming electronic equipments.

1.2 Electronics Cooling Techniques

The need for the heat removal from electronic components tremendously increases every single year. According to Moore's law, transistor number per chip doubles every 18 months.
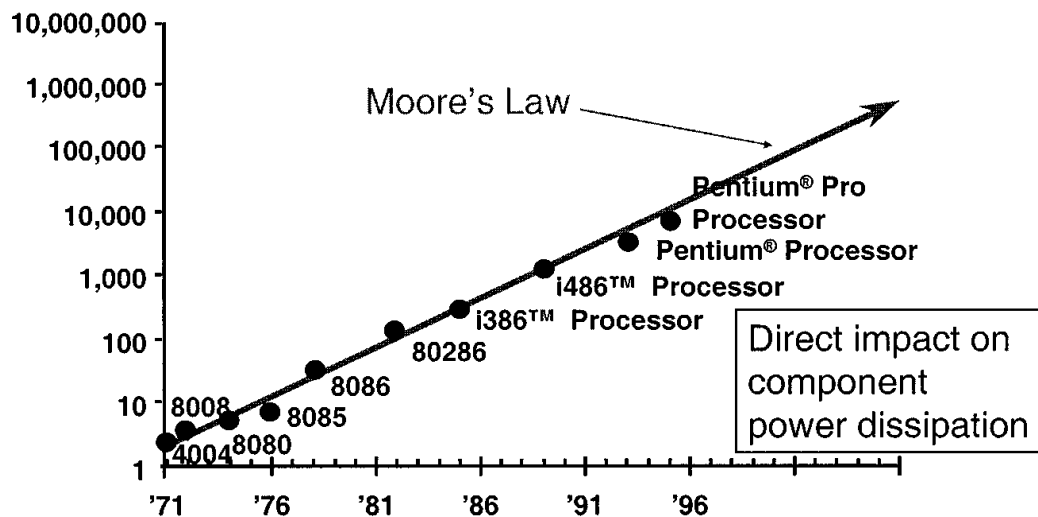
Figure 1.1 Moore's Law, Schmidt [3]

It seems that Moore's law applies even today. This augmentation in transistor number brings about the requirement of high heat dissipation from the components.

At the early stages of the electronics technology, primitive cooling methods were sufficient. By primitive cooling technique, it is meant that the heat is solely dissipated by natural convection over the fins with increased surface area. As the time went by and operation power of electronic components increased, this cooling technique could not meet the increased demand for the heat removal. Then, external fans are implemented to create forced convection on the surface of these fins. The fans are used even today especially for desktop computers where the space constraint is not an issue, but the space limitation is a big problem in notebook or netbook computers. Heat pipes are utilized in these systems. In addition to a heat pipe, a pump that provides motion of the liquid and a heat exchanger through which heat is dissipated to the surroundings by the help of an external fan should be implemented in a place where enough room is available. Although the use of a liquid as the coolant provides higher heat removal rates compared to conventional air cooling methods, it has some disadvantages. Most crucial drawback of this system is the reliability issue. There might be permanent damage on the electronic components in case of leakage problem in the connections or in any other components of the system. Channels used as a heat sink in cooling of electronic components can be classified based on their hydraulic diameter, from bigger to smaller, conventional channels, minichannels and microchannels, respectively. Since Tuckerman and Pease proved in 1981 that microchannels have high heat dissipation capacity for small volumes, many other studies have been conducted [1]. Today especially for military applications, electronic devices are cooled by microchannel heat sinks owing to their high area to volume ratio; hence, higher heat dissipation rates.

The use of vapor compression refrigeration cycles is also an alternative cooling method for electronic devices. These cycles are composed of four main components, evaporator, compressor, condenser and expansion valve. This method is also effective for cooling; however, it has the same reliability problems. There are other advanced cooling methods, such as, air jet impingement, spray cooling and immersion cooling.

Air jet impingement is beneficial for removing heat from local hot spots; however, high pressure drop due to the high speed of air is the main drawback of this cooling method. Also in high speed air flow, noise might be another problem. Like air jet impingement method, spray cooling is also utilized for local hot spots but instead of air, liquid is used as the coolant. Coolant is directly in contact with die in spray cooling. When the liquid gets in contact with the die surface, it starts to evaporate. The condensed liquid is again sprayed on the die surface. The crucial point in spray cooling is the usage of a dielectric liquid as the liquid is in direct contact with the electronic component [4].

1.3 Literature Survey

Tuckerman and Pease [1] are the pioneers of the investigation of microchannel heat sinks. Many researchers compared their numerical or analytical studies with Tuckerman and Pease's. They theoretically calculated that the minimum thermal resistance was obtained when the fin efficiency was maximum, the channel width and wall thickness were equal to each other. Tuckerman and Pease were able to dissipate 790 W/cm^2 heat flux when the increase in the temperature of the substrate was 71°C from inlet temperature of the coolant fluid. Three similar geometries were manufactured and tested under different heat loads and it was found that the thermal resistance was approximately 0.1 °C/W

Kim and Husain [5] performed an optimization study with channels of trapezoidal cross section unlike the more frequent rectangular channel studies. They used the channel width at the top and bottom and fin thickness as the optimization variables. Their objective function was the thermal resistance. A surrogate-based optimization technique was used. Some design points were selected and at these points the objective function values were calculated via three dimensional Navier-Stokes and energy equations. Then, the optimization procedure is followed.

Kim and Husain [6] conducted a similar study but in their study, there were two objective functions. One was the thermal resistance and the other was the pumping

power. Pumping power is quite important in optimization studies of the microchannels because it is the limiting factor for the volumetric flow rate of the working fluid. Many studies take the pumping power as a constraint like done in the present study, but Kim and Husain [6] used it as an objective function. Later, they performed an optimization study with same method but using variable thermophysical properties [7].

Liu and Garimella [8] developed five analytical models to find the optimum channel dimensions. The first model combined conductive, convective and caloric thermal resistances by adding them all. The second model was based on a fin analysis and evaluated the fluid temperature distribution for one dimension, throughout the channel. The distinction of the third model from the second was the evaluation the fluid temperature distribution in two dimensions, so the third model was more reliable than the second one. The fourth model was different than the other models in a way that it did not neglect the axial conduction in the fin. The fifth model inspected the geometry in terms of a porous medium model. When compared with the numerical studies in the literature under 8% difference was observed in the thermal resistances. Also the difference between each model was under 6%.

Ryu et al [9] performed a numerical study which minimized the thermal resistance. They kept the pumping power constant and the design variables were the channel depth, channel width and the number of the channels. They used a random search technique as the optimization tool. Contrary to most of the studies dealing with the optimization of microchannels, they investigated the effect of the entrance region and handled the geometry as three dimensional. They found that the entrance region effects should be taken into account especially for higher pumping powers.

Kleinstruer and Koo [10] examined the effect of viscous dissipation in the microchannels and microtubes. They found that viscous dissipation effect on the friction factor became important for water especially for the channels with small hydraulic diameter which are lower than 50 μm. There are also other parameters affecting viscous dissipation such as the aspect ratio, thermophysical properties of

the fluid and the fluid velocity. The variation of viscosity throughout the channel due to the temperature change in the fluid also has great importance on the viscous dissipation. The variation of the viscosity for equivalent temperature changes compared to those of the other thermophysical properties is quite more; hence, it should not be ignored when calculating the viscous dissipation term. They concluded that flows with low specific heat and high viscosity may increase the effect of viscous dissipation even for low mean velocity values. In addition to these parameters, a high aspect ratio for the channel may also enhance the viscous dissipation effects.

Sabry [11] investigated the transverse temperature gradient effect on fin efficiency for microchannel design. He constructed an analytical model in two dimensions. This model formed the fourth model mentioned in the study of Liu and Garimella [8]. As this model includes the axial conduction in the fin region and evaluates the fluid temperature distribution in two dimensions, it yields more realistic results among the analytical studies.

Li and Peterson [2] conducted a numerical study solving three dimensional conjugate heat transfer for constant pumping power and channel height. They kept pumping power at lower values in order to get fully developed flow. Optimization was carried out when the pumping power was at 0.05 W which is reasonable value for pumps used in microchannels. Kim and Husain [12] stated that a realistic interval of pumping powers is between 0.01 and 0.8 W. Li and Peterson [2] compared their study with Tuckerman and Pease's and they observed that for a given pumping power, thermal resistance could be reduced by 20% as a results of dimensional optimization. This shows the necessity for optimizing the dimensions of the channels.

Kim S.J. [13] inspected three optimization models which are fin, porous and numerical model using random search method. He compared these models and noted that for large aspect ratios, fin model did not accurately predict the actual phenomena. The reason is mainly the assumptions made when building the fin

6

model; namely, a constant heat transfer coefficient along the channel height, a uniform temperature at any axial location and negligible axial conduction along the channel. Due to these assumptions, the fin model should be carefully implemented.

He noted that results for aspect ratios higher than eight do not match with numerical results. On the contrary, porous model gives better results than the fin model for a wide range of aspect ratios.

Shao et.al [14] performed an optimization study using a sequential quadric programming procedure. They developed a model based on thermal resistance network which is similar to the first model of the present study. They compared their optimization study with a CFD software and observed that the relative error was lower than 5%.

1.4 The Present Study

The present study has two main parts. In the first part, a CFD modeling of existing microchannel heat sinks has been carried out for performance evaluation. The geometric modeling was done using the software GAMBIT while the thermal analysis was performed using FLUENT. The developed model was first validated by comparing the results with those available in the literature, and a very good agreement has been reached. The model was then applied to eight different metal-polymer microchannel heat sinks that were designed, fabricated and partially tested by a fellow student [15]. The goal was to find out how much heat could be provided to the system while keeping the substrate temperature below 85°C under constant pumping power requirement.

The second part of this work includes the dimensional optimization of microchannel heat sinks. Taking the objective function as the total thermal resistance, the optimum geometries have been obtained for the mentioned metal-polymer heat sinks as well as more conventional silicon ones. In addition, for the sake of conducting an optimization study for a contemporary electronic device, the Intel Core i7-900 Desktop Processor Extreme Edition Series is considered as a reference

processor which is reported to dissipate 130 W of heat and to have chip core dimensions of 1.891 cm × 1.44 cm. A dimensional optimization study has been performed for various copper and silicon microchannel heat sinks to cool down this processor.

The major contribution of the present study is that the effects of the thermophysical property variations with respect to temperature, and the thermally and hydrodynamically developing regions have been taken into account. Hence, it can be said that the present work can handle a wider range of pumping power and temperature interval compared to the other optimization studies available in the literature.

CHAPTER 2

FUNDAMENTALS OF HEAT TRANSFER AND LIQUID FLOW IN MICROCHANNELS

Extensive research has been performed in an effort to understand the fundamentals of flow and heat transfer in microchannels. A few books have been published in the area. Among them, the book authored by Kandlikar et al. [16] covers the single-phase flow of gases and liquids, two phase flow, and some biological applications. The book includes the effects of the entry region and roughness in single phase flow, and also focuses on microchannel system design for chip cooling. Various parameters affect the thermal and hydrodynamic characteristics of the flow in microchannels. Some background on laminar single phase liquid flow is included in this chapter.

2.1 Classification of Channels

Flow and heat transfer characteristics of channels change with the size of the channels. Kandlikar and Grande 2003 [17], classified the channels based on their smallest dimension, D, as listed in Table 2.1

Table 2.1 Channel size classification, Kandlikar and Grande [17]

Conventional Channels	D > 3mm
Minichannels	3 mm > D > 200 μm
Microchannels	200 μm > D > 10 μm
Transitional Microchannels	10 μm > D > 1 μm
Transitional Nanochannels	1 μm > D > 0.1 μm
Molecular Nanochannels	0.1 μm > D

According to Kandlikar and Grande [17], *D* is the diameter for circular channels. If the channel is not circular, it may be the smaller edge of the channel in case of rectangular channels. As can be seen from Table 2.1, the channels inspected in the present study are classified as microchannels.

2.2 Validation of the Continuum Theory in Microchannels

When the length scale is around micro and nanometers in channels, classical continuum modeling may not be valid. Whether it is valid or not can be determined by the Knudsen number which is defined as the ratio of the molecular mean free path to the characteristic length.

$$Kn = \frac{\lambda}{L}$$
(2.1)

If $Kn \leq 10^{-3}$ the flow is considered to be a continuum,

$0.001 \leq Kn \leq 0.1$ slip flow regime,

$10 \leq Kn$ a free molecular flow.

Navier-Stokes equations give accurate results provided that the molecular mean free path, λ, is much smaller than characteristic length *L*.

In the slip flow regime classical Navier-Stokes equations are solved by modified boundary conditions. At the solid-fluid interface, slip and temperature jump boundary conditions are applied. Although the slip and temperature jump boundary conditions yield satisfactory results for gaseous flow, there is no general agreement on the boundary conditions for the liquid flows. Viskanta et al. [18] stated that the Knudsen number for water was nearly 3.5×10^{-5} for microchannels with 100 μm hydraulic diameter. It can be said that for Knudsen numbers less than 10^{-3}, the flow can be modeled by a continuum model. Since the Knudsen number of a liquid is much lower than that of a gas, it seems logical to use the continuum model for liquid flow in microchannels.

2.3 Transition Reynolds Number

As very well known, Reynolds number is a dimensionless parameter that determines whether the flow is laminar or turbulent. It is defined as

$$Re = \frac{\rho \, u_m D_h}{\mu} = \frac{u_m D_h}{\nu}$$

(2.2)

Where the u_m is the mean velocity, ν is the kinematic viscosity and D_h is the hydraulic diameter of the channel. For microchannels of rectangular cross-section as depicted in Figure 2.1, the hydraulic diameter is defined as

$$D_h = \frac{4 \, H_c \, w_c}{2 \, (H_c + w_c)}$$

(2.3)

Lee et al. [19] performed an experimental study using water as the coolant to understand whether classical correlations are valid or not for developing flow in microchannels which have hydraulic diameters ranging from 318 μm to 903 μm. They claim that "Beyond the range of Reynolds numbers of approximately 1500-2000, the experimental results show a change in slope, reflecting a transition from laminar flow." According to Kandlikar et al. [16], although the first studies inspecting microchannels asserted transition from laminar to turbulent flow to be sooner than that in conventional channels, most of the recent studies have a general opinion that the size of the channel does not have an effect on the

11

transition Reynolds number. However, it is noted that the channel surface roughness influences the transition [16].
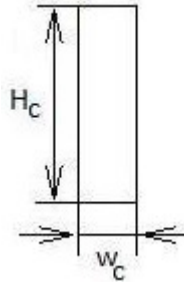
Figure 2.1 Channel height and width of a channel

2.4 Pressure Drop

Pressure drop is a crucial parameter when optimizing microchannels. It is dependent on the friction factor, mean velocity, length and the hydraulic diameter of the channel.

The pressure drop is defined as

$$\Delta P = \frac{2\, f\, \rho\, u_m^2\, L}{D_h} \qquad (2.4)$$

where f is the Fanning friction factor that depends on the conditions stated below [16],

- The Reynolds number,
- channel surface conditions,
- hydrodynamically fully developed or developing flow conditions,
- geometry of the channel (aspect ratio, hydraulic diameter etc.).

The Fanning friction factor is proportional to the pressure drop; therefore, it is essential to keep it under a certain value in order to get a low thermal resistance for constant pumping power.

The pumping power is equal to the multiplication of the volumetric flow rate and the pressure drop throughout the channel.

$$P = \Delta P \, \dot{Q} \tag{2.5}$$

2.4.1 Hydrodynamically Fully Developed Laminar Flow Conditions

The Poiseuille number which is constant for fully developed flow conditions for certain geometries is equal to the multiplication of the Fanning friction factor and the Reynolds number. Poiseuille numbers for different aspect ratios are given in Table 2.2 and also as a formulation in (2.6) [16]. In Table 2.2, the dimensions *x* and *y* are as illustrated in Figure 2.2.
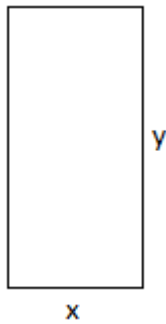
x is short side of the channel

y is long side of the channel

Figure 2.2 Cross Section of a Channel

Table 2.2 Po numbers for different aspect ratios, Kandlikar et al. [16]

Aspect Ratio *(y/x)*	*Po = f Re*
1	14.23
2	15.55
3	17.09
4	18.23
6	19.70
8	20.58
∞	24

Poiseuille number formulation dependent on aspect ratio is given by Kandlikar et al. [16]

$$
\begin{aligned}
\text{Po} = \text{f} * \text{Re} \\
= 24 * \big(1 - 1.3553\alpha_c + 1.94677\,\alpha_c{}^2 - 1.7012\,\alpha_c{}^3 + 0.9564\,\alpha_c{}^4 \qquad (2.6)\\
- 0.2537\,\alpha_c{}^5\big)
\end{aligned}
$$

Where $\alpha_c = x/y$.

Hence, the poiseuille number is only dependent on the channel geometry for fully developed flow conditions [16].

2.4.2 Hyrodynamically Developing Laminar Flow

One of the most important drawbacks of using microchannels in cooling applications is the high pressure drop due to small hydraulic diameters. Therefore, the length of the channel is desired to be as short as possible. However, this way the hydrodynamic entrance length becomes a considerable portion of the channel length in microchannels. Hence, the hydrodynamically developing region along the channel needs to be considered, and many researchers have focused on the hydrodynamic entrance region in microchannels for years.

The apparent friction factor "accounts for pressure drop due to friction and developing region effects" [16].

The pressure drop that represents the developing region is defined as

$$\Delta p = \frac{2(f_{app}Re)\mu\, u_m\, x}{D_h{}^2} = \frac{2(fRe)\mu u_m x}{D_h{}^2} + K(x)\frac{\rho\, u_m^2}{2} \tag{2.7}$$

Where *K(x)* is the incremental pressure defect that stands for "the difference between the apparent friction factor over a length *x* and the fully developed friction factor *f*" [16].

$$K(x) = \left(f_{app} - f\right)\frac{4\, x}{D_h} \tag{2.8}$$

The dimensionless length is defined as

$$x^+ = \frac{x}{D_h Re}. \tag{2.9}$$

The multiplications of the apparent friction factor and the Reynolds number for different aspect ratios are listed [16]. Also, curve-fit equations of these values are provided.

Apparent friction factors in terms of the dimensionless lengths and aspect ratios are given in Table 2.3. Linear interpolation may be utilized for values not listed in the table.

Table 2.3 Laminar developing flow friction factor for rectangular channels, Kandlikar et al. [16]

| $x^+ = (x/D_\text{h})/Re$ | $f_\text{app}Re$ | | | |
	$\alpha_\text{c} = 1.0$	$\alpha_\text{c} = 0.5$	$\alpha_\text{c} = 0.2$	$\alpha_\text{c} \leq 0.1$ $\alpha_\text{c} \geq 10$
0	142.0	142.0	142.0	287.0
0.001	111.0	111.0	111.0	112.0
0.003	66.0	66.0	66.1	67.5
0.005	51.8	51.8	52.5	53.0
0.007	44.6	44.6	45.3	46.2
0.009	39.9	40.0	40.6	42.1
0.01	38.0	38.2	38.9	40.4
0.015	32.1	32.5	33.3	35.6
0.02	28.6	29.1	30.2	32.4
0.03	24.6	25.3	26.7	29.7
0.04	22.4	23.2	24.9	28.2
0.05	21.0	21.8	23.7	27.4
0.06	20.0	20.8	22.9	26.8
0.07	19.3	20.1	22.4	26.4
0.08	18.7	19.6	22.0	26.1
0.09	18.2	19.1	21.7	25.8
0.10	17.8	18.8	21.4	25.6
0.20	15.8	17.0	20.1	24.7
>1.0	14.2	15.5	19.1	24.0

In the present study, moderate values are calculated using linear interpolation method. Curve-fit equations of apparent friction factor for the laminar and developing region are available in APPENDIX A

In order to understand where the flow reaches fully developed flow conditions, these curve-fit equations are plotted. Philips [20] and Kandlikar et al. [16] plotted f_{app} Re versus the dimensionless length.
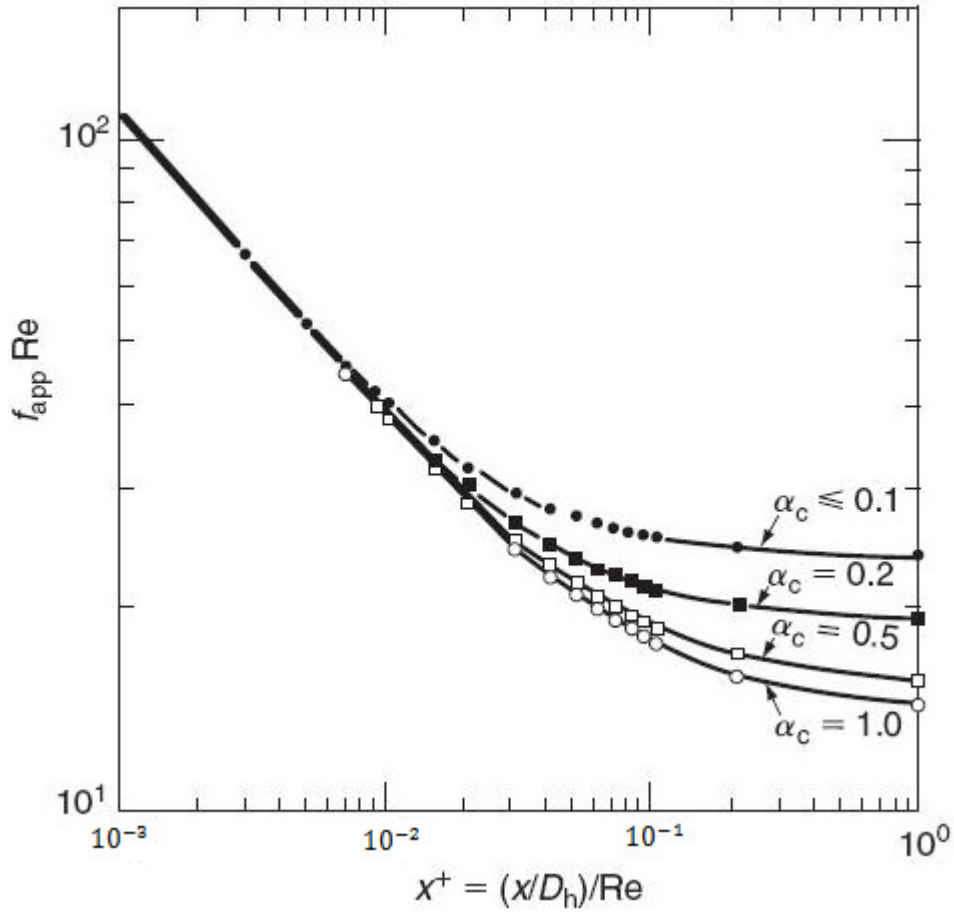
Figure 2.3 Laminar developing region friction factor in terms of the dimensionless length for different aspect ratios, Philips [20] and Kandlikar [16]

As can be seen from Table 2.3 and Figure 2.3, when dimensionless length is approximately 10^0 or greater, flow conditions become fully developed. Therefore, the critical hydrodynamically developing length for rectangular channels can be described as

$$x_{fd,h} = Re\ D_h \qquad (2.10)$$

For locations further than x^+, hyrodynamically fully developed flow conditions are acquired and Poiseuille number takes constant values. However, when the entrance region composes a considerable part of the channel, the entrance effects should be put into account in microchannels.

2.5 Thermal Considerations for Laminar Flow in Rectangular Microchannels

As the Knudsen number is lower than 10^{-3} for water flow in microchannels, the continuum theory is valid. In other words, the thermal solution methods for the microchannels are not so different from those for the conventional channels. Newton's law of cooling is applicable for rectangular microchannels.

$$q = h_{av} \, A \left(T_s(x, y, z) - T_{fluid}(x, y, z) \right) \tag{2.11}$$

In (2.11), q is the heat transfer rate between the channel wall and the fluid, h_{av} is average heat transfer coefficient and A is the heat transfer surface area of the channel. The channel surface temperature and the fluid temperature difference is not constant throughout the channel for constant heat flux case because in the thermally developing region the temperature difference is quite small compared to that in the fully developed region. However, the heat transfer coefficient at the entrance region is higher than that in the thermally fully developed region. Having considerable differences in the thermal characteristics in the flow direction makes it obligatory to examine the entrance region effects carefully. Moreover, the heat transferred to the fluid can be expressed by the help of the first law of thermodynamics, neglecting the kinetic and potential energy effects, as

$$q = \dot{m} \, C_p \, (T_o - T_i) \tag{2.12}$$

where T_o is the outlet temperature of the fluid and T_i the is inlet temperature.

The heat transfer coefficient can be found in terms of the Nusselt number which is defined as,

$$Nu = \frac{h \, D_h}{k}. \tag{2.13}$$

The Nusselt number and the heat transfer coefficient are constants provided that the flow is thermally developed, the fluid thermophysical properties are constant and the channel geometry is fixed. If the flow is in the thermally developing region, the Nusselt number and the heat transfer coefficient vary along the channel.
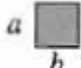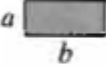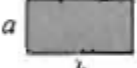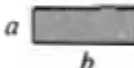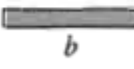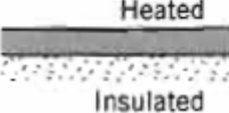
To be able to conduct a theoretical study, some simplifications have to be made. For example, the fluid temperature may be taken as one or two dimensional, also heat transfer coefficient may be assumed as constant throughout the channel even if some part of the flow is in the developing region. Chapter 4 gives detailed information about the simplifications used in this study. Based on these simplifications, various analytical models are derived.

2.5.1 Thermal Considerations for Laminar Thermally Fully Developed Flow in Rectangular Channels

The Nusselt number changes with respect to the aspect ratio of the channel and the boundary conditions applied at the channel walls. For the fully developed conditions, the Nusselt number takes a constant value. Uniform heat flux and uniform surface temperature boundary conditions bring about different Nusselt numbers. They are given in Table 2.4 for different cross sections.

Table 2.4 Nusselt numbers for uniform heat flux and uniform surface temperature for different cross sections, [21].

Cross Section	$\dfrac{b}{a}$	$Nu_D \equiv \dfrac{hD_h}{k}$ (Uniform q_s'')	$Nu_D \equiv \dfrac{hD_h}{k}$ (Uniform T_s)
○	—	4.36	3.66
□ (square, sides a, b)	1.0	3.61	2.98
▭ (a, b)	1.43	3.73	3.08
▭ (a, b)	2.0	4.12	3.39
▭ (a, b)	3.0	4.79	3.96
▭ (a, b)	4.0	5.33	4.44
▭ (b)	8.0	6.49	5.60
Heated	∞	8.23	7.54
Insulated	∞	5.39	4.86
△	—	3.11	2.49

In the literature, various boundary conditions are defined. They are presented as equations depending on the aspect ratio, $\alpha_c = a/b$, a being the short side, b, the long side of the channel [16].

Constant wall temperature:

$$Nu_T = 7.541\,(1 - 2.610\alpha_c + 4.970\,\alpha_c^2 - 5.119\,\alpha_c^3 + 2.702\,\alpha_c^4 \\ - 0.548\,\alpha_c^5)$$

(2.14)

Constant circumferential wall temperature, uniform axial heat flux:

$$Nu_{H1} = 8.235\,(1 - 2.0421\,\alpha_c + 3.0853\,\alpha_c^2 - 2.4765\,\alpha_c^3 + 1.0578\,\alpha_c^4 - 0.1861\,\alpha_c^5)$$

(2.15)

Circumferentially and axially constant wall heat flux:

$$Nu_{H2} = 8.235\,(1 - 10.6044\,\alpha_c + 61.1755\,\alpha_c^2 - 155.1803\,\alpha_c^3 + 176.9203\,\alpha_c^4 - 72.9236\,\alpha_c^5)$$

(2.16)

In addition to these, there are some boundary conditions that cannot be classified as mentioned above due to the non-uniform temperature and heat flux conditions. Nusselt numbers for three side and four side heated channels are mentioned in the literature [16, 20, 22].

Table 2.5 Nusselt numbers for laminar fully developed flow, Kandlikar et al. [16]

$\alpha_c = a/b$	$\mathrm{Nu_{fd,3}}$	$\mathrm{Nu_{fd,4}}$
0	8.235	8.235
0.10	6.939	6.700
0.20	6.072	5.704
0.30	5.393	4.969
0.40	4.885	4.457
0.50	4.505	4.111
0.70	3.991	3.740
1.00	3.556	3.599
1.43	3.195	3.740
2.00	3.146	4.111
2.50	3.169	4.457
3.33	3.306	4.969
5.00	3.636	5.704
10.00	4.252	6.700
>10.00	5.385	8.235

In the Table 2.5, for three and four side heated cases, the Nusselt numbers are given. *a* is the unheated side of the channel in the case of three-sided heating. Related curve-fit equations are given in APPENDIX A.

Like the majority of the studies in the literature, the top surface of the channel is insulated in the present study. That is why, three side heated case is considered for thermally fully developed flow conditions.

2.5.2 Thermal Consideration of Laminar Thermally Developing Flow in Rectangular Channels

Thermal entry length is defined as:

$$x_{fd,t} = 0.1 \, Re \, Pr D_h \qquad (2.17)$$

While for circular tubes, the constant in the thermal entry length formula is 0.05, it is determined as 0.1 for rectangular microchannels [16,20]. Nusselt numbers for four side heated case are given in Table 2.6 for different aspect ratios and dimensionless lengths [16].

Table 2.6 Nusselt numbers for laminar thermally developing and four side heated case [16]

x^*	$\alpha_c \leq 0.1^*$	$Nu_{x,4}$ $\alpha_c = 0.25$	$\alpha_c = 0.333$	$\alpha_c = 0.5$	$\alpha_c = 1.0$	$\alpha_c \geq 10^{**}$
0.0001	31.4	26.7	27.0	23.7	25.2	31.6
0.0025	11.9	10.4	9.9	9.2	8.9	11.2
0.005	10	8.44	8.02	7.46	7.1	9.0
0.00556	9.8	8.18	7.76	7.23	6.86	8.8
0.00625	9.5	7.92	7.5	6.96	6.6	8.5
0.00714	9.3	7.63	7.22	6.68	6.32	8.2
0.00833	9.1	7.32	6.92	6.37	6.02	7.9
0.01	8.8	7	6.57	6.05	5.69	7.49
0.0125	8.6	6.63	6.21	5.7	5.33	7.2
0.0167	8.5	6.26	5.82	5.28	4.91	6.7
0.025	8.4	5.87	5.39	4.84	4.45	6.2
0.033	8.3	5.77	5.17	4.61	4.18	5.9
0.05	8.25	5.62	5.00	4.38	3.91	5.55
0.1	8.24	5.45	4.85	4.22	3.71	5.4
1	8.23	5.35	4.77	4.11	3.6	5.38

$x^* = x/(Re \Pr D_h)$ *- Parallel Plates, both sides heated; **- Parallel plates, one side heated. For moderate values, curve fit equations are provided in APPENDIX A

Curve fit equations of this table can be used for three side heated case by benefiting from the formula below:

For $0.1 < \alpha_c < 10$

$$Nu_{x,3}(x^*, \alpha_c) = Nu_{x,4}(x^*, \alpha_c) \frac{Nu_{fd,3}(x^*_{fd}, \alpha_c)}{Nu_{fd,4}(x^*_{fd}, \alpha_c)} \qquad (2.18)$$

For $\alpha_c \leq 0.1$ and $\alpha_c \geq 10$ values for the four side heated case may be used for the three side heated case.

By the help of fully the developed Nusselt numbers for three and four side heated cases, the Nusselt numbers for thermally developing flow for the three side heated case can be found.

CHAPTER 3

NUMERICAL SIMULATIONS

For the simulations, the geometric modeling is performed using the software GAMBIT while the thermal analysis is performed with FLUENT. The model is applied to eight different metal-polymer microchannel heat sinks that were designed, fabricated and partially tested by a fellow student [15]. These metal-polymer microchannel heat sinks are simulated to find out how much heat could be provided to the systems while keeping the substrate temperatures below 85°C under a constant pumping power requirement. To keep the pumping power constant and sustain the substrate temperature under 85°C, simulations are performed iteratively. Substrate is the solid layer at the bottom of the microchannel heat sink. The simulations can be regarded as a pre-evaluation before conducting experiments in a parallel study [15] mentioned above.

3.1 Governing Equations

The numerical solution is based on three main conservation laws, conservation of mass, momentum and energy. The equations are given below [23].

Conservation of mass:

$$\frac{D\rho}{Dt} + \rho \nabla \cdot \boldsymbol{v} = 0 \qquad (3.1)$$

ρ is density of the fluid, **v** is the velocity vector and $\frac{D}{Dt}$ is the material derivative

$$\frac{D}{Dt} = \frac{\partial}{\partial t} + u\frac{\partial}{\partial x} + v\frac{\partial}{\partial y} + w\frac{\partial}{\partial z}. \qquad (3.2)$$

If the fluid is incompressible, the time derivative of the density may be neglected, and the continuity equation in Cartesian coordinates takes the form

$$\frac{\partial u}{\partial x} + \frac{\partial v}{\partial y} + \frac{\partial w}{\partial z} = 0 \qquad (3.3)$$

where u,v,w are the velocity components of flow.

2-D Conservation of momentum (Navier-Stokes) equation in x direction [23]:

$$\rho\frac{Du}{Dt} = -\frac{\partial P}{\partial x} + \frac{\partial}{\partial x}\left(2\mu\frac{\partial u}{\partial x} - \frac{2\mu}{3}\left(\frac{\partial u}{\partial x} + \frac{\partial v}{\partial y}\right)\right) + \frac{\partial}{\partial y}\left(\mu\left(\frac{\partial u}{\partial y} + \frac{\partial v}{\partial x}\right)\right) + gx \qquad (3.4)$$

P is the pressure vector, μ is the dynamic viscosity, g is the gravitational acceleration.

If the flow is assumed to be incompressible, and the dynamic viscosity and the density are assumed constant, the x-momentum equation reduces to

$$\rho\left(\frac{\partial u}{\partial t} + u\frac{\partial u}{\partial x} + v\frac{\partial u}{\partial y}\right) = -\frac{\partial P}{\partial x} + \mu\left(\frac{\partial^2 u}{\partial x^2} + \frac{\partial^2 u}{\partial y^2}\right) + gx. \qquad (3.5)$$

For three dimensions in Cartesian coordinates, the steady state, incompressible, constant density and dynamic viscosity, Navier-Stokes equations are of the form

$$\rho\left(u\frac{\partial u}{\partial x} + v\frac{\partial u}{\partial y} + w\frac{\partial u}{\partial z}\right) = -\frac{\partial P}{\partial x} + \mu\left(\frac{\partial^2 u}{\partial x^2} + \frac{\partial^2 u}{\partial y^2} + \frac{\partial^2 u}{\partial z^2}\right) + gx \qquad (3.6)$$

$$\rho\left(u\frac{\partial v}{\partial x}+v\frac{\partial v}{\partial y}+w\frac{\partial v}{\partial z}\right)=-\frac{\partial P}{\partial y}+\mu\left(\frac{\partial^2 v}{\partial x^2}+\frac{\partial^2 v}{\partial y^2}+\frac{\partial^2 v}{\partial z^2}\right)+gy \tag{3.7}$$

$$\rho\left(u\frac{\partial w}{\partial x}+v\frac{\partial w}{\partial y}+w\frac{\partial w}{\partial z}\right)=-\frac{\partial P}{\partial z}+\mu\left(\frac{\partial^2 w}{\partial x^2}+\frac{\partial^2 w}{\partial y^2}+\frac{\partial^2 w}{\partial z^2}\right)+gz \tag{3.8}$$

in *x*, *y* and *z* directions, respectively.

The first law of thermodynamics states that

$$\rho c_p \frac{DT}{Dt}=\nabla\cdot(k\,\nabla T)+q'''+\beta\,T\frac{DP}{Dt}+\mu\Phi \tag{3.9}$$

where q''' is the internal heat generation, β is the thermal expansion coefficient, Φ is the viscous dissipation term, and c_p is the specific heat.

With the assumption of constant thermal conductivity and dynamic viscosity, the steady state, incompressible flow *($\beta = 0$)*, with no internal heat generation, (3.9) in Cartesian coordinates reduces to

$$\rho c_p\left(u\frac{\partial T}{\partial x}+v\frac{\partial T}{\partial y}+w\frac{\partial T}{\partial z}\right)=k\left(\frac{\partial^2 T}{\partial x^2}+\frac{\partial^2 T}{\partial y^2}+\frac{\partial^2 T}{\partial z^2}\right)+\mu\Phi \tag{3.10}$$

where Φ is given by,

$$\Phi=2\left(\left(\frac{\partial u}{\partial x}\right)^2+\left(\frac{\partial v}{\partial y}\right)^2+\left(\frac{\partial w}{\partial z}\right)^2\right)$$
$$+\left(\left(\frac{\partial u}{\partial y}+\frac{\partial v}{\partial x}\right)^2+\left(\frac{\partial v}{\partial z}+\frac{\partial w}{\partial y}\right)^2+\left(\frac{\partial w}{\partial x}+\frac{\partial u}{\partial z}\right)^2\right) \tag{3.11}$$
$$-\frac{2}{3}(\frac{\partial u}{\partial x}+\frac{\partial v}{\partial y}+\frac{\partial w}{\partial z})^2\,.$$

3.2 Calculation of the Pumping Power Based on Experimental Conditions

In order to run the optimization code which will be explained in Chapter 5, the pressure drop through the channel should be determined. To conduct a realistic analysis, an existing pump used in a parallel experimental study [15] is considered. It is investigated how much flow the system is able to pump without having any leakage from the connections and any stability problem. The experimental set up is tested at room temperature with water (at 300 K), and it is observed that 5 milliliters per minute can be pumped through 200-10CH device without any problems. Hence, the required pumping power could be calculated. For all geometries analyzed in this chapter, the pumping power calculated below is considered.

Channel dimensions are for the tested device are given in Table 3.1

Table 3.1 Experimented device dimensions, 200-10 CH

Channel length, L	0.0186 m
Channel width, w_c	200 μm
Channel height, H_c	20 μm
Channel number, n	10
Wall thickness	56 μm

The volumetric flow rate, $\dot{Q}$, may be calculated as

$$\dot{Q} = u_m A_c \, n = 5 \frac{\text{ml}}{\text{min}} = \frac{5 \times 10^{-6}}{60} \frac{\text{m}^3}{\text{s}} \qquad (3.12)$$

Where u_m is the mean velocity in the channel. The flow rate per channel is $\frac{\dot{Q}}{n}$.

$$u_m = \frac{\dot{Q}}{A\,n} = 2.08\,\frac{m}{s} \tag{3.13}$$

$$Re = \frac{u_m\,D_h}{\nu} = 88.3 \tag{3.14}$$

$$\Delta P = \frac{2\,f\,\rho\,u_m{}^2 L}{D_h} \tag{3.15}$$

In the pressure drop calculation given in (3.15) all the parameters except f are known.

To find f, Poiseuille number may be used. Using (2.6), Po number for three side heated case for hydrodynamically fully developed flow may be calculated as

$$Po = f * Re = Po\left(\frac{1}{\alpha_c}\right) = Po(\mathrm{H_c/w_c}) = Po(0.1)$$
$$= 24 * \left(1 - 1.3553\alpha_c + 1.94677\,\alpha_c{}^2 - 1.7012\,\alpha_c{}^3 + 0.9564\,\alpha_c{}^4 \right. \tag{3.16}$$
$$\left. - 0.2537\,\alpha_c{}^5\right) = 21.1759.$$

The equation above gives reasonable values when the aspect ratio is smaller than 1. Therefore, the aspect ratio of the channel is taken as $\frac{1}{\alpha_c}$, where $\alpha_c = w_c/H_c$.

In order to understand whether the fully developed assumption holds, the dimensionless hydrodynamic entry length should be examined. The dimensionless length is defined as

x^+ = Dimensionless Hydrodynamic length = $\frac{L}{D_h Re}$ = 5.79

The dimensionless length should be greater than 1 for the flow to be hydrodynamicaly fully developed.

It is not necessary for the current calculations but if the dimensionless hydrodynamic entry length were below 1, it would be required to calculate the dimensionless entry length and then the Poiseuille number. Local Po numbers are given in the form of Table 3.2.

Table 3.2 Laminar flow entrance region Poiseulle number for rectangular channels, [16]

	$f_{app}Re$			
$x^+ = (x/D_h)/Re$	$\alpha_c = 1.0$	$\alpha_c = 0.5$	$\alpha_c = 0.2$	$\alpha_c \leq 0.1$ $\alpha_c \geq 10$
0	142.0	142.0	142.0	287.0
0.001	111.0	111.0	111.0	112.0
0.003	66.0	66.0	66.1	67.5
0.005	51.8	51.8	52.5	53.0
0.007	44.6	44.6	45.3	46.2
0.009	39.9	40.0	40.6	42.1
0.01	38.0	38.2	38.9	40.4
0.015	32.1	32.5	33.3	35.6
0.02	28.6	29.1	30.2	32.4
0.03	24.6	25.3	26.7	29.7
0.04	22.4	23.2	24.9	28.2
0.05	21.0	21.8	23.7	27.4
0.06	20.0	20.8	22.9	26.8
0.07	19.3	20.1	22.4	26.4
0.08	18.7	19.6	22.0	26.1
0.09	18.2	19.1	21.7	25.8
0.10	17.8	18.8	21.4	25.6
0.20	15.8	17.0	20.1	24.7
>1.0	14.2	15.5	19.1	24.0

There are also curve fit equations in APPENDIX A for different aspect ratios. For intermediate values linear interpolation is used.

$$\Delta P = \frac{2f\rho \, u_m{}^2 L}{D_h} = 1.06 \text{ MPa} \qquad (3.17)$$

$$\text{Pumping Power} = \Delta P * \dot{Q} = 0.088 \text{ W} \qquad (3.18)$$

The pumping power is determined to be approximately 0.088 W. This value is a reasonable number for syringe pumps as surveyed in the literature. As it is not possible to enter the pumping power as a boundary condition in Fluent software, some iterations were needed to be performed not to exceed this value by more than 5%.

3.3 Geometry

In most studies related to the optimization of microchannels, a rectangular cross-section is considered, as done in this study. Metal-polymer microchannels as shown in Figure 3.1 are analyzed, and optimized.

Parylene top wall

Copper side walls

Titanium – Gold metal layer

Parylene electrical insulation layer

Heat Flux to the heat sink
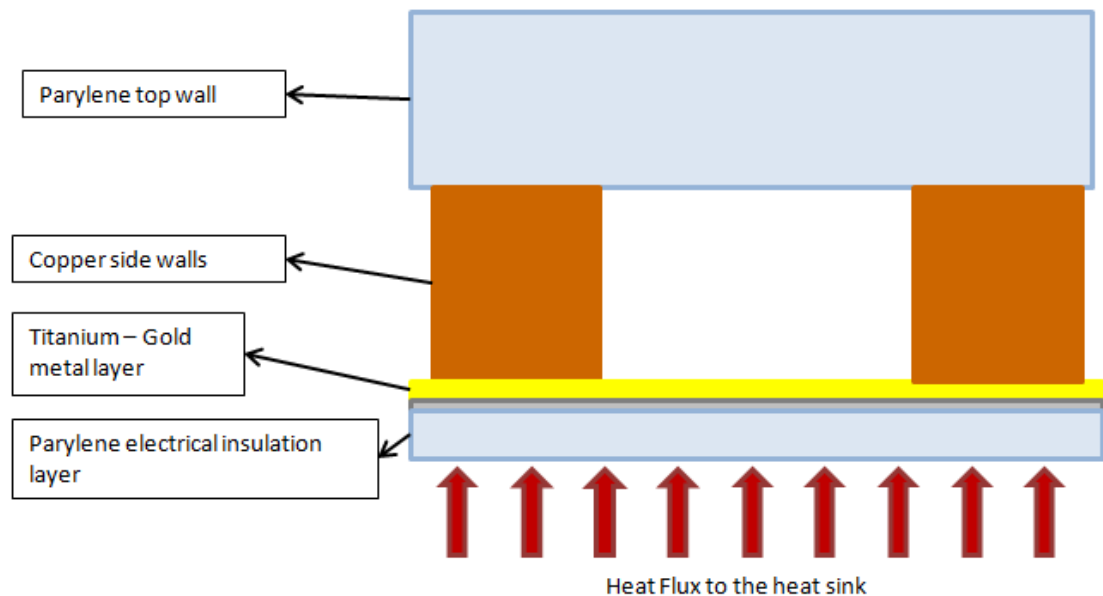
Figure 3.1 Schematic view of main geometry

In this chapter, analyses for existing channels [15] with known geometrical parameters are performed.
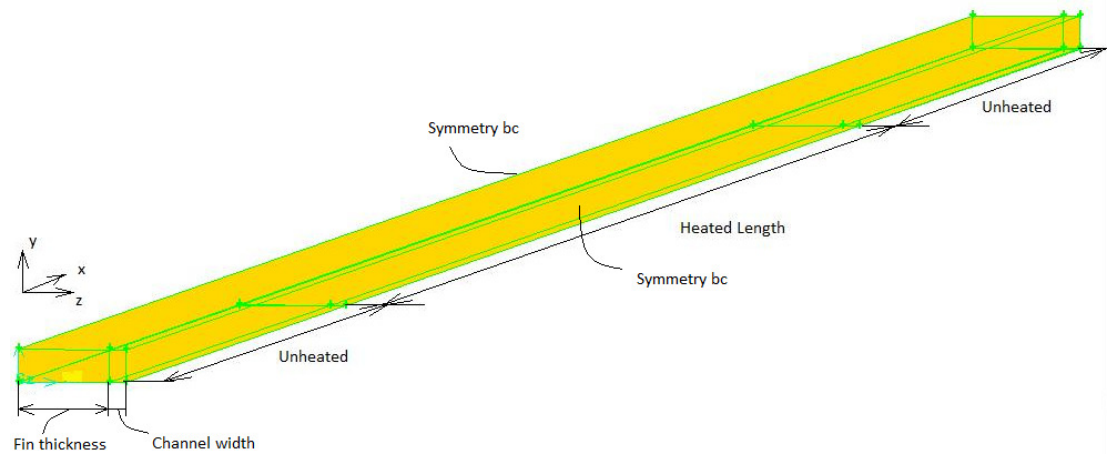
Figure 3.2 Three dimensional geometry of a 20-20 CH

Figure 3.2 shows the three dimensional simplified geometry of a metal-polymer heat sink. On the two vertical sides, symmetry boundary conditions are applied. A constant heat flux is applied at the bottom for the heated length. The heated part corresponds to the middle of the channel. There are two unheated sections of equal length before and after the heated part. This particular geometry, denoted by 20-20 CH, corresponds to a heat sink of 20 channels with 20 μm height and width. Detailed information on the channel dimensions can be found in the following section.

3.3.1 Main Dimensions

3.3.1.1 Fixed Dimensions

Starting from bottom to top, there are three main layers at the bottom of the geometry as can be seen from Figure 3.1, parylene, titanium and gold layers. The channel walls are made from copper, and are of 20 μm height. At the top, there is a thermal insulation layer 200 μm height. The thickness of each layer is presented in Table 3.3.

Table 3.3 Fixed dimensions

Layer	Thickness
Parylene insulation	200 nm
Titanium	50 nm
Gold	500 nm
Copper walls (Height)	20 μm
Parylene top wall	15 μm

The three layers at the bottom are there due to manufacturing concerns. The thin parylene layer provides electrical insulation of the electronic device. Titanium layer serves as cohesive material between two materials. Finally, the gold layer serves as a seed layer for Cu wall. Among the three layers, only the parylene layer is modeled in Gambit. Titanium layer is neglected in simulations because its conduction thermal resistance is very low. On the other hand, the gold layer is identified as shell conduction in Fluent.

3.3.1.2 Varying Dimensions

In order to evaluate the effect of the channel geometry on the thermal and hydrodynamic characteristics of the microchannel, eight different heat sinks of various geometries are assessed for different flow conditions. In these geometries

the height of the channel is kept constant but the channel width, w_c, and the number of channels, n, are changed for constant total width.

In addition to multi channels, single channel heat sinks are also analyzed. The analyzed heat sinks are listed in the Table 3.4.

Table 3.4 Analyzed devices

	Device Code	Width (µm)	Height (µm)	Length (mm)		Number of Channels	Wall Thickness (µm)	Total Device Width (mm)
				Heated	Total			
Single Channels	200-1CH	200	20	10	18.6	1	50	0.3
	200-1CH-SH	200	20	6	14.8	1	50	0.3
	100-1CH	100	20	10	18.6	1	100	0.3
Multi Channels	200-10CH	200	20	10	18.6	10	56	2.56
	100-10CH	100	20	10	18.6	10	167	2.67
	50-10CH	50	20	10	18.6	10	222	2.72
	20-10CH	20	20	10	18.6	10	232	2.52
	20-20CH	20	20	10	18.6	20	110	2.6

CH- Channel, SH-Short

The total device width for the single channels is 0.3 mm, but the wall thickness and the channel width are different for each case. Also the heated and total lengths are different. The constant heat flux boundary condition is not applied for the whole channel length. The heated parts correspond to the middle of the channel. The rest is reserved for fluidic connections.

3.4 CFD Simulations

3.4.1 Validation

In order to validate their numerical results, many researchers have compared them with Tuckerman and Pease's [1] study. They used silicon channels of geometry shown in Figure 3.3. There are three cases in Tuckerman and Pease's experimental study which are compared with numerical studies in the literature. In the present work, first, the same cases are considered for validation purposes before proceeding with the CFD simulations of the metal-polymer heat sinks. Detailed information on the geometries, boundary conditions and the mesh structure are taken from the study by Liu and Garimella [8] to make the comparisons under exactly the same conditions. The comparison of the results are given in Table 3.5.
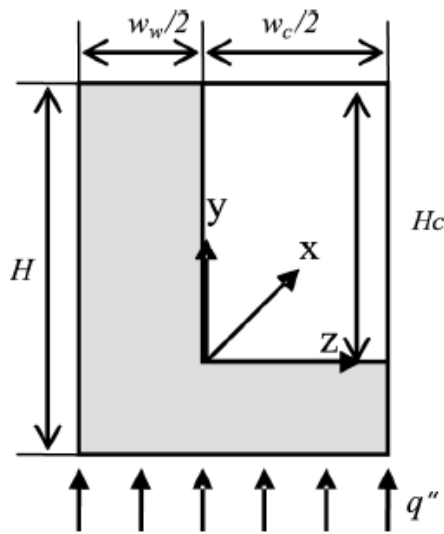
Figure 3.3 Silicon channels used in the experiments of Tuckerman and Pease, [8]

Symmetry boundary conditions were applied on both sides of the geometry and there was uniform heat flux at the bottom.

Table 3.5 Comparison of numerical studies with the experiments of Tuckerman and Pease [1]

	Case 1	Case2	Case 3
w_c (μm)	56	55	50
w_w (μm)	44	45	50
H_c (μm)	320	287	302
H (μm)	533	430	458
ΔP (kPa)	103.42	117.21	213.73
$q^{''}$ (W/cm^2)	181	277	790
R_{exp} (°C/W) Tuckerman and Pease [1]	0.110	0.113	0.090
R_{num} (°C/W) Liu and Garimella [8]	0.115	0.114	0.093
R_{num} (°C/W) Ryu et.al [9]	0.111	0.117	0.092
R_{num} (°C/W) Hussain 2008 [7]	0.115	0.097	0.081
R_{num} (°C/W) Present Study	0.115	0.114	0.0935

As can be seen from the Table 3.5, the thermal resistance values obtained in the current study agrees with very well Tuckerman and Pease's and other numerical results especially with Liu and Garimella's, for all cases. The results prove that the developed CFD model can be used for further analyses.

3.4.2 Mesh Structure of the Present Study

Liu and Garimella [8], used 500×14×60 grid structure to solve Tuckerman and Pease's [1] geometry and obtained satisfactory results. 500×14×60 represents the number of grid interval in x, y and z directions, respectively. Similar grid intervals

are selected in the present study to simulate the metal-polymer channels. A 3-D view of the computational domain of the 20-20CH heat sink and the coordinate system are given in Figure 3.2.

Table 3.6 Grid structure of the geometries

Device Code		Width (μm)	Height (μm)	Grid Structure (x,y,z)
Single Channels	200-1CH	200	20	930×13×74
	200-1CH-SH	200	20	740×13×74
	100-1CH	100	20	930×13×75
Multi Channels	200-10CH	200	20	930×23×65
	100-10CH	100	20	930×23×66
	50-10CH	50	20	930×23×77
	20-10CH	20	20	930×23×76
	20-20CH	20	20	930×23×65

The regions near to the solid-fluid interface are meshed denser with successive ratio of 1.016. This implementation is expected to give more accurate results than equally meshed geometries because the velocity and the heat flux gradients are higher at the fluid-solid interface. On the other hand, the meshes where adiabatic or symmetry boundaries are present are coarser. The 2-D mesh structure of the 20-20 CH device cross-section in y-z plane is shown in Figure 3.4.
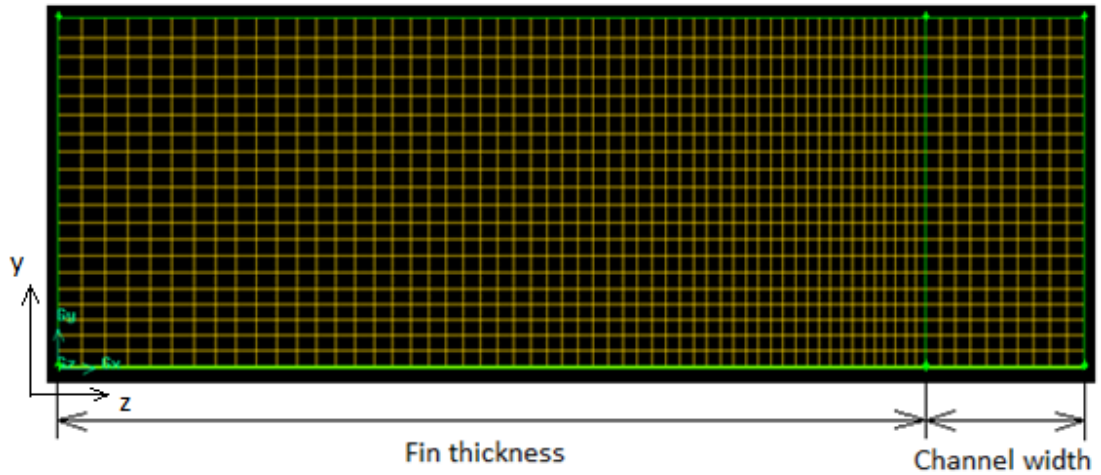
Figure 3.4 Mesh structure of 20-20 CH cross-section in y-z plane

The mesh statistics are presented in Table 3.7

Table 3.7 Mesh statistics

Device Code		Width (μm)	Height (μm)	Grid Structure (x,y,z)	Number of Nodes	Average Element Width (μm)
Single Channels	200-1CH	200	20	930×13×(24+50)	963480	2
	200-1CH-SH	200	20	740×13×(24+50)	766640	2
	100-1CH	100	20	930×13×(50+25)	976500	2
Multi Channels	200-10CH	200	20	930×23×(15+50)	1428480	2
	100-10CH	100	20	930×23×(42+24)	1473120	2
	50-10CH	50	20	930×23×(56+12)	1495440	2
	20-10CH	20	20	930×23× (58+10)	1517760	1
	20-20CH	20	20	930×23×(56+10)	1450800	1

y direction grid structure : (Wall side mesh number + Fluid side mesh number)

Channel inlet and outlet faces are meshed with quad-map scheme and the volume is meshed with the help of the source faces by the Cooper scheme.

In order to find out the effect of the mesh structure on the thermal resistance, the 200-1CH device is modeled with both 930×13×(24+50) and 930×8×(12+25) (nearly half of it) mesh structures. Thermal resistance differences are given in Table 3.8.

Table 3.8 Mesh independence

Mesh Structure	Thermal Resistance	Error %
930×13×(24+50)	15.871	0.2772
930×8×(12+25)	15.827	

As can be seen from the table, despite lowering the cell number nearly to half, the thermal resistance difference is below 1%. Therefore, it can be said that 930×13× (24+50) mesh structure and close to average element width for this geometry gives satisfactory results.

3.4.3 Boundary Conditions and Solver Settings

Firstly, the boundary conditions are defined on the geometry constructed in the software Gambit. Then the geometry file is exported to Fluent. There are three main boundary conditions: fluid inlet and outlet temperatures, and constant heat flux conditions at the bottom. These boundary conditions determine the hydrodynamic and thermal characteristics of the flow. By benefiting from the symmetry of the channels, only half of a channel is inspected providing a reduction in the computational time. Half of the channel reflects the characteristics of all geometry. The computational domain may be illustrated as in Figure 3.5 and Figure 3.6.
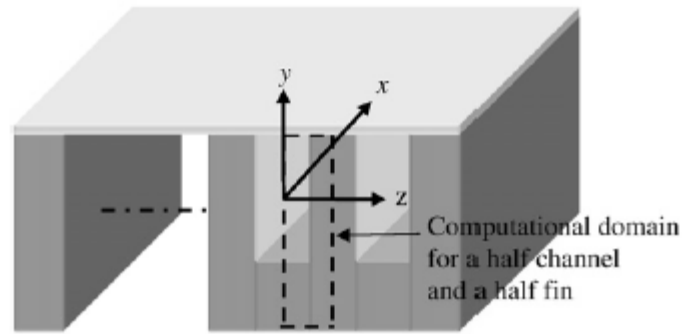
Figure 3.5 Computational domain, Kou et al. [24]
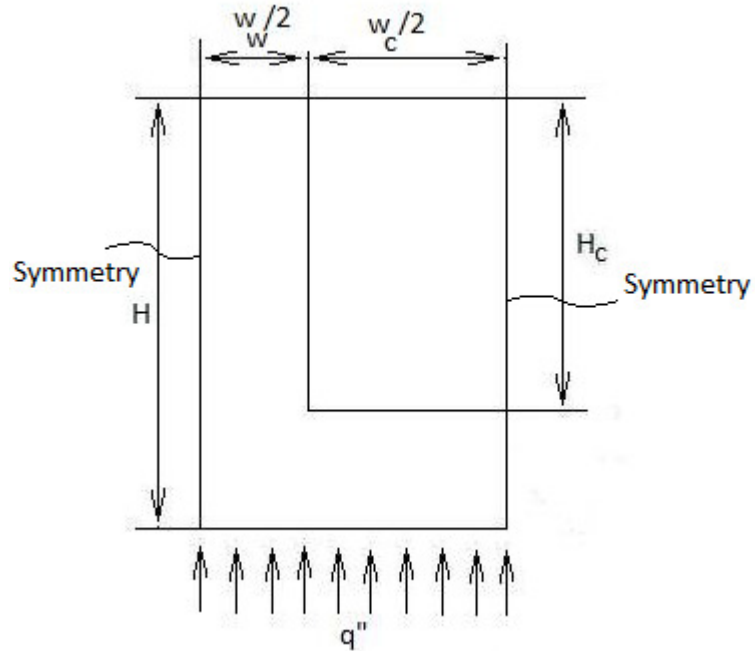
Figure 3.6 Symmetry and constant heat flux boundary conditions

Boundary condition types and boundary conditions for various devices are listed in and , respectively.

Table 3.9 Boundary condition types

Boundary Condition	
Fluid İnlet	Water coolant velocity inlet at 300 K
Fluid outlet	Pressure outlet at 0 Pa (gauge)
Solid Bottom	For heated parts heat flux is entered For insulated parts, the heat flux is 0
External Walls	Adiabatic (0 heat flux)
Side walls	Symmetry boundary conditions.

External walls are the surfaces in the solid region near to fluid inlet and outlet.

Table 3.10 Boundary conditions of the devices

	Device Code	Width (μm)	Height (μm)	Length (mm)		Number of Channels	Wall Thickness (μm)	Total Device Width (mm)	T enter (K)	u (m/s)	Heat Flux (W/cm2)
				Heated	Total						
Single Channel	200-1CH	200	20	10	18.6	1	50	0.3	300	7.7	115.6
	200-1CH-SH	200	20	6	14.8	1	50	0.3	300	8.3	154.3
	100-1CH	100	20	10	18.6	1	100	0.3	300	10.4	81
Multi Channel	200-10CH	200	20	10	18.6	10	56	2.56	300	2.4	69.2
	100-10CH	100	20	10	18.6	10	167	2.67	300	3.4	44.8
	50-10CH	50	20	10	18.6	10	222	2.72	300	4.5	30.3
	20-10CH	20	20	10	18.6	10	232	2.52	300	5.41	19
	20-20CH	20	20	10	18.6	20	110	2.6	300	3.8	25.7

Table 3.11 Material and coolant specifications

Coolant	Water with variable properties
Solid-Fin	Copper with variable properties
Solid Layer	Titanium with variable properties
	Gold with variable properties
	Parylene C with variable properties

Channel material and coolant specifications are given in Table 3.11. Variable thermophysical properties are used for water. Fifth degree polynomials are fitted for water properties and piecewise linear properties are entered for solids at 200, 300 and 400 K. Detailed information on property calculations is given in APPENDIX B.

Solution settings have a great importance in obtaining satisfactory results. Most of the solver settings are kept as the default values because those are optimized by the software. Convergence criterion is 0.001 for continuity and momentum equations. On the other hand, convergence criterion for the energy equation is 10^{-6}. A 3-D double precision solution is sought. Main solver settings adjusted in Fluent are given in the Table 3.12.

Table 3.12 Solution settings

Viscous Model	Laminar with viscous heating
Solution Controls	Pressure= 0.3
	Density= 1
	Body Forces= 1
	Momentum= 0.7
Discretization	Pressure= Standard
	Momentum= First Order Upwind
	Energy = First Order Upwind
Pressure-Velocity Coupling	Simple

3.4.4 Simplification of the Geometry

The main structure of the geometry was given in Figure 3.1. As the titanium layer is so thin that it has nearly no effect on thermal characterization of the microchannel. Channel walls are made of copper, and due to its high thermal conductivity, it is expected that it will have a good contribution in dissipating heat.

On the outermost surfaces of the microchannel heat sink, there will be natural convection due to the temperature difference between the surfaces and the ambient. It is necessary to calculate how much heat is dissipated from these surfaces to see its effect on the maximum temperature of the walls.

In order to assess the influence of natural convection on the thermal resistance of the channel, the heat transfer coefficient on the outer surface of the walls should be calculated.

A correlation that is valid for all Ra_L values by Churchill and Chu [21] for a vertical plate is of the form

$$\overline{Nu_L} = \left(0.825 + \frac{0.387\,Ra_L^{\left(\frac{1}{6}\right)}}{(1 + (\frac{0.492}{Pr})^{\frac{9}{16}})^{\frac{8}{27}}}\right)^2 \tag{3.19}$$

$$Ra_L = \frac{g\,\beta\,(T_s - T_\infty)L^3}{\nu\alpha} \tag{3.20}$$

The ambient air is assumed to be at T_{air}=300 K and P_{air}=90 kPa (assumed suitable for Ankara).

For 200-1CH coded device, copper wall, parylene top and copper surface temperature at the exit is 328 K when the pumping power is 0.088 W, flow rate is 1.85 ml/min and maximum substrate temperature is 355 K. Detailed information can be found in Table 3.13.

The film temperature is

$$T_f = \frac{300 + 328}{2} = 314\text{ K} \tag{3.21}$$

Then the thermophysical properties of air are

ρ=0.99015803 kg/m^3, C_p= 1.00757 kJ/kgK, μ=1.913×10^{-5} N s /m², k=0.0273545W/m K, ν =1.913×10^{-5} m²/s, α =2.76×10^{-5} m²/s, Pr=0.7049.

Density is found by the help of ideal-gas equation. ν and α are functions of density so they are also calculated for 90 kPa atmospheric presssure.

$$L = 20\ \mu m, \qquad \beta = \frac{1}{314\ K}$$

$$Ra_L = \frac{g\,\beta\,(T_s - T_\infty)L^3}{\nu\alpha} = \frac{9.81\frac{m}{s^2}\frac{1}{314\,K}(328 - 300)K\,(20 \times 10^{-6}m)^3}{1.913 \times 10^{-5}\frac{m^2}{s}\,2.76 \times 10^{-5}\ m^2/s} \tag{3.22}$$

$$= 1.33 \times 10^{-5}$$

$$\overline{Nu}_L = (0.825 + \frac{0.387 \, Ra_L^{\left(\frac{1}{6}\right)}}{(1 + (\frac{0.492}{Pr})^{\frac{9}{16}})^{\frac{8}{27}}})^2 = 0.7654 \tag{3.23}$$

$$\bar{h}_L = \frac{\overline{Nu}_L \, k}{L} = 1046 \frac{W}{m^2 K} \tag{3.24}$$

An exact natural convection analysis is beyond the scope of this thesis. Hence, for an order of magnitude analysis, the same heat transfer coefficient will be assumed for the horizontal surface.

$$q_{vertical} = A \, \bar{h}_L \, (T_s - T_\infty)$$
$$= (20 \times 10^{-6} m \times 0.0186 \, m \times 2 + 20 \times 10^{-6} m \times 50$$
$$\times 10^{-6} m \times 4) \times 1046 \frac{W}{m^2 K} \times (328 - 300)K = 0.022W \tag{3.25}$$

$$q_{horizontal} = A \, \bar{h}_L \, (T_s - T_\infty)$$
$$= (0.0186 \, m \times 0.3 \times 10^{-3} m) \times 1046 \frac{W}{m^2 K} \times (328 - 300)K \tag{3.26}$$
$$= 0.16 \, W$$

$$q_{total,loss} = q_{horizontal} + q_{vertical} = 0.182 \, W \tag{3.27}$$

The total heat load given to the system is $q_{load} = 3.47$ W as stated in Table 3.13. The heat transferred through natural convection is about 5% of the total heat given to the system. Therefore, the assumptions of an insulated top surface and symmetry boundary conditions for the side walls are proved to be valid.

3.5 Evaluation of the Results

In this part, the objective is to compare heat dissipation capacities of various metal-polymer microchannels under two main constraints one of which is that the substrate temperature is not allowed to exceed 85°C, and the second is that the same constant pumping power, 0.088 W, is applied to all of the channels. The pumping power cannot be an input to the CFD code, thus, an iterative procedure has been followed, and a value which is within 5% of 0.088 W is considered valid.

The simulation results are given in Table 3.13

Table 3.13 Analysis Results

	Device Code	Width (µm)	Height (µm)	Length (mm) Heated	Length (mm) Total	Number of Channels	Wall Thickness (µm)	Total Device Width (mm)	T enter (K)	T outlet (K)	u (m/s)	q (W)	Heat Flux (W/cm2)	T_{max} (K)	Pres Drop(Pa)	Pumping Power (W)
Single Channel	200-1CH	200	20	10	18.6	1	50	0.3	300	327	7.7	3.5	115.6	355	2991031	0.092
	200-1CH-SH	200	20	6	14.8	1	50	0.3	300	320	8.3	2.8	154.3	355	2728611	0.091
	100-1CH	100	20	10	18.6	1	100	0.3	300	328	10.4	2.4	81	356	4285020	0.089
Multi Channel	200-10CH	200	20	10	18.6	10	56	2.56	300	344	2.4	17.7	69.2	356	858625	0.083
	100-10CH	100	20	10	18.6	10	167	2.67	300	342	3.4	12	44.8	354	1308246	0.089
	50-10CH	50	20	10	18.6	10	222	2.72	300	344	4.5	8.2	30.3	354	1973512	0.089
	20-10CH	20	20	10	18.6	10	232	2.52	300	353	5.4	4.8	19	356	3979084	0.086
	20-20CH	20	20	10	18.6	20	110	2.6	300	352	3.8	6.7	25.7	355	2871860	0.089

In order to check the accuracy of the CFD code, the outlet temperature of the fluid is also calculated theoretically and is compared with the CFD result.
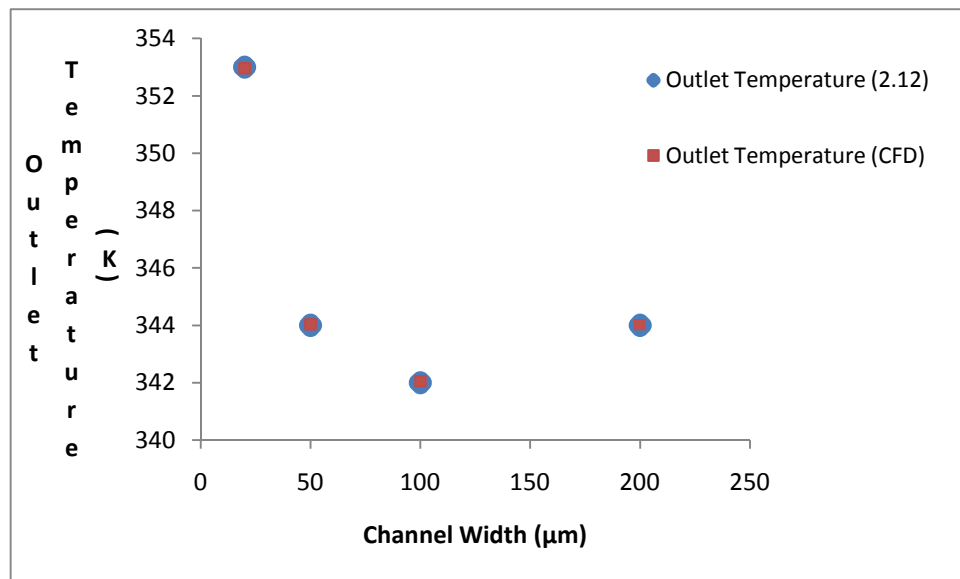
Figure 3.7 Comparison of theoric outlet temperature and CFD result of fluid outlet temperature for multichannels

Although the thermophysical properties of water are assumed to be constant at 315 K for the theoretical calculations, the results are nearly the same with the CFD results as can be seen in Figure 3.7. The maximum error between the compared data point is under 1%.

3.5.1 Thermal Evaluation

The metal-polymer microchannel heat sinks of ten channels with previously listed dimensions are compared in terms of their heat dissipation capacities. Detailed information on the results can be found in Table 3.13.
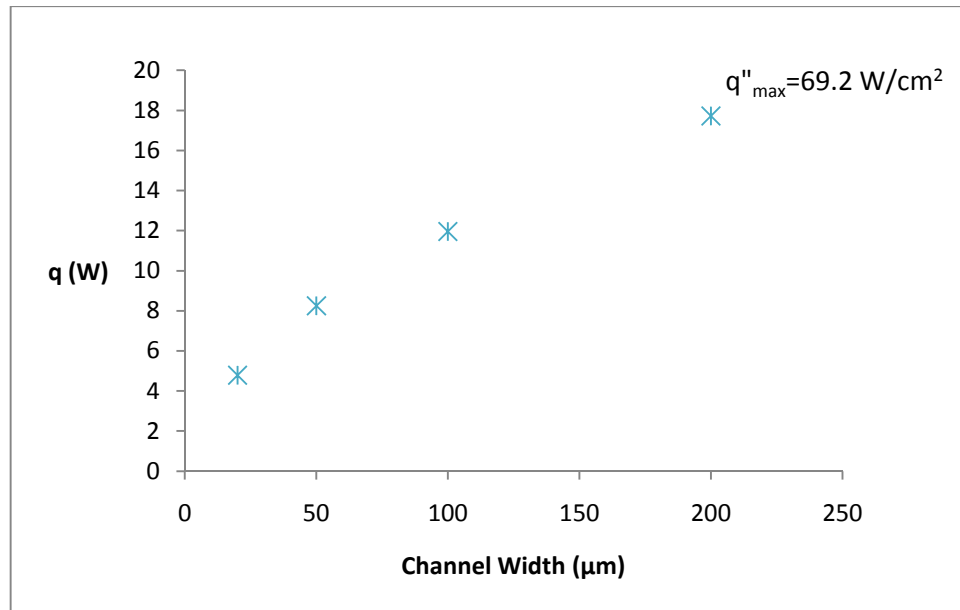
Figure 3.8 Heat dissipation capacity of 10-channel heat sinks

Figure 3.8 shows that when the channel width increases, heat dissipation rates also increases because for constant pumping power, higher volumetric flow rates can be pumped for larger channel width. In other words, instead of having large fin thickness, enlarging the channel width provides higher heat removals for the same number of channels.

It is expected to see a similar trend for single channels. As can be seen from Table 3.13, the heat dissipation rate increases when the channel width is increased for constant total width. Results indicated that it is possible to remove heat flux values as much as 154 W/cm^2.

One other parameter that augments the heat dissipation rate is the number of the channels. When the performances of 10-channel and 20-channel heat sinks of 20 μm channel width are compared in Table 3.13, an increase in the heat transfer rate is observed as the number of the channels increases.

The inner surface temperature of the side walls are presented in Figure 3.9. As expected, the maximum wall temperature is attained at the end of the heated section.
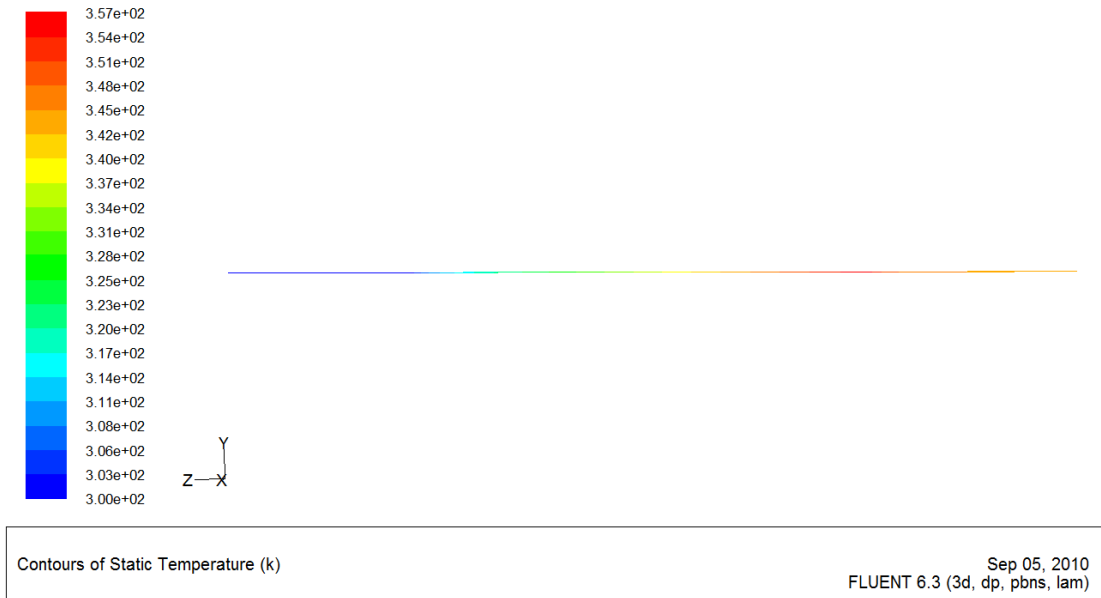
Figure 3.9 Inner surface temperature of the side wall, 200-10CH
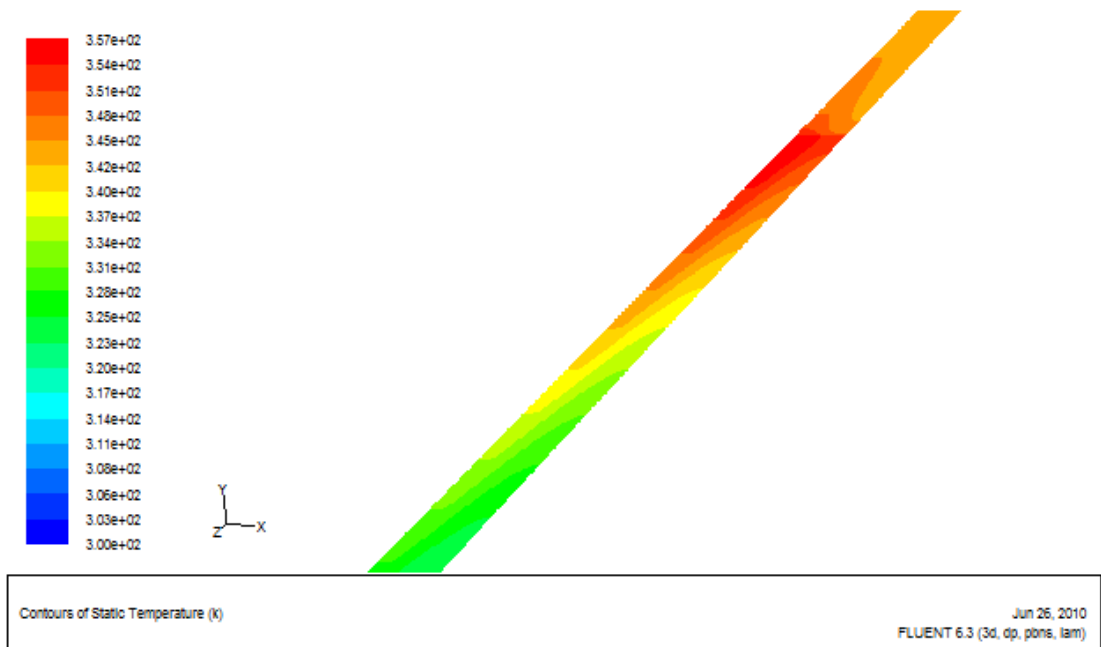
Figure 3.10 Substrate temperature distribution for 200-10CH

The maximum temperature value in microchannels occurs at the end of the heated section in z direction according to the coordinate system shown in Figure 3.10, and on the bottom substrate surface touching the heat source as indicated in the figure.

3.5.2 Hydrodynamic Evaluation

In addition to thermal evaluation, it is also crucial to evaluate the microchannels hydrodynamically. Pressure drop is one of the most important parameters when dealing with microchannels because it is directly related to the pumping power. The maximum pressure drop observed in the simulation results is within the range that the microchannels can resist [15]. Generally, to reduce the pumping power and to prevent large temperature differences between the channel inlet and outlet, the channel length is kept short. Therefore, the pressure drop value is desired to be low. The pressure drop for the fully developed flow is given by (2.4).

For a low pressure drop, the friction factor, fluid density, mean velocity and channel length are required to be small; on the other hand, hydraulic diameter of the channel should be large. Widening the channel width also lowers the mean velocity; consequently, the pressure difference between the inlet and the outlet is reduced. Pressure drop versus channel width relation under constant pumping power, channel height and number of channels is given in Figure 3.11,
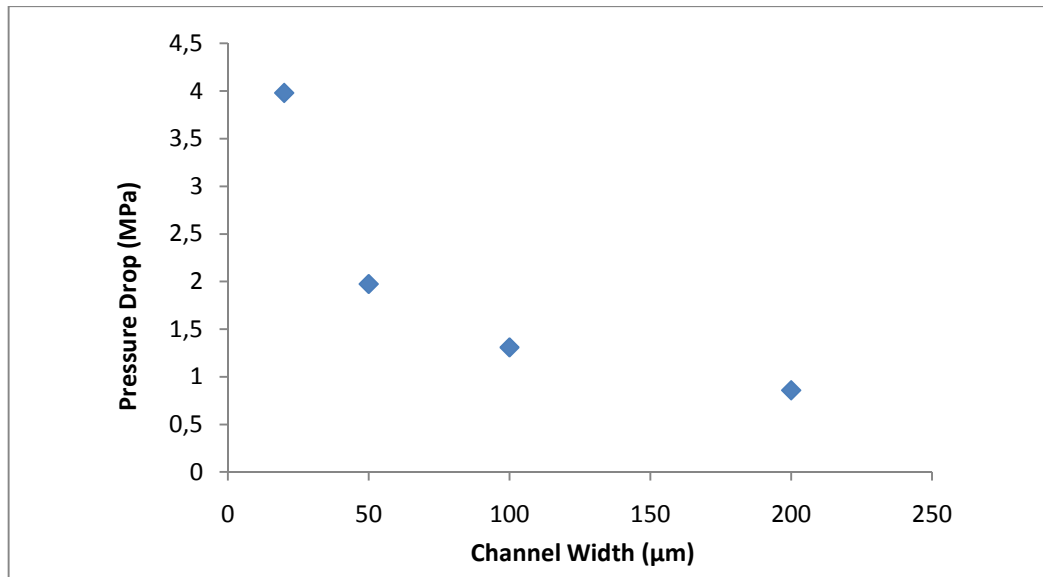
Figure 3.11 Pressure drop versus channel width for multichannels

Decrease in the pressure drop is observed as the channel width is increased.

Pressure variation throughout the channel is expected to have sharp decrease at the inlet of the channel because of the entrance region effects. Then, the decline trend continues gradually. The pressure distribution along the channel is shown in Figure 3.12.
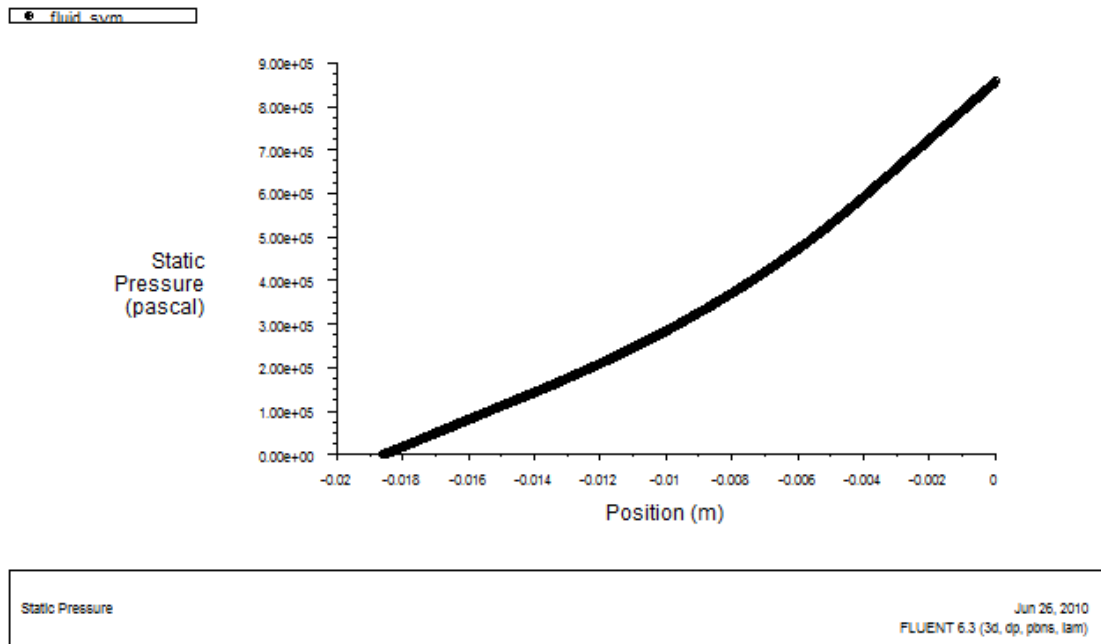
Figure 3.12 Pressure throughout the channel, 200-10CH

As expected, at the entrance regions, a sharp pressure drop is observed. After fully developed flow conditions are reached, the pressure decreases more gradually.

Velocity profile throughout the channel develops till the flow reaches the fully developed condition. Figure 3.13 shows that the flow reached the fully developed region at the exit of the channel. For 200-10CH, velocity vectors are shown in the figure,
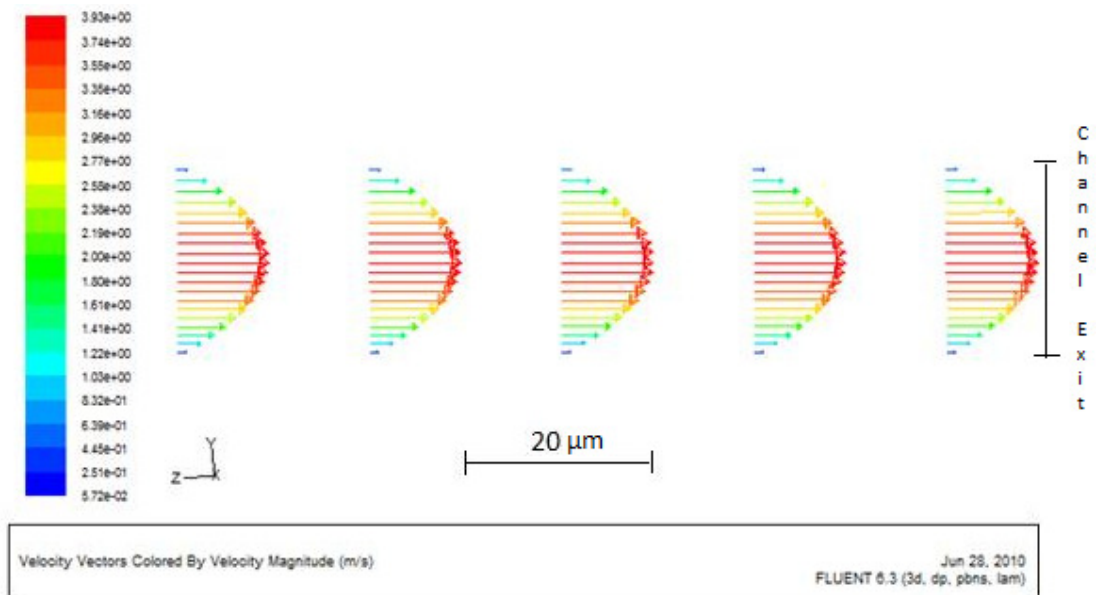
Figure 3.13 Velocity vectors at the exit of the channel

Fluid regions close to the wall have lower velocity values than in the center of the channel due to no-slip boundary condition on the channel walls.

CHAPTER 4

OPTIMIZATION-THEORY

The main objective of the optimization study is to determine the heat sink geometries that yield the minimum thermal resistance under certain constraints related to the fabrication and operation. In this chapter, the models used in the optimization processes are derived. Four main optimization models will be considered. The first model includes the summation of conductive, convective and caloric thermal resistances. The second model is based on an adiabatic tip fin analysis and evaluates the fluid temperature distribution for one dimension throughout the channel. The third is distinguished from the second in evaluating the fluid temperature distribution in two dimensions so the third model is more reliable than the second one. The fourth model is different than the other models in that it does not neglect the axial conduction in the fin. The models are presented in detail by Liu and Garimella [8]. For the first and the fourth models, the studies by Sabry [11] and Shao et al. [14], were also helpful in understanding the derivation of the two models, respectively. Although the derivation of the models is well presented in the mentioned literature, they are repeated here step by step for the sake of completeness.

4.1 Assumptions

To be able to derive the thermal resistance equations analytically, some simplifications have to be made. The main assumptions are given by Liu and Garimella [8] as

- Steady-state flow and heat transfer;
- Negligible radiation;
- Uniform heat flux at the bottom;
- Hydrodynamically and thermally fully developed flow;
- Laminar and incompressible flow;
- Constant but variable with respect to inlet and outlet temperature thermophysical properties;
- Negligible contact resistance between substrate layers;
- Negligible axial conduction for fluid;
- Negligible axial conduction for solid fin except model 4;
- Averaged heat transfer coefficient for cross section in the fluid domain.

4.2 Boundary Conditions

The heat sink geometry and the coordinate system are illustrated in Figure 4.1 and 4.2, respectively. There are two main boundary conditions for the base of the fin [8].
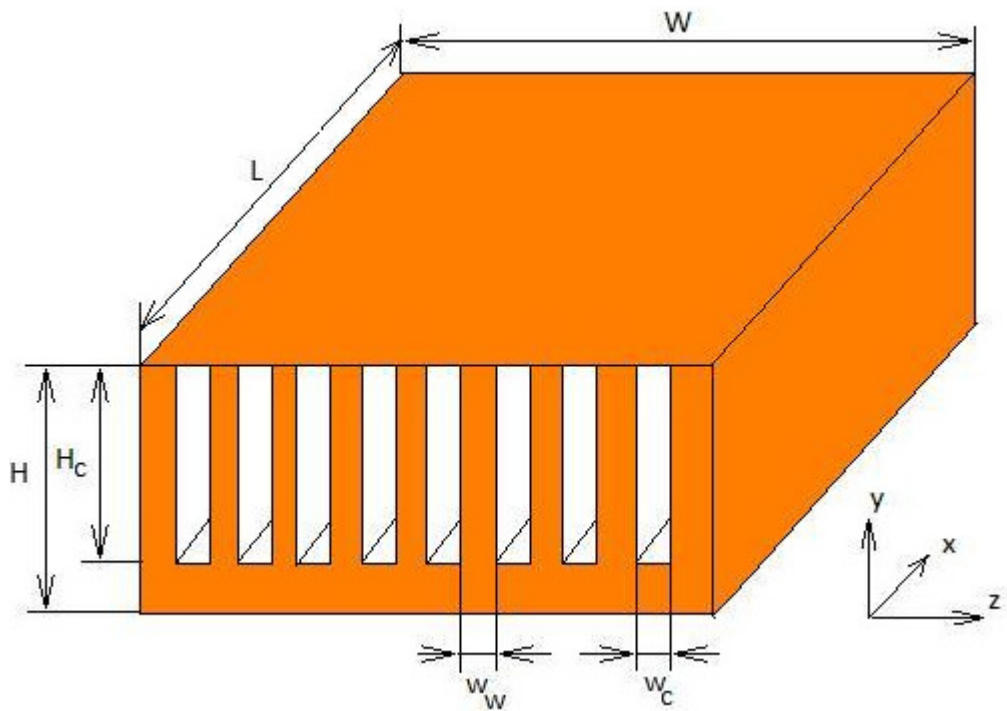
Figure 4.1 Shape of a rectangular microchannel heat sink
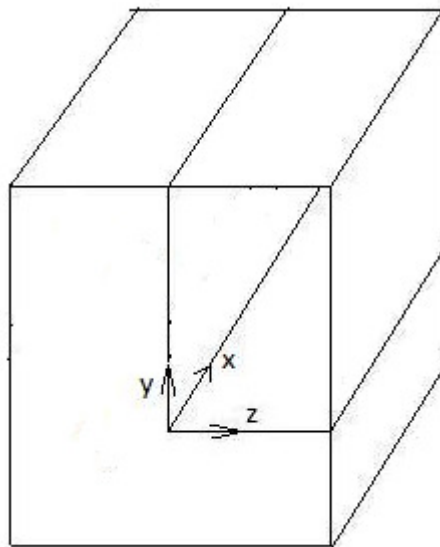
Figure 4.2 Coordinate system of the geometry

The first boundary condition is the uniform heat flux being supplied from the bottom of the substrate.

$$-k_s \frac{dT}{dy} = q'' \ at \ y = 0 \qquad (4.1)$$

This boundary condition might be useful when determining the substrate temperature distribution but the boundary condition is sought for the fin base. As heat transferred from the exposed surface to the fluid (at y=0) and through the fins are different, this boundary condition may not reflect the actual heat flux at the fin base.

If it is thought that all heat goes through the fin base, the boundary condition can be given as;

$$-k_s \frac{dT}{dy} = \frac{(w_c + w_w)}{w_w} q'' \ at \ y = 0 \qquad (4.2)$$

Heat transfer to the fluid through fin is

$$q_{fin} = h \ (H_c L) \ \eta \ (T_b - \bar{T}_f) \qquad (4.3)$$

Heat transfer to the fluid through the exposed channel base is

$$q_{substrate} = h \left(\frac{w_c}{2}L\right)(T_b - \bar{T}_f). \qquad (4.4)$$

The ratio of the fin heat transfer to the exposed substrate is

$$\frac{2H_c\eta}{w_c} = 2\eta\alpha_c \qquad (4.5)$$

where α_c is defined for Chapter 4 as

$$\alpha_c = \frac{H_c}{w_c} = \frac{\text{long side of the channel}}{\text{short side of the channel}}. \qquad (4.6)$$

The fin heat transfer to the fluid is equal to the fin base boundary condition. The case where all the heat flows through the fin base was given in (4.2), the ratio of the

fin heat transfer to the exposed substrate is also known. Hence, the fin base boundary condition can be calculated as

$$\frac{q_{fin\,base}}{q_{substrate}} = 2\eta\alpha_c \qquad (4.7)$$

$$q_{fin\,base} + q_{substrate} = \frac{(w_c + w_w)}{w_w} q" \qquad (4.8)$$

The solution of (4.2) and (4.10) yields the boundary condition at the base of the fin as

$$-k_s \frac{dT}{dy} = \frac{2\eta\alpha_c}{2\eta\alpha_c + 1} \frac{(w_c + w_w)}{w_w} q" \; at \; y = 0. \qquad (4.9)$$

This boundary condition is more realistic than the uniform heat flux assumption at the base of the fin because the heat flux is not equally distributed at y=0.

As the present study deals with the temperature distribution within the solid fin, substrate resistance is calculated separately and then added to other resistance values obtained for the maximum temperature of the solid fin.

$$R_{substrate} = \frac{t_{gold}}{k_{gold}\,(L*W)} + \frac{t_{titanium}}{k_{titanium}\,(L*W)} + \frac{t_{parylene}}{k_{parylene}\,(L*W)} \qquad (4.10)$$

t is thickness of the substrate material.

$$R_{total} = R_{fin} + R_{substrate} \qquad (4.11)$$

4.3 Model 1, Resistance Analysis

Under the assumption of thermally and hydrodynamicaly fully developed flow and the other assumptions stated in Chapter 4.1, Liu and Garimella [8] considered three

main resistances, conduction in the substrate, convection through fin and channel base surfaces and also resistance of the fluid. Shao et al. [14] also conducted a study using the thermal resistance model, and suggested the thermal resistance network given in Figure 4.3.
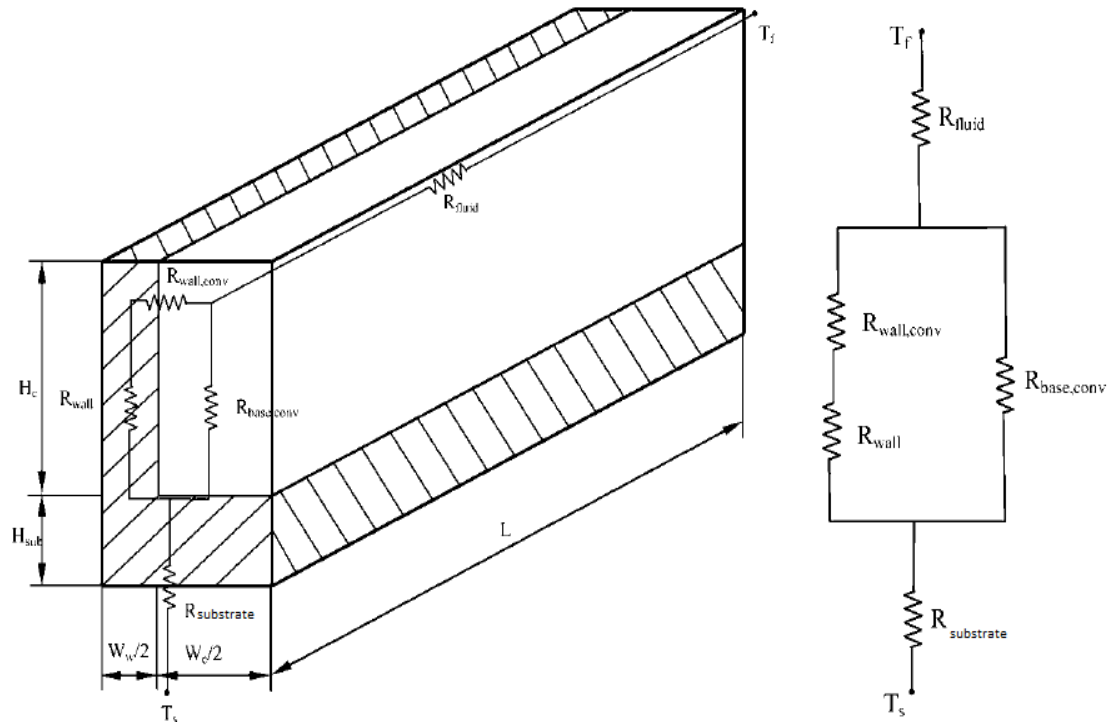
Figure 4.3 Thermal resistance network, [14].

The fin resistance is given by

$$R_{fin} = R_{wall,conv} + R_{wall} = \frac{1}{2\, n\, h\, L\, \eta H_c} \qquad (4.12)$$

where n is the number of the channels, η is the fin efficiency with adiabatic fin tip assumption.

$$\eta = \frac{tanh\,(m\,H_c)}{m\,H_c} \qquad (4.13)$$

$$m = \left(\frac{2\,h}{k_{fin}\,w_w} \right)^{\frac{1}{2}} \tag{4.14}$$

k_{fin} is the thermal conductivity of the fin material, w_w is the fin thickness.

$$R_{base,conv} = \frac{1}{n\,h\,L\,w_c} \tag{4.15}$$

$$R_{fluid} = \frac{1}{\rho_f\,\theta\,C_p} \tag{4.16}$$

ρ_f is the density of the fluid, θ is the volumetric flow rate, c_p is the specific heat of the fluid.

$$R_{substrate} = \frac{t_{gold}}{k_{gold}\,(L*W)} + \frac{t_{titanium}}{k_{titanium}\,(L*W)} + \frac{t_{parylene}}{k_{parylene}\,(L*W)} \tag{4.17}$$

$$R_{total,model\ 1} = R_{substrate} + \left(\frac{1}{R_{fin}} + \frac{1}{R_{base,conv}} \right)^{-1} + R_{fluid} \tag{4.18}$$

$$R_{total,model\ 1} = \frac{t_{gold}}{k_{gold}\,(L*W)} + \frac{t_{titanium}}{k_{titanium}\,(L*W)} + \frac{t_{parylene}}{k_{parylene}\,(L*W)}$$
$$+ \frac{1}{\rho_f\,\theta\,C_p} + \frac{1}{nhL(2\eta H_c + w_c)} \tag{4.19}$$

4.4 Model 2, Fin analysis

This model investigates the temperature distribution of the solid fin which neglects the axial conduction throughout the channel. The fluid side temperature distribution is one dimensional only in x direction, the fluid temperature is averaged

for each cross-section. The energy balance for the fins is written in y direction by the help of the schematic in Figure 4.4 as given by (4.20)
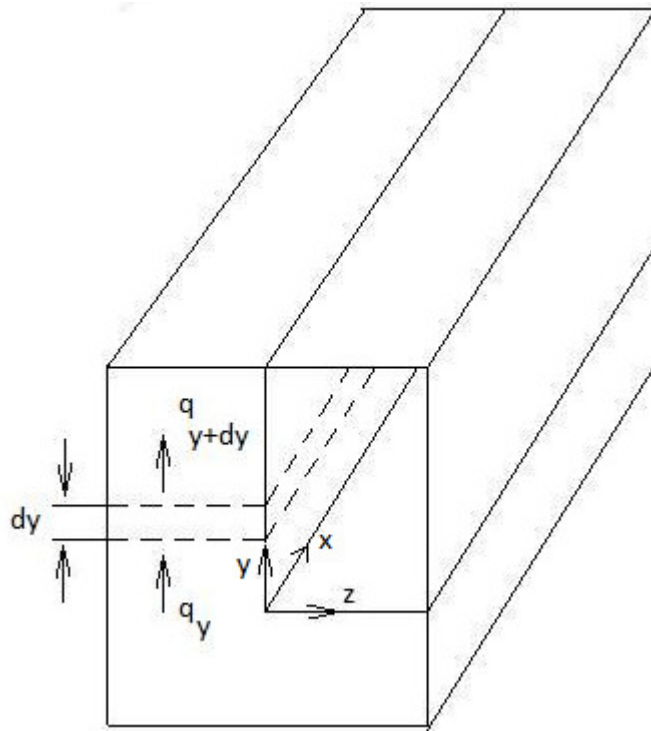
Figure 4.4 Energy balance in y direction for solid fin

$$q_y + h\, L\, dy\, \left(T(x,y) - T_f(x)\right) = q_y + \frac{dq_y}{dy}\, dy. \tag{4.20}$$

where

$$q_y = -k_{fin}\, A\, \frac{dT(x,y)}{dy} = -k_{fin}\, L\, \frac{w_w}{2}\, \frac{dT(x,y)}{dy}. \tag{4.21}$$

Substitution (4.21) in (4.20) yields

$$\frac{d^2 T(x,y)}{dy^2} = \frac{-2\, h}{k_{fin} w_w}\left(T(x,y) - T_f(x)\right) \tag{4.22}$$

with boundary conditions

63

$$-k_s \frac{dT}{dy} = \frac{2\eta\alpha_c}{2\eta\alpha_c + 1} \frac{(w_c + w_w)}{w_w} q" \; at \; y = 0, \tag{4.23}$$

$$\frac{dT(x,y)}{dy} = 0 \; at \; y = H_c. \tag{4.24}$$

The temperature distribution which includes the fluid temperature distribution may be found as

$$T(x,y) = T_f + \frac{1}{m\,k_{fin}} \frac{q"}{2\,\eta\,\alpha_c + 1} \frac{2\,\eta\,\alpha_c}{w_w} \frac{w_c + w_w}{sinh\,(m\,H_c)} \frac{cosh(m\,(H_c - y))}{sinh\,(m\,H_c)} \tag{4.25}$$

where

$$m = \left(\frac{2\,h}{k_{fin}\,w_w} \right)^{\frac{1}{2}}. \tag{4.26}$$

As can be seen from (4.26) the temperature distribution of the solid fin is dependent on the fluid, so it is necessary to find the fluid temperature distribution.
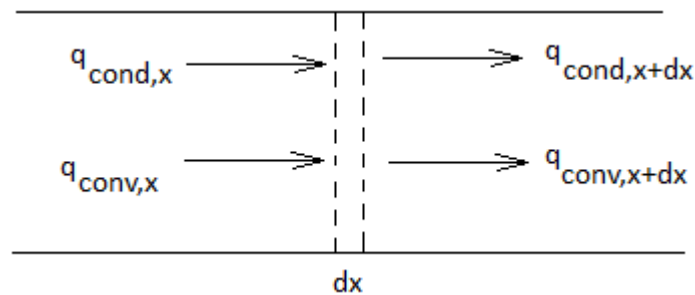
Figure 4.5 Enery balance for fluid domain in x-direction

The energy balance for the fluid in the x-direction is shown schematically in Figure 4.5

$$q_{conv,x} = u\,H_c\rho\,w_c\,C_p\,T(x) \tag{4.27}$$

$$q_{conv,x+dx} = u \, H_c \rho \, w_c \, C_p \, T(x) + \frac{d(u \, H_c \rho \, w_c \, C_p \, T(x))}{dx} \, dx \qquad (4.28)$$

Neglecting the axial conduction throughout the channel in the fluid domain, the energy balance can be written as,

$$u \, H_c \rho \, w_c \, C_p \, T(x) + q'' \, (w_c + w_w) \, dx$$
$$= u \, H_c \rho \, w_c \, C_p \, T(x) + \frac{d(u \, H_c \rho \, w_c \, C_p \, T(x))}{dx} \, dx \, . \qquad (4.29)$$

If average fluid temperature at the entrance of the channel is $T_f(x = 0) = T_0$

$$T_f(x) = T_0 + \frac{q'' \, (w_c + w_w) \, x}{\rho_f C_p \, u_m \, H_c w_c} \, . \qquad (4.30)$$

Substitution of this equation into T(x,y) in (4.25) yields

$$T(x, y) = T_0 + \frac{q'' \, (w_c + w_w) \, x}{\rho_f C_p \, u_m \, H_c w_c}$$
$$+ \frac{1}{m} \frac{q''}{k_{fin}} \frac{2 \, \eta \, \alpha_c}{2 \, \eta \, \alpha_c + 1} \frac{w_c + w_w}{w_w} \frac{\cosh(m \, (H_c - y))}{\sinh \, (m \, H_c)} \, . \qquad (4.31)$$

Then the total thermal resistance takes the form

$$R_{total,model2} = \frac{\Delta T}{q'' \, (L * W)} + R_{substrate} = \frac{T(L, 0) - T_0}{q'' \, (L * W)}$$
$$= R_{substrate} + \frac{(w_c + w_w)}{W \rho_f C_{p,f} \, u_m \, H_c w_c} \qquad (4.32)$$
$$+ \frac{1}{m \, (L \, W \, k_{fin})} \frac{2 \, \eta \, \alpha_c}{2 \, \eta \, \alpha_c + 1} \frac{w_c + w_w}{w_w} \frac{\cosh(m \, (H_c - y))}{\sinh \, (m \, H_c)}$$

c_p is the specific heat of the fluid.

4.5 Model 3, Fin-Fluid Coupled Approach

Liu and Garimella [8] implemented a one dimensional fluid temperature distribution in model two; on the other hand, model 3 includes two dimensional fluid temperature distribution throughout the channel and in y direction, parallel to the fin surface. As the fluid velocity is present only through the channel, other components of the velocity are counted zero in energy equation for the fluid domain. Excluding normal to the fin surface direction, conduction in all directions is neglected [11]. The reason why the z direction conduction is not neglected is that this surface is dominant in terms of the heat transfer rate in the channel.

The energy equation was obtained in the previous model. If it is written for two dimensional fluid temperature distribution, the following differential equation is obtained

$$\frac{d^2 T(x,y)}{dy^2} = \frac{-2\,h}{k_{fin}w_w}\Big(T(x,y) - T_f(x,y)\Big) \tag{4.33}$$

with the boundary conditions

$$-k_s \frac{dT}{dy} = \frac{2\eta\alpha_c}{2\eta\alpha_c + 1} \frac{(w_c + w_w)}{w_w} q" = j \;\; at\; y = 0 \tag{4.34}$$

where, to prevent complexity, boundary condition at y=0 is denoted by j,

$$\frac{dT(x,y)}{dy} = 0 \; at\; y = H_c. \tag{4.35}$$

The energy equation in the fluid domain is

$$\nabla \cdot \Big(\rho_f C_{p,f} \,\vec{V}\, T_f\,(x,y,z)\Big) = k_{fluid}\nabla^2 T_f(x,y,z) \tag{4.36}$$

If the conductions in the axial and y directions are neglected,

$$\rho_f C_{p,f} \, u \, \frac{\partial T_f\,(x,y,z)}{\partial x} = k_f \frac{\partial^2 T_f\,(x,y,z)}{\partial z^2}. \tag{4.37}$$

If this equation is integrated over the z direction from 0 to $\frac{w_c}{2}$

66

$$u_m \left(\frac{w_c}{2}\right)\frac{\partial}{\partial x}\int_0^{\frac{w_c}{2}} \frac{u}{\left(\frac{w_c}{2}\right)u_m}T_f(x,y,z)dz = \frac{k_{fluid}}{\rho_f C_{p,f}}\frac{\partial T_f(x,y,z)}{\partial z}\Big|_0^{\frac{w_c}{2}} \qquad (4.38)$$

where

$$u_m = \frac{1}{(w_c/2)}\int_0^{\frac{w_c}{2}} u\,dz \qquad (4.39)$$

$$\overline{T}_f(x,y) = \int_0^{\frac{w_c}{2}} \frac{u}{\left(\frac{w_c}{2}\right)u_m}T_f(x,y,z)dz \qquad (4.40)$$

and the boundary conditions at the fin-fluid interface are

$$-k_{fin}\frac{\partial T_s(x,y)}{\partial z}\Big|_{z=0} = h\big(T_s - \overline{T}_f(x,y)\big) = -k_f\frac{\partial \overline{T}_f(x,y)}{\partial z}\ at\ z = 0. \qquad (4.41)$$

If these boundary conditions are substituted into (4.38), the differential equation

$$u_m \left(\frac{w_c}{2}\right)\frac{\partial}{\partial x}\overline{T}_f(x,y) = \frac{1}{\rho_f C_{p,f}}\left(0 - \left(h\left(\overline{T}_f(x,y) - \overline{T}_s(x,y)\right)\right)\right) \qquad (4.42)$$

is obtained. When simplified, the equation becomes

$$u_m\rho_f C_{p,f}w_c\frac{\partial \overline{T}_f(x,y)}{\partial x} = 2h\left(\overline{T}_s(x,y) - \overline{T}_f(x,y)\right) \qquad (4.43)$$

where

$$h = \frac{Nu\,k_{fluid}}{D_h} \qquad (4.44)$$

$$\frac{1}{2}u_m\rho_f C_{p,f}w_c D_h\frac{\partial \overline{T}_f(x,y)}{\partial x} + k_{fluid}Nu\,\overline{T}_f(x,y) = k_{fluid}Nu\,\overline{T}_s(x,y) \qquad (4.45)$$

Non-dimensionalization yields,

$$\overline{T}_f(X,Y) = \overline{T}_f(x,y) - T_0 \qquad (4.46)$$

$$\overline{T}_s(X,Y) = \overline{T}_s(x,y) - T_0 \qquad (4.47)$$

$$X = \frac{x}{a} \ and \ Y = \frac{y}{a} \qquad (4.48)$$

$$a = \frac{u_m \rho_f C_{p,f} w_c D_h}{2 \, k_{fluid} Nu}. \qquad (4.49)$$

Hence,

$$\overline{T}_f(0,Y) = 0 \qquad (4.50)$$

$$k_{fluid} Nu \frac{\partial \overline{T}_f(X,Y)}{\partial X} + k_{fluid} Nu \, \overline{T}_f(X,Y) = k_{fluid} Nu \, \overline{T}_s(X,Y). \qquad (4.51)$$

Simplification yields

$$\frac{\partial \overline{T}_f(X,Y)}{\partial X} + \overline{T}_f(X,Y) = \overline{T}_s(X,Y) \qquad (4.52)$$

$\overline{T}_f(X,Y)$ may be written as

$$\overline{T}_f(X,Y) = \int_0^X T(\tau,Y) e^{-(X-\tau)} d\tau. \qquad (4.53)$$

If (4.33) is non-dimensionalized and the non-dimensionalized fluid temperature distribution is implemented, the following equation is obtained.

$$\frac{\partial^2 \overline{T}_s(X,Y)}{\partial Y^2} = \beta \left(\overline{T}_s(X,Y) - \int_0^X T(\tau,Y) e^{-(X-\tau)} d\tau \right) \qquad (4.54)$$

$$\beta = \frac{a^2}{\lambda^2} \tag{4.55}$$

$$\lambda^2 = \frac{k_s w_w D_h}{2\, k_{fluid} Nu} \tag{4.56}$$

Taking the Laplace transform of both sides of the (4.54) over X,

$$\frac{\partial^2 \overline{T}_s(s,Y)}{\partial Y^2} = \beta \left(\frac{s\, \overline{T}_s(s,Y)}{s+1} \right). \tag{4.57}$$

The boundary conditions are

$$-k_s \frac{\partial \overline{T}_s(s,Y)}{\partial Y}\Big|_{Y=0} = \frac{j\, a}{s} \tag{4.58}$$

$$-k_s \frac{\partial \overline{T}_s(s,Y)}{\partial Y}\Big|_{Y=\tilde{H}_c} = 0 \quad \tilde{H}_c = \frac{H_c}{a} \tag{4.59}$$

Applying the boundary conditions,

$$\overline{T}_s(s,Y) = \frac{j\, a}{k_s\, s\, \sqrt{\gamma}} \frac{\cosh\left(\sqrt{\gamma}\,(Y - \tilde{H}_c)\right)}{\sinh(\sqrt{\gamma}\, H_c)}, \qquad \gamma = \frac{\beta\, s}{s+1}, \tag{4.60}$$

$$\overline{T}_s(X,Y) = L^{-1}\left[\overline{T}_s(s,Y) \right], \tag{4.61}$$

$$\overline{T}_s(X,Y) = \frac{j\, a}{k_s \tilde{H}_c\, \beta} \left\{ (1+X) + \frac{\beta}{2}(Y - \tilde{H}_c)^2 - \frac{\beta\, \tilde{H}_c^2}{6} \right.$$
$$\left. + 2 \sum_{n=1}^{\infty} (-1)^n \frac{(s_n + 1)^2}{s_n} \cos\left(\frac{n\, \pi\, (Y - \tilde{H}_c)}{\tilde{H}_c} \right) e^{s_n X} \right\} \tag{4.62}$$

where

$$s_n = \frac{-(n\, \pi)^2 / \tilde{H}_c^2}{\beta + n^2 \pi^2 / \tilde{H}_c^2}. \tag{4.63}$$

69

According to Liu and Garimella [8], "the first three terms adequately represent the thermal resistance model."

$$R_{total,model\,3} = \frac{\Delta T}{q''\,(L\,W)} + R_{substrate} = R_{substrate} + \frac{\overline{T}_s(L,0) - T_0}{q''(L\,W)}$$

$$= R_{substrate} + \frac{j\,a}{k_s \tilde{H}_c\,\beta}\left(\left(1 + \frac{L}{a}\right) + \frac{1}{3}\beta\,\tilde{H}_c^2\right)\frac{1}{L\,W} \tag{4.64}$$

4.6 Model 4, Fin-Fluid Coupled Approach 2

The difference of the fourth model from the third is the addition of the axial conduction in the solid fin domain. This modification makes this model the most complex among the four models. Sabry [11] developed this model to investigate the transverse temperature gradient effect on the fin efficiency for microchannel design. Liu and Garimella [8] also derived this model with different boundary conditions than those of Sabry [11] at the base of the fin.

Energy equations for the solid and the fluid domains are

$$\nabla^2 T_s(x,y,z) = 0 \tag{4.65}$$

$$\nabla \cdot \left(\rho_f C_{p,f}\,\vec{V}\,T_f\,(x,y,z)\right) = k_{fluid}\nabla^2 T_f(x,y,z). \tag{4.66}$$

The boundary conditions at the fin-fluid interface are,

$$-k_s\frac{\partial T_s}{\partial z} = -k_{fluid}\frac{\partial T_f}{\partial z} = h\left(T_i - \overline{T}_f\right)\ at\ z = 0 \tag{4.67}$$

where T_i is the solid fin temperature at solid-fluid interface

$$\overline{T}_f(x,y) = \int_0^{\frac{w_c}{2}} \frac{u}{\left(\frac{w_c}{2}\right) u_m} T_f(x,y,z) dz \qquad (4.68)$$

$$u_m = \frac{1}{(w_c/2)} \int_0^{\frac{w_c}{2}} u dz. \qquad (4.69)$$

The boundary conditions are

$$\frac{\partial T_s}{\partial y}\Big|_{y=H_c} = \frac{\partial T_s}{\partial x}\Big|_{x=0} = \frac{\partial T_s}{\partial x}\Big|_{x=L} = \frac{\partial T_s}{\partial z}\Big|_{z=\frac{-w_w}{2}} = \frac{\partial T_f}{\partial z}\Big|_{y=\frac{w_c}{2}} = 0 \qquad (4.70)$$

Integrating the energy equation over z from $\frac{-w_w}{2}$ to 0 and multiplying with k_s

$$k_s \frac{w_w}{2}\left(\frac{\partial^2}{\partial x^2} + \frac{\partial^2}{\partial y^2}\right)\overline{T}_s + k_s \frac{\partial T_s}{\partial z}\Big|_{\frac{-w_w}{2}} = 0, \qquad (4.71)$$

$$\overline{T}_s = \int_{\frac{-w_w}{2}}^0 T_s dz. \qquad (4.72)$$

Using (4.67), (4.71) can be written as

$$k_s \frac{w_w}{2}\left(\frac{\partial^2}{\partial x^2} + \frac{\partial^2}{\partial y^2}\right)\overline{T}_s - h(T_i - \overline{T}_f) = 0. \qquad (4.73)$$

Since the fin material is highly conductive and $\frac{h(w_w/2)}{k_s} \ll 1$, it can be assumed that

$$T_i = \overline{T}_s \qquad (4.74)$$

Then (4.73) becomes

$$k_s \frac{w_w}{2}\left(\frac{\partial^2}{\partial x^2} + \frac{\partial^2}{\partial y^2}\right)\overline{T}_s - h(\overline{T}_s - \overline{T}_f) = 0. \qquad (4.75)$$

71

On the other hand, the fluid domain equation is integrated over z from 0 to $\frac{w_c}{2}$. The conduction in x and y directions, i.e the $k_{fluid} \frac{\partial^2 T_f}{\partial x^2} + k_{fluid} \frac{\partial^2 T_f}{\partial y^2}$ terms are neglected in the energy equation of the fluid domain. Thus, the energy equation takes the form

$$\frac{w_c}{2} u_m \frac{\partial}{\partial x} \int_0^{\frac{w_c}{2}} \frac{u}{u_m} T_f \, dz = \frac{k_{fluid}}{\rho_f C_{p,f}} \frac{\partial T_f}{\partial z} \Big|_0^{\frac{w_c}{2}} . \tag{4.76}$$

Benefiting from the boundary conditions (4.67), the energy equation can be written as

$$u_m \frac{w_c}{2} \frac{\partial}{\partial x} \overline{T}_f + \frac{1}{\rho_f C_{p,f}} h(\overline{T}_f - \overline{T}_s) = 0. \tag{4.77}$$

Hence, the two main energy equations (4.75) and (4.77) are derived.

These equations may be non-dimensionalized to obtain

$$X = \frac{x}{L} , \qquad Y = \frac{y}{H_c} \tag{4.78}$$

$$\overline{T}_s(X,Y) = \frac{\overline{T}_s(x,y) - T_0}{\Delta T}. \tag{4.79}$$

The definition of ΔT comes from the boundary condition (4.9) at the base of the fin.

Multiplying the heat flux by the area at the fin-fluid interface yields

$$\frac{2\eta \alpha_c}{2\eta \alpha_c + 1} \frac{(w_c + w_w)}{w_w} q''(\frac{w_w}{2} L) = h \, H_c L \, \Delta T \tag{4.80}$$

or

72

$$\Delta T = \frac{2\eta\alpha_c}{2\eta\alpha_c + 1} \frac{(w_c + w_w)}{2\,h\,H_c}\, q". \tag{4.81}$$

The following two non-dimensionalized equations are obtained as

$$\left(A^2 \frac{\partial^2}{\partial X^2} + \frac{\partial^2}{\partial Y^2}\right)\overline{T}_s - (mH_c)^2(\overline{T}_s - \overline{T}_f) = 0 \tag{4.82}$$

$$\frac{\partial \overline{T}_f}{\partial X} + S(\overline{T}_f - \overline{T}_s) = 0 \tag{4.83}$$

where

$$m = \left(\frac{2\,h}{k_{fin}\,w_w}\right)^{\frac{1}{2}}, \tag{4.84}$$

$$A = \frac{H_c}{L}, \tag{4.85}$$

$$S = \frac{h\,L}{\rho_f C_{p,f} u_m \frac{w_c}{2}}. \tag{4.86}$$

(4.83) may be written as

$$\left(\frac{\partial}{\partial X} + S\right)\overline{T}_f - S\,\overline{T}_s = 0, \tag{4.87}$$

$$\overline{T}_f = \frac{S\,\overline{T}_s}{(\frac{\partial}{\partial X} + S)}. \tag{4.88}$$

Substitution of $\overline{T}_f$ in (4.82) yields

73

$$\left(A^2 \frac{\partial^2}{\partial X^2} + \frac{\partial^2}{\partial Y^2} - (mH_c)^2\right)\left(\frac{\partial}{\partial X} + S\right)\overline{T}_s + S\,(mH_c)^2\,\overline{T}_s = 0. \tag{4.89}$$

Using the separation of variables method as

$$\overline{T}_s = \overline{T}_{s,1}(Y) + \overline{T}_{s,2}(X,Y), \tag{4.90}$$

the differential equation takes the form

$$\left(A^2 \frac{\partial^2}{\partial X^2} + \frac{\partial^2}{\partial Y^2} - (mH_c)^2\right)\left(\frac{\partial}{\partial x} + S\right)\left(\overline{T}_{s,1}(Y) + \overline{T}_{s,2}(X,Y)\right)$$
$$+ S(mH_c)^2\left(\overline{T}_{s,1}(Y) + \overline{T}_{s,2}(X,Y)\right) = 0. \tag{4.91}$$

(4.89) can be written as

$$\left(A^2 \frac{\partial^2}{\partial X^2} + \frac{\partial^2}{\partial Y^2} - (mH_c)^2\right)\left(\frac{\partial}{\partial x} + S\right)\overline{T}_{s,1} = 0 \tag{4.92}$$

$$\left(A^2 \frac{\partial^2}{\partial X^2} + \frac{\partial^2}{\partial Y^2} - (mH_c)^2\right)\left(\frac{\partial}{\partial X} + S\right)\overline{T}_{s,2} + S\,(mH_c)^2\,\overline{T}_{s,2} + S\,(mH_c)^2\,\overline{T}_{s,1}$$
$$= 0 \tag{4.93}$$

Boundary conditions may be written in the dimensionless form as

$$\frac{\partial \overline{T}_s(X,Y)}{\partial Y}\Big|_{Y=0} = -(mH_c)^2 \qquad \frac{\partial \overline{T}_s}{\partial X}\Big|_{X=0} = \frac{\partial \overline{T}_s}{\partial X}\Big|_{X=1} = \frac{\partial \overline{T}_s}{\partial Y}\Big|_{Y=1} = 0 \quad (4.94)$$

$$\frac{\partial \overline{T}_{s,1}(X,Y)}{\partial Y}\Big|_{Y=0} = -(mH_c)^2 \qquad \frac{\partial \overline{T}_{s,1}}{\partial X}\Big|_{X=0} = \frac{\partial \overline{T}_{s,1}}{\partial X}\Big|_{X=1} = \frac{\partial \overline{T}_{s,1}}{\partial Y}\Big|_{Y=1}$$
$$= 0 \tag{4.95}$$

$$\frac{\partial \overline{T}_{s,2}(X,Y)}{\partial Y}\Big|_{Y=0} = 0 \qquad \frac{\partial \overline{T}_{s,2}}{\partial X}\Big|_{X=0} = \frac{\partial \overline{T}_{s,2}}{\partial X}\Big|_{X=1} = \frac{\partial \overline{T}_{s,2}}{\partial Y}\Big|_{Y=1}$$
$$= 0 \tag{4.96}$$

As $\overline{T}_{s,1}$ is only a function of Y, (4.92) may be written as

$$\frac{\partial^2 \overline{T}_{s,1}}{\partial Y^2} - (mH_c)^2 \overline{T}_{s,1} = 0. \tag{4.97}$$

Solving for $\overline{T}_{s,1}$ yields

$$\overline{T}_{s,1}(Y) = \frac{m\,H_c}{Sinh(m\,H_c)} Cosh\big((1-Y)(mH_c)\big). \tag{4.98}$$

$\overline{T}_{s,2}$ may be found using

$$\left(A^2 \frac{\partial^2}{\partial X^2} + \frac{\partial^2}{\partial Y^2} - (mH_c)^2\right)\left(\frac{\partial}{\partial X} + S\right)\overline{T}_{s,2} + S\,(mH_c)^2\,\overline{T}_{s,2}$$
$$= -S\,(mH_c)^2\,\overline{T}_{s,1}. \tag{4.99}$$

Three boundary conditions in X and two boundary conditions in Y direction are needed:

$$\left(A^2 \frac{\partial^2}{\partial X^2} + \frac{\partial^2}{\partial Y^2} - (mH_c)^2\right)\overline{T}_{s,2}|_{X=0} = 0, \tag{4.100}$$

$$\frac{\partial \overline{T}_{s,2}}{\partial X}|_{X=0,1} = \frac{\partial \overline{T}_{s,2}}{\partial Y}|_{Y=0,1} = 0. \tag{4.101}$$

As may be observed from the boundary conditions in Y direction, $\overline{T}_{s,2}$ is symmetric at Y=0 and Y=1, so half range cosine Fourier series expansion can be applied in the $0 \leq Y \leq 1$ interval as

$$\overline{T}_{s,2}(X,Y) = \sum_{n=0}^{\infty} Cos(n\pi Y)f_n(X). \tag{4.102}$$

Then, (4.99) becomes

$$f_n'''(X) + Sf_n''(X) - \left(\frac{(n\pi)^2 + (mH_c)^2}{A^2}\right)f_n'(X) - \frac{(n\pi)^2 S}{A^2}f_n(X)$$

$$= \frac{-2S}{A^2}\int_0^1 (mH_c)^2 T_1(Y)Cos(n\pi Y)dy , \tag{4.103}$$

$$v_n = \left(\frac{(n\pi)^2 + (mH_c)^2}{A^2}\right), \tag{4.104}$$

$$z_n = \frac{(n\pi)^2 S}{A^2}. \tag{4.105}$$

(4.103) may be written as

$$f_n'''(X) + S\,f_n''(X) - v_n\,f_n'(X) - z_n f_n(X) = -\frac{S\,b_n}{A^2}, \tag{4.106}$$

$$b_n = 2\,(m\,H_c)^2 \quad for \ n = 0 , \tag{4.107}$$

$$b_n = \frac{2\,(m\,H_c)^4}{(m\,H_c)^2 + n^2\pi^2} \quad for \ n > 0 . \tag{4.108}$$

The boundary conditions in terms of $f_n(X)$ are

$$[f_n''(X) - v_n f_n(X)]|_{X=0} = 0 , \tag{4.109}$$

76

$$f_n'(X)\big|_{X=0,1} = 0 \,. \tag{4.110}$$

Superposition yields,

$$\overline{T}_s = \overline{T}_{s,1}(Y) + \overline{T}_{s,2}(X,Y), \tag{4.111}$$

$$\overline{T}_s(X,Y) = \frac{m\,H_c}{Sinh(m\,H_c)}\,Cosh\big((1-Y)(mH_c)\big) + \sum_{n=0}^{\infty} Cos(n\pi Y)f_n(X). \tag{4.112}$$

Liu and Garimella [8] state that "the first term of the infinite series adequately represents the complete series and the deviation from the complete series is under five percent."

$$f_0(X) = SX + \sum_{i=1}^{2}\left(\frac{C_{0i}}{W_{0i}}\right)e^{W_{0i}X} + C_{0,3} \,, \tag{4.113}$$

$$W_{01} = -\frac{S}{2} + \sqrt{\left(\frac{S}{2}\right)^2 + \left(\frac{m\,H_c}{A}\right)^2} \,, \tag{4.114}$$

$$W_{02} = -\frac{S}{2} - \sqrt{\left(\frac{S}{2}\right)^2 + \left(\frac{m\,H_c}{A}\right)^2} \,, \tag{4.115}$$

$$C_{01} = -S\frac{(e^{W_{02}} - 1)}{(e^{W_{02}} - e^{W_{01}})}, \tag{4.116}$$

$$C_{02} = -S\frac{(e^{W_{01}} - 1)}{(e^{W_{02}} - e^{W_{01}})}, \tag{4.117}$$

77

$$C_{03} = \left(\frac{SA}{mH_c}\right)^2, \tag{4.118}$$

$$R_{total,model4} = R_{substrate} + \frac{\Delta\overline{T}}{q''(LW)} = R_{substrate} + \frac{T(1,0) - T_0}{q''(LW)}\Delta T$$

$$= R_{substrate}$$

$$+ \frac{2\eta\alpha_c}{2\eta\alpha_c + 1} \frac{(w_c + w_w)}{2\,h\,H_c}\left[mH_c \frac{Cosh(mH_c)}{Sinh(mH_c)} + S\right. \tag{4.119}$$

$$\left. + \sum_{i=1}^{2}\left(\frac{C_{0i}}{W_{0i}}\right)e^{W_{0i}} + C_{0,3}\right]\frac{1}{(LW)}.$$

As $(mH_c/A) \gg S/2$ the equation above reduces to

$$R_{total,model4} = R_{substrate}$$

$$+ \frac{2\eta\alpha_c}{2\eta\alpha_c + 1} \frac{(w_c + w_w)}{2\,h\,H_c}\left[mH_c \frac{Cosh(mH_c)}{Sinh(mH_c)} + S\right.$$

$$\left. + \left(\frac{SA}{mH_c}\right)^2\right]\frac{1}{LW}. \tag{4.120}$$

4.7 Verification of the Analytical Models

In order to understand whether the models derived here analytically give accurate results, these models are compared with other numerical, experimental and analytical studies in the literature. Again the geometries used by Tuckerman and Pease [1] are considered. They tested three different heat sink geometries for different flow and thermal conditions. Their experimental results set the basis for comparison. In addition to the four analytical models, a CFD model is also implemented to evaluate the thermal resistances. Table 4.1 summarizes the results of comparison. For the channel geometry and flow conditions given in Table 3.5,

Tuckerman and Pease's study is repeated analytically in order to check the validity of the models derived in Chapter 4.

Table 4.1 Comparison of analytical and numerical studies in the present study with literature

Thermal Resistance (°C/W)	Case 1		Case 2		Case 3	
	X	Y	X	Y	X	Y
$R_{Total, Model\ 1}$	0.112	0.1119	0.112	0.1119	0.091	0.0906
$R_{Total, Model\ 2}$	0.112	0.1117	0.112	0.1117	0.091	0.0903
$R_{Total, Model\ 3}$	0.106	0.1078	0.106	0.1071	0.087	0.0879
$R_{Total, Model\ 4}$	0.106	0.1069	0.106	0.1064	0.087	0.0872
$R_{Exp, Tuc\ and\ Pease, [1]}$	0.110		0.113		0.090	
$R_{Num, Liu\ and\ Gar[8]}$	0.115		0.114		0.093	
$R_{Num, Present\ study}$	0.115		0.114		0.093	

X= Thermal Resistances of Analytical Models by Liu and Garimella [8]

Y= Thermal Resistances of Analytical Models by Present Study

The difference between the analytical models is under 2%; therefore, the computer code is validated. The analytical models are also compared with numerical results. The highest error between the analytical results in the present study and the numerical study of Liu and Garimella [8] is under 8% among the three cases listed in Table 4.1. It can be said with confidence that the analytical models developed here can be implemented in the optimization study.

CHAPTER 5

OPTIMIZATION-CALCULATIONS

After obtaining the thermal resistance models, optimization procedure can be followed. There are four main thermal resistance models as explained in Chapter 4. These models build up the theoretical basis of the optimization. Each optimization model consists of an objective function. In this study the objective functions; namely, the thermal resistances are written in terms of w_c and w_w, the channel width and the fin thickness, respectively. These two parameters are called the design variables in optimization studies. The aim of this optimization study is to find the optimum values of these design variables in a given interval. This interval is specified by some limitations; for example, Ryu et al. [9] states that microchannels with channel height that is higher than ten times the channel width are difficult to produce. Hence the interval of the design variables is limited by some optimization constraints. Another example of optimization constraints is the pumping power. It is determined by the pump used in the design and pipe connections in the experimental set-up. Hence, it is not possible to exceed the specified limit of pumping power. The multiplication of the pressure drop through the channel and the volumetric flow rate gives the pumping power for a specified geometry of the channel. The pressure drop is considered constant for a given pumping power in this optimization study.

5.1 General Terms in Optimization

5.1.1 Objective Function

The objective function is the function to be minimized or maximized at the optimum design variable values. The thermal resistance is to be minimized in this study.

Four analytical models have been developed to obtain the thermal resistance values of microchannel heat sinks.

Some assumptions are made when developing these models; therefore, each model has its own characteristics. Models derived in the previous chapter yielded thermal resistance values represented by equations (4.19, 32, 64, 120).

5.1.2 Design variables

Each objective function has two variables, w_c and w_w. In this optimization study, optimum values of w_c and w_w where the objective function, thermal resistance, is minimum are sought.

5.1.3 Optimization Constraint

Due to fabrication issues, it is necessary to establish some limitations on the interval of design variables. Ryu et al. [9] claims that microchannels with too high or low aspect ratios are difficult to produce. The aspect ratio of the channel should not be lower than 0.1 if the aspect ratio is defined as $\alpha_c = \frac{w_c}{H_c}$. Moreover, the fin thickness needs to be higher than at least 10 μm. Pumping power is related to pump and pipe connections in the experimental set-up that is why it is not possible to exceed specified limit of pumping power. Pumping power and pressure drop are kept constant in this optimization study for the sake of comparison for each model.

5.2 Optimization Model

In the literature, most of the studies use surrogate based optimization method. Surrogate based models depend on taking limited data and using these data

developing a function that represents the objective function. This function is formed by various surrogate models most of which are based on regression analysis. Generally, the thermal analysis of microchannels is performed numerically, which is convenient for limited data. On the other hand, in the current study, as the objective functions may be evaluated analytically even for numerous data, it is not necessary to build up an objective function for specified data points.

In the present study, the objective function has two design variables.

If the validity interval of the design variables are defined as

$$w_{w,lb} \leq w_w \leq w_{w,ub}$$

$$w_{c,lb} \leq w_c \leq w_{c,ub}$$

with, lb= lower bound, ub= upper bound.

By incrementing these two intervals such that

$$n = \frac{w_{w,ub} - w_{w,lb}}{incw_w} \tag{5.1}$$

$$m = \frac{w_{c,ub} - w_{c,lb}}{incw_c} \tag{5.2}$$

where

$incw_w$ = step size in the w_w interval, 1 μm

$incw_c$ = step size in the w_c interval, 1 μm

an $(n \times m)$ matrix is formed as follows.

$$
\begin{bmatrix}
R(w_{c,lb}, w_{w,lb}) & R(w_{c,lb} + incw_c, w_{w,lb}) & \cdot & \cdot & \cdot & \cdot & R(w_{c,ub}, w_{w,lb}) \\
R(w_{w,lb} + incw_w) & & & & & & \cdot \\
\vdots & & & & & & \vdots \\
\vdots & & & & & & \vdots \\
\vdots & & & & & & \vdots \\
\vdots & & & & & & \cdot \\
R(w_{c,lb}, w_{w,ub}) & & \cdot & \cdot & \cdot & \cdot & \cdot & R(w_{c,ub}, w_{w,ub})
\end{bmatrix}
$$

The thermal resistances are evaluated for each combination of w_c and w_w. The computer code generates the resistance matrix shown above and picks the smallest value. This way, the optimum w_c and w_w combination is found minimizing the thermal resistance. As the number of calculation points increase, so does the sensitivity of the optimization. One drawback; on the other hand, is the increased computational effort.

5.3 Optimization Flowchart

The optimization code has been developed using Matlab. The flowchart of the code is given in the Figure 5.1. Firstly, the step size of the data points is determined. This stage strongly affects the computational time because the number of calculations is decided in this step. After then, the temperature dependent thermophysical properties are introduced. The following step is defining the microchannel's total dimensions and the main parameters related to the fluid characteristics of the system. It is necessary to estimate the fluid temperature at the outlet of the channel before the theoretical calculations because the thermopyhsical properties are determined based on the inlet and outlet temperatures of the fluid. Next, the optimization constraints that limit the interval of design variables are entered. Before conducting theoretical calculations, it is essential to define some parameters such as the hydraulic diameter, the fin efficiency and introduce Poiseulle and Nusselt number correlations for both fully developed and developing flow conditions. Finally, the respective optimization model is applied and the resistance

83

matrix is formed. Then the minimum thermal resistance is obtained. If the outlet temperature of the fluid is far away from the estimated one, calculations are repeated until the convergence criterion is obtained. The convergence is reached when the difference in the dynamic viscosity between two successive iterations is under 10^{-9}. Finally, the optimum channel dimensions and minimum thermal resistance are achieved. Detailed information about the optimization calculations is given in APPENDIX C.
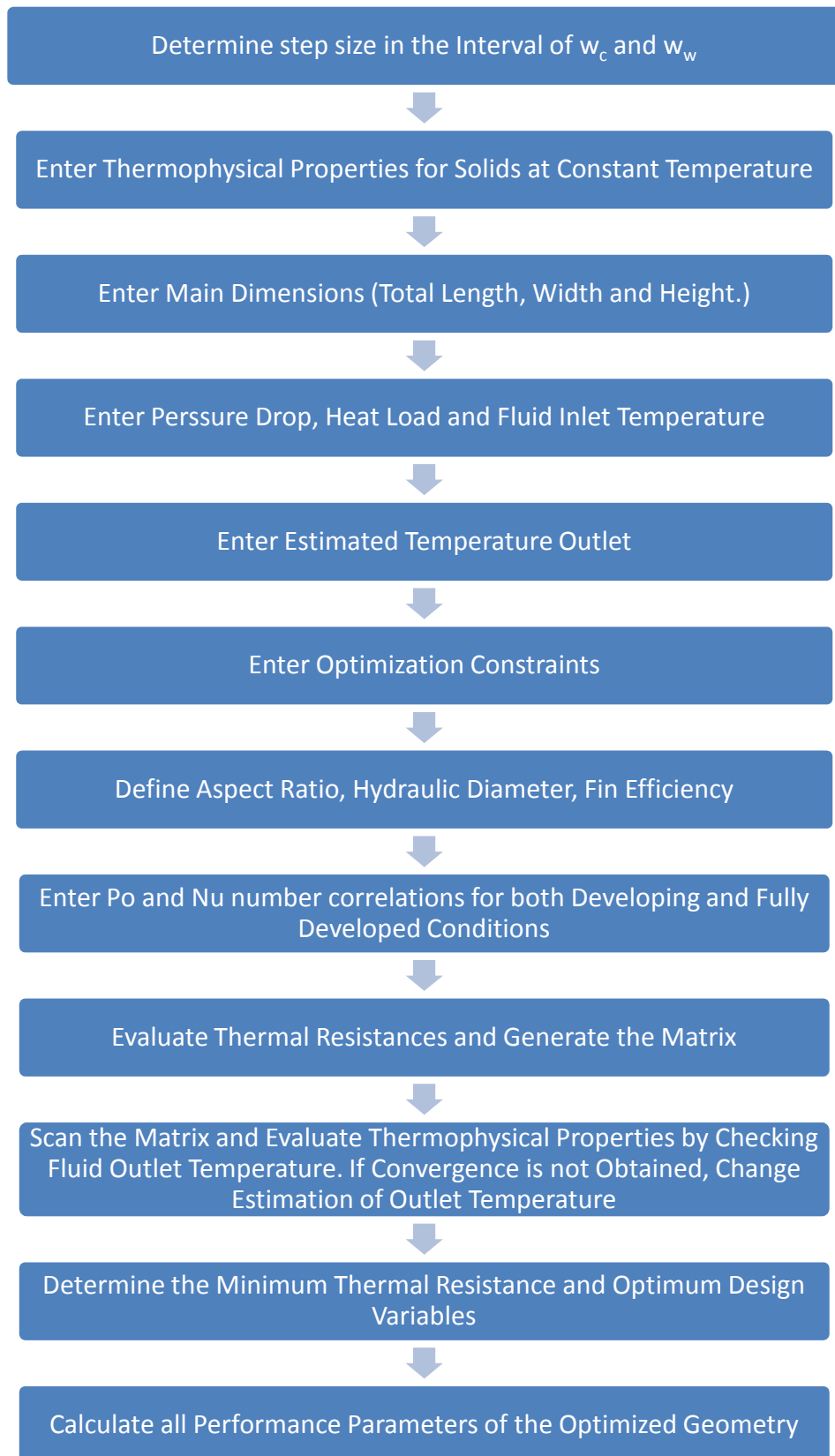
Figure 5.1 Optimization flow chart

5.4 Optimization Model and Computer Code Validation

In order to validate the computer code developed in this study, the results are compared with available optimization models in the literature. Liu and Garimella [8] performed an optimization study by taking the first derivatives of the objective function with respect to the two design variables, namely, the channel width and the fin thickness, and equating them to zero. They used the commercial computer software Matlab and obtained satisfactory results. Deviation between the four models was under 10 percent. In this study, the code development procedure is different. The objective function is evaluated at numerous w_c and w_w combinations and a matrix is generated. Then, the minimum thermal resistance is detected as mentioned in the previous sections.

5.4.1 Validation of the Optimization Computer Code against the Literature

In this step, the study of Liu and Garimella [8] is repeated. They used constant thermophysical properties at 300 K, silicon as the fin and substrate material, and constant Nu number for fully developed flow. Some parameters used in their study are listed in Table 5.1.

Table 5.1 Main parameters of the optimized geometry, [8]

Pressure Drop	60 kPa
Heat Load	$100 \ \dfrac{\text{W}}{\text{cm}^2}$
Total Channel Width (W)	1 cm
Total Channel Length (L)	1cm
Channel Height (H_c)	400 µm
Substrate Thickness (t)	100 µm

Comparison of the optimization results are depicted in Table 5.2. As can be observed from the table, the agreement is very good despite the different calculation methodologies. The slight differences between the results are thought to be within the microchannel fabrication tolerances.

Table 5.2 Comparison of the optimization results with literature

Model	w_c (μm)		w_w (μm)		$\alpha_c = \dfrac{w_c}{H_c}$		$R_{tot}\left(\dfrac{{}^\circ C}{W}\right)$	
	X	Y	X	Y	X	Y	X	Y
1	64	65.88	18	18.94	0.16	0.165	0.0965	0.095
2	65	65.88	19	18.94	0.162	0.165	0.0965	0.095
3	65	66.46	24	24.89	0.162	0.166	0.0973	0.096
4	61	62.74	16	16.74	0.152	0.157	0.0907	0.090

X= Liu and Garimella [8] (constant properties at 300 K)

Y= Present Study (constant properties at 300 K)

5.4.2 Modified Code with Thermophysical Properties Evaluated at the Fluid Mean Temperature

The aim of this study is to observe the effect of temperature on fluid properties and confirm the validity of this addition to the computer code. Instead of evaluating the thermophysical properties of the fluid at the inlet temperature (300 K), an area weighted average of the inlet and the exit temperatures is considered. Except this difference, all the flow conditions and the main dimensions are the same as those for the previous validation study given in Table 5.1. The comparison of the results is given in Table 5.3. Although there is not much change in the optimized geometry, a small reduction is observed in the thermal resistance values.

5.4.3 Addition of the Entrance Effects

In order to further improve the fluid temperature dependent computer code, the hydrodynamically and thermally developing correlations are also mounted in this stage. Hence the present study has two new contributions. The results are presented in Table 5.3. The main parameters are the same with those in Table 5.1.

Table 5.3 Comparison of the present optimization code results with literature

		Models			
		1	2	3	4
w_c (μm)	X	65.88	65.88	66.46	62.74
	Y	65.88	65.3	65.9	62.7
	Z	71	71	72	67
w_w (μm)	X	18.94	18.94	24.89	16.7
	Y	18.94	18.9	24.9	16.7
	Z	20.3	20.3	27	18
$\alpha_c = \dfrac{w_c}{H_c}$	X	0.165	0.165	0.166	0.157
	Y	0.165	0.165	0.166	0.157
	Z	0.1775	0.1775	0.18	0.1675
$R_{tot} \left(\dfrac{°C}{W}\right)$	X	0.095	0.095	0.096	0.090
	Y	0.0937	0.0937	0.0943	0.0886
	Z	0.0913	0.0913	0.0917	0.0858

X = Present Study (constant properties at 300 K)

Y = Present Study (constant properties at the area weighted average of the inlet and outlet temperatures)

Z = Present Study (constant properties at the area weighted average of the inlet and outlet temperatures, developing flow)

As can be seen from the table, making the computer code sensitive to the developing flow conditions and temperature dependent fluid properties does have an effect on the results. It is believed that these modifications made the computer code more accurate and applicable to a wider range of geometry and flow conditions. The results indicate that before applying fully developed flow

conditions, evaluation of whether the flow is fully developed or not is so crucial in microchannel optimization studies.

5.5 Geometry and Flow Conditions for the Present Study

In the literature, a considerable amount of studies evaluated microchannel heat sinks under $100\frac{W}{cm^2}$ constant heat flux condition for a 1cm×1cm chip size that is why the validation of the present optimization study is conducted using this geometry. However, considering the recent features of electronic devices, a processor designed with the most current technology is also investigated. Intel Core i7-900 Desktop Processor Extreme Edition Series is taken as the reference processor the thermal characteristics of which are examined. According to the data sheet of this processor [25], the thermal design power is determined as 130 W.

5.5.1 Geometrical Consideration

Die dimensions of this processor is 18.91× 14.4 mm so the heat flux is calculated to be 47.74 W/cm². The long side of the die is taken as length of the microchannel. Main dimensions of the optimization study is given in Table 5.4

Table 5.4 Heat load and main dimensions of Intel Core i7-900

Heat Load	130 W
Heat Flux	$47.74\ W/cm^2$
Total Channel Length	1.891 cm
Total Channel Width	1.44 cm

In order to inspect the effects of fin and substrate material on the thermal characteristics of the system, two main substrate and fin structures are considered in the optimization study. The first case investigated silicon fins and substrates. In the other case, metal-polymer heat sinks are considered for which the fins are

made of copper and the substrate is composed of parylene, titanium and gold layers of different thicknesses.

5.5.1.1 Silicon Fin Structure

In numerical studies on microchannels in the literature, the channel material is silicon for both the fins and the substrate. Durability to high temperature changes, easiness of production and good electric insulation property makes silicon a reasonable alternative as a microchannel material. Considering the studies in the literature and manufacturing limitations, three different channel heights are inspected. Analyzed channel heights and substrate thicknesses are given in Table 5.5.

Table 5.5 Substrate and fin dimensions of the optimization geometry for silicon fin structure

Layer	Thickness
Silicon Substrate	100 µm
Silicon Fins	300, 400, 500 µm

5.5.1.2 Copper Fin Structure

Similar to the structure presented in Chapter 3, the fin material is copper and the substrate is composed of three different layers. The investigated geometry is described in Table 5.6. Starting from bottom, a 200 nm thin parylene layer, which performs duty of providing electrical insulation between the electronic device and the microchannels, forms the bottom layer, then at the middle a 50 nm titanium layer exists to stick parylene and 500 nm gold layers. The gold layer serves as the seed layer for the copper walls. The heat flux is provided to the system via the gold layer due to its high electrical conductivity.

Table 5.6 Substrate and fin dimensions of optimization geometry for copper fin structure

Layer	Thickness
Parylene insulation	200 nm
Titanium	50 nm
Gold	500 nm
Copper walls	20,70, 300 μm

One of the most important advantages of this structure is that the microchannels can be produced as an integrated part of the electronic chip [15]. Considering the manufacturing constraints, the channel heights are selected as 20 and 70 μm. Despite the fact that it is not possible to produce a channel of 300 μm height using the reported fabrication technique, this height is also considered because of two main reasons. One is the possibility of production of this channel in the future. Another reason is to have a chance to compare this geometry with silicon fin structures.

5.5.2 Hydrodynamic Considerations

According to Kim and Hussain [12], the pumping power in microchannels ranges from 0.01 W to 0.8 W under considering of micropump characteristics. During parallel experiments [15], a 5 milliliter per minute flow rate has been reached for a 10-channel heat sink of 200 μm channel width, and 20 μm height. Calculations indicated that the corresponding pumping power at 300 K the fluid temperature would be 0.088 W. After making some modifications in the experimental set-up, 10 milliliters per minute water is pumped through the same channel geometry. The pumping power corresponding to this flow rate is determined as 0.35 W. The design parameters for the examined cases are given in Table 5.7.

Table 5.7 Design parameters for examined cases

Heat Load	47.74 W/m^2	
Geometry	Silicon Fin Structure	Copper Fin Structure
Pumping Power	0.088 W,0.35 W	
Channel Height	300,400,500 µm	20,70,300 µm

5.6 Optimization Results

The purpose of the optimization study was to minimize the thermal resistance within a specific interval of design variables. Various parameters are examined in order to understand their effects on the thermal resistance. These parameters are mainly, the channel height, the fin material and the pumping power. In addition to these parameters, the thermal resistance values indicated a variation among the four analytical models for the same conditions. Each analytical model for which detailed information was given in the previous chapter, has its own characteristics.

 Table 5.8 and Table 5.9 list the optimization results.

Table 5.8 Optimization results for 0.35 W pumping power for various channel heights

		Channel Height (µm)	Model 1	Model 2	Model 3	Model 4
Silicon Fin Structure	Optimum W_C (µm)	300	116	116	111	109
	Optimum W_W (µm)		18	18	19	16
	$R_{min}(°C/W)$, T_{max} (°C)		0.076, 36.9	0.076, 36.9	0.0695, 36	0.0681, 35.8
	Optimum W_C (µm)	400	109	109	106	91
	Optimum W_W (µm)		22	22	25	16
	$R_{min}(°C/W)$, T_{max} (°C)		0.0658, 35.5	0.0658, 35.5	0.0617, 35	0.0572, 34.4
	Optimum W_C (µm)	500	103	103	103	100
	Optimum W_W (µm)		24	24	24	22
	$R_{min}(°C/W)$, T_{max} (°C)		0.0579, 34.5	0.0579, 34.5	0.056, 34.2	0.053, 33.9
Copper Fin Structure	Optimum W_C (µm)	70*	70	70	70	70
	Optimum W_W (µm)		2	2	1	1
	$R_{min}(°C/W)$, T_{max} (°C)		0.1677, 48.8	0.1677, 48.8	0.1253, 46.8	0.1338, 44.4
	Optimum W_C (µm)	300	116	116	113	111
	Optimum W_W (µm)		11	11	12	10
	$R_{min}(°C/W)$, T_{max} (°C)		0.0755, 36.8	0.0755, 36.8	0.0694, 36	0.0779, 37.1

*No lower limit for w_w

Table 5.9 Optimization results for 0.088 W pumping power for various channel heights

		Channel Height (µm)	Model 1	Model 2	Model 3	Model 4
Silicon Fin Structure	Optimum W_C (µm)	300	149	149	142	139
	Optimum W_W (µm)		18	18	18	15
	$R_{min}(°C/W)$, T_{max} (°C)		0.1111, 41.4	0.1111, 41.4	0.0985, 39.8	0.097, 39.61
	Optimum W_C (µm)	400	152	152	146	143
	Optimum W_W (µm)		24	24	25	21
	$R_{min}(°C/W)$, T_{max} (°C)		0.0987, 39.8	0.0987, 39.8	0.0904, 38.7	0.0885, 38.5
	Optimum W_C (µm)	500	142	142	138	134
	Optimum W_W (µm)		27	27	31	24
	$R_{min}(°C/W)$, T_{max} (°C)		0.0876, 38.3	0.0876, 38.3	0.0818, 37.6	0.0792, 37.3
Copper Fin Structure	Optimum W_C (µm)	70*	70	70	70	70
	Optimum W_W (µm)		1.2	1.2	0.2	0.1
	$R_{min}(°C/W)$, T_{max} (°C)		0.273, 62.5	0.2722, 62.4	0.1819, 50.6	0.1759, 49.9
	Optimum W_C (µm)	70	308	308	256	256
	Optimum W_W (µm)		10	10	10	10
	$R_{min}(°C/W)$, T_{max} (°C)		0.3404, 71.2	0.3404, 71.2	0.212, 54.6	0.221, 55.7
	Optimum W_C (µm)	300	149	149	143	142
	Optimum W_W (µm)		11.3	11.3	11	10
	$R_{min}(°C/W)$, T_{max} (°C)		0.1092, 41.2	0.1092, 41.2	0.0974, 39.7	0.1058, 40.7

*No lower limit for w_w

Detailed information on the optimization results can be found in APPENDIX D.

As can be seen from the tables above, the thermal resistance decreases when the channel height increases at constant pumping power. The maximum rise in the fluid temperature is determined as 44°C, which corresponds to a maximum substrate temperature of 71°C for model 1 with 70 µm channel height and 0.088 W pumping power. The maximum operating temperature of the electronic device is assumed to be 85°C. Channels of 70 µm height and 0.088 W pumping power have the greatest thermal resistance among the examined cases. Lower pumping power means lower volumetric flow rate and this situation brings about a considerable increase in the maximum temperature on the substrate. Neither thermally nor hydrodynamically, fully developed flow conditions could be reached except in channels with 20 and 70 µm height. Although the fully developed flow conditions are assumed when deriving the analytical models, it is observed that the flow conditions are in the developing region. That is why the developing region correlations are used in the calculations for the Nusselt and Poiseuille numbers. As the thermal resistance models are derived analytically, it is inevitable to make some assumptions that simplify the energy and momentum equations. As this study does not pursue the goal of estimating the exact temperature distribution or the accurate thermal resistance values, but aims to obtain the optimized dimensions rather, these simplifications may be regarded as satisfactory.

In order to interpret the results clearly, the variation of the thermal resistance with the channel height, is plotted in Figure 5.2.
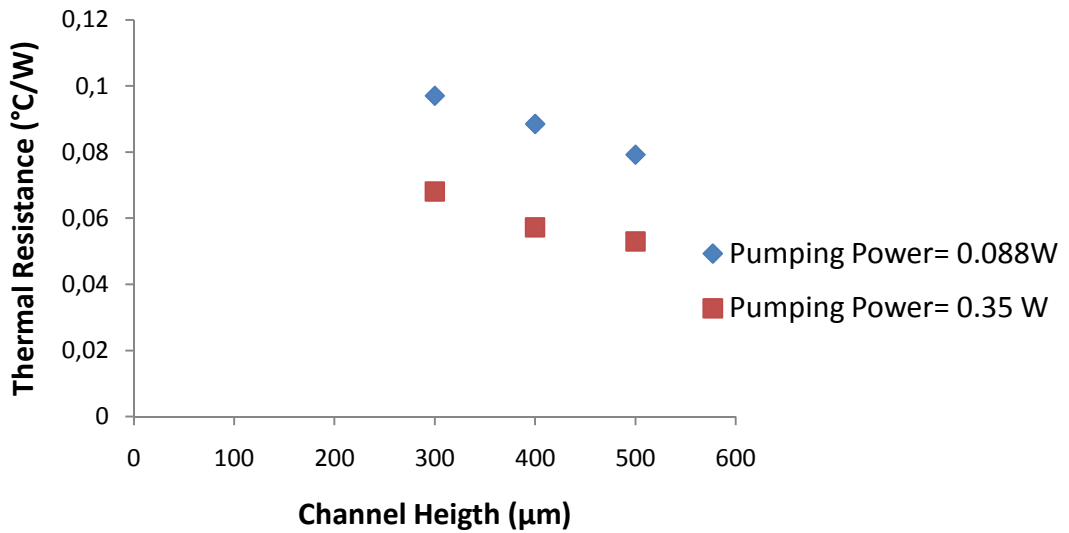
Figure 5.2 Thermal resistance versus channel height at constant pumping power for silicon fin structure

Pressure drop values that correspond to 0.35 W pumping power is the lowest for the deepest channel due to the higher hydraulic diameter. Greater pumping power means greater volumetric flow rate thereby enabling the system to remove more heat from the electronic device.

Figures 5.3 and 5.4 illustrate the variation of the thermal resistances with the model used, for a pumping power of 0.35 and 0.088 W, respectively.
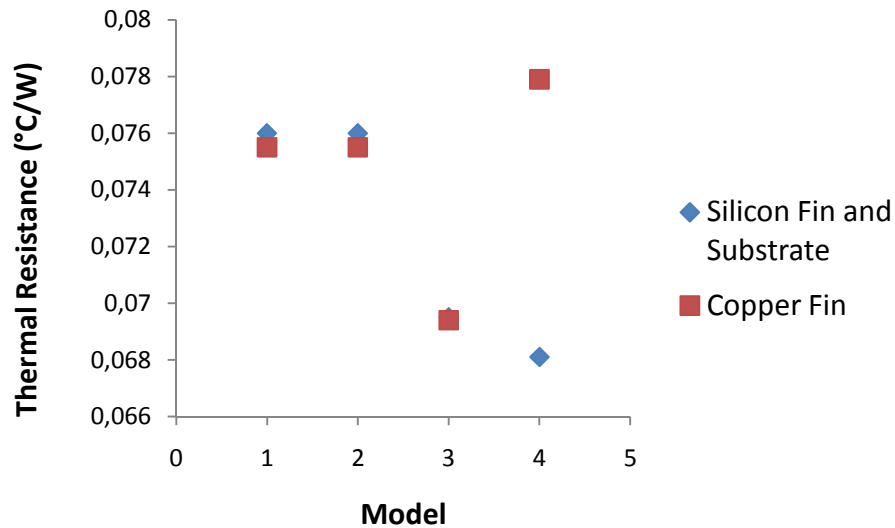
Figure 5.3 Comparison of analytical models for a channel with 300 μm height and 0.35 W pumping power

As can be observed from Figure 5.3, excluding the model 4, thermal resistance values for silicon and copper fin structures are close to each other. The feature that distinct the fourth model from the others is that the axial conduction in the solid fin region is put into account. About three times greater thermal conductivity of copper than silicon leads a little bit different results for the thermal resistance values. Adding the axial conduction term into the energy equation reduced the maximum temperature of the silicon substrate. This is because of the temperature variation throughout the channel length. On the other hand, the temperature difference between two ends of the substrate might be nearly the same for copper fin structure because of the low Biot number of the copper fins.
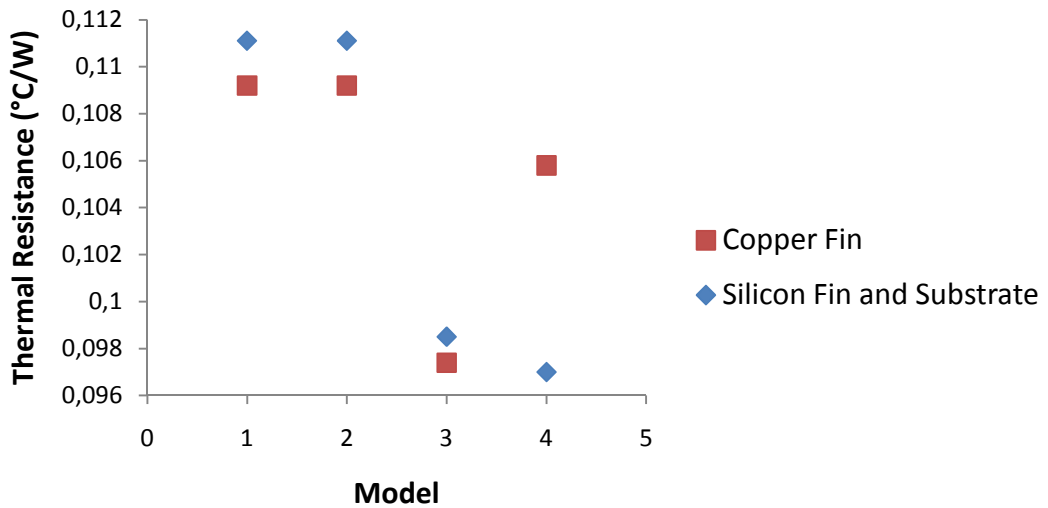
Figure 5.4 Comparison of analytical models for a channel with 300 µm height and
0.088 W pumping power

Similar results are observed for lower pumping powers but in this case the thermal
resistances are higher than those for the 0.35 W pumping power, and the
differences between the thermal resistance values of copper and silicon structures
are slightly more pronounced.
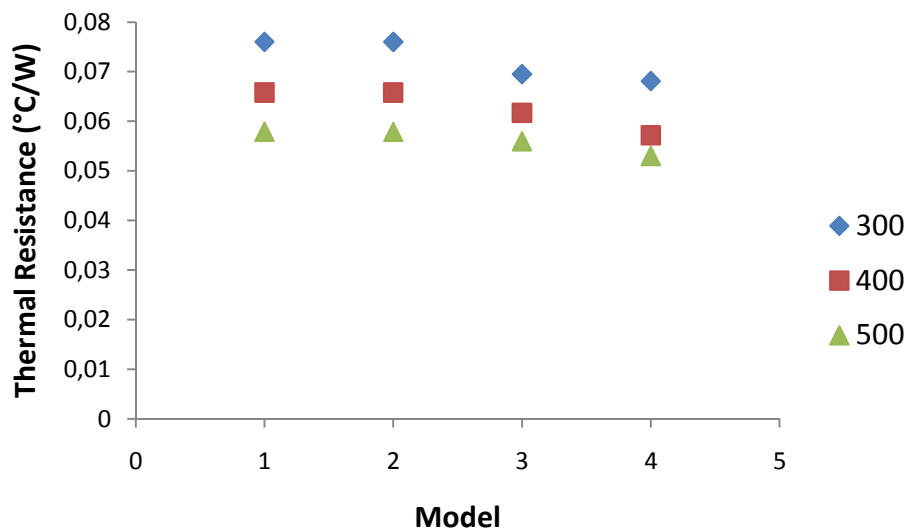
Figure 5.5 Thermal resistances for different channel heights for each model at 0.35
W pumping power for silicon fin structure

Figure 5.5 proves that as the height of the channels increase, lower thermal resistances are obtained. The reason is the increased hydraulic diameters leading to lower pressure drops and higher Nusselt numbers. These two parameters make the channels perform better both hydrodynamically and thermally.
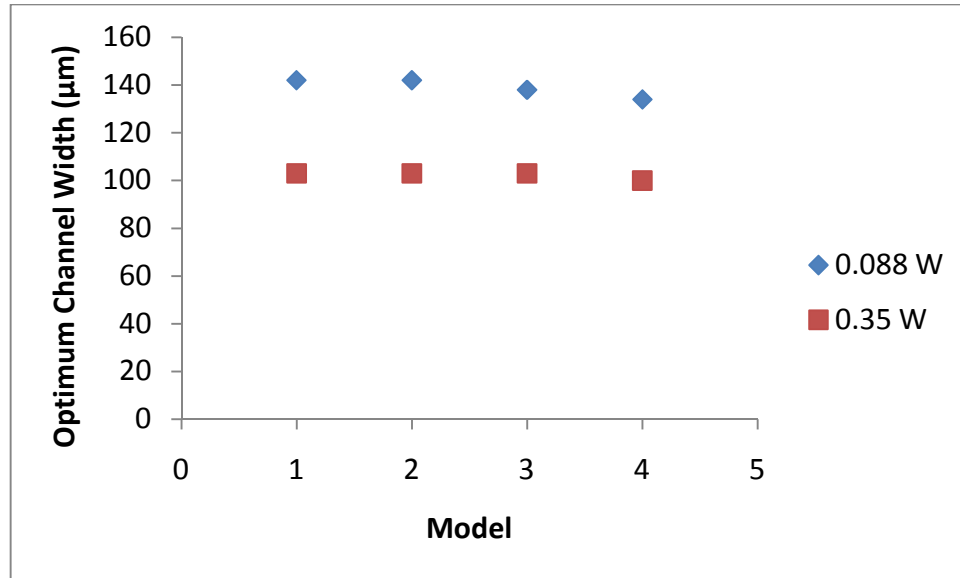
Figure 5.6 Optimum channel width obtained with the four optimization models for silicon channels of 500 μm height

As illustrated in Figure 5.6, the optimum channel width values are so close for each model. Optimization results for lower pumping power results in a wider channel width in order to reduce the pressure drop.
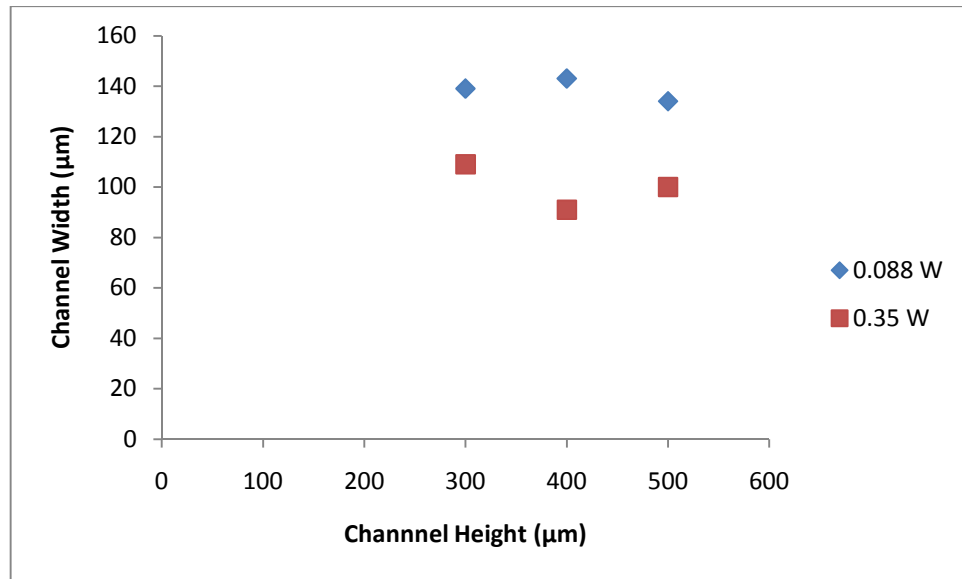
Figure 5.7 Optimum channel width versus channel height for silicon fin structure using model 4

Optimum channel widths are given in Figure 5.7 for different channel heights at two different pumping powers.

CHAPTER 6

DISCUSSION AND CONCLUSION

A novel microchannel optimization code has been developed for the optimum geometric parameters yielding the minimum total thermal resistance for various microchannel heat sinks. To the best of the author's knowledge, this is the first analytical microchannel optimization study that considers the effects of the thermophysical property variations with temperature, and of the thermal and hydrodynamic entrance regions.

6.1 Summary

The work performed within the scope of this thesis may be summarized in two parts. In the first part, a CFD modeling of already fabricated microchannel heat sinks has been carried out for performance evaluation. The software GAMBIT was utilized for the geometric modeling, and the thermal analysis was performed using the software FLUENT. The developed model was first validated against those available in the literature, and a very good agreement has been reached. The model was then applied to eight different metal-polymer microchannel heat sinks that were designed, fabricated and partially tested by Koyuncuoğlu et al. [15]. The heat removal performances of the heat sinks have been investigated considering a maximum chip operating temperature of 85°C for a few constant pumping power conditions.

The second part of the study included the dimensional optimization of microchannel heat sinks. The Intel Core i7-900 Desktop Processor Extreme Edition Series has been considered as a reference processor in the optimization study. The processor is reported to dissipate 130 W of heat and to have chip core (die) dimensions of 1.891 cm × 1.44 cm. Taking the objective function as the total thermal resistance, the optimum geometries have been obtained for the mentioned metal-polymer heat sinks as well as silicon structures with the intension of cooling down this processor.

6.2 Conclusions

Thermal modeling of the metal-polymer microchannels indicated that it is possible to remove heat flux values around 150 W/cm^2. It has been illustrated that the optimized geometries have small aspect ratios, i.e. much greater channel height compared to the channel width. Hence, it is suggested that for the investigated metal-polymer heat sinks, the channel height should be increased as much as allowed by the fabrication constraints.

The analyses proved that channels with larger width can reach relatively higher heat transfer rates at constant pumping power. Instead of designing thick fins, increasing the channel width, hence, reducing the pressure drop yields enhanced volumetric flow, and heat dissipation rates. It has been observed that single channels and multiple channels with greater channel widths have higher heat dissipation capacities.

Furthermore, it has been shown that using an optimized geometry, it is possible to dissipate the reported 130 W heat load of the Intel Core i7-900 Desktop Processor without exceeding a substrate temperature of 85°C. The maximum substrate temperature has been observed to be 71°C for the metal-polymer channels of 70 μm height for 0.088 W pumping power. For this condition, the optimum channel width and fin thickness are determined to be 308 μm and 10 μm, respectively. On the other hand, using a silicon structure of 300 μm channel height, a maximum

substrate temperature of 41℃ was attained at the same pumping power, corresponding to a channel width and fin thickness of 149 µm and 18 µm, respectively.

6.3 Future Work

In the present optimization study, the thermal resistance formulae are derived analytically. For this, some simplifying assumptions, such as, fully developed flow, negligible viscous dissipation and axial conduction in the fluid, are made. Their effects on the thermal performance might be inspected in a future numerical study.

The present work can handle many other working liquids; however, the models should be modified for gaseous flow. For gaseous flow, the characteristics of the flow may change. Slip flow boundary conditions may be applied at the solid-fluid boundaries. Additionally, incompressible flow assumption will not be valid.

Heat sink materials other than copper and silicon may be tried without changing the present code. On the other hand, optimization of channels of non-rectangular cross-sections may require significant change in the derivations.

The results of the numerical simulations obtained in the present study may be compared with experimental data when available.

Considering the optimization results, the metal-polymer heat sinks may be re-designed and fabricated for improved performance.

REFERENCES

[1] Tuckerman, D. B. and Pease, R. F. W., "High performance heat sink for VLSI", *IEEE Electron Dev.Lett.*, EDL-2, (5), 126–129, 1981.

[2] J. Li and G.P. Peterson, "3-Dimensional numerical optimization of silicon-based high performance parallel microchannel heat sink with liquid flow," *International Journal of Heat and Mass Transfer* 50, no. 15-16 (July 2007): 2895-2904.

[3] Roger Schmidt, "Challenges in Electronic Cooling—Opportunities for Enhanced Thermal Management Techniques—Microprocessor Liquid Cooled Minichannel Heat Sink," *Heat Transfer Engineering* 25, no. 3 (2004): 3

[4] Emrah Alpsan, "Experimental Investigation and Numerical Analysis of Microchannel Heatsinks for Phased Array Radar Cooling Applications," M.S. Thesis, June 1, 2008.

[5] Afzal Husain and Kwang-Yong Kim, "Thermal Optimization of a Microchannel Heat Sink With Trapezoidal Cross Section," *Journal of Electronic Packaging* 131, no. 2 (June, 2009): 021005-6

[6] Afzal Husain and Kwang-Yong Kim, "Multiobjective Optimization of a Microchannel Heat Sink Using Evolutionary Algorithm," *Journal of Heat Transfer* 130, no. 11 (November, 2008): 114505-3.

[7] Afzal Husain and Kwang-Yong Kim, "Optimization of a microchannel heat sink with temperature dependent fluid properties," *Applied Thermal Engineering* 28, no. 8-9 (June 2008): 1101-1107.

[8] Dong Liu and Suresh V. Garimella, "Analysis and optimization of the thermal performance of microchannel heat sinks," *International Journal of Numerical Methods for Heat & Fluid Flow* 15, no. 1 (2005): 7-26.

[9] J. H. Ryu, D. H. Choi, and S. J. Kim, "Numerical optimization of the thermal performance of a microchannel heat sink," *International Journal of Heat and Mass Transfer* 45, no. 13 (June 2002): 2823-2827.

[10] J. Koo and C. Kleinstreuer, "Viscous dissipation effects in microtubes and microchannels," *International Journal of Heat and Mass Transfer* 47, no. 14-16 (July 2004): 3159-3169.

[11] Mohamed-Nabil Sabry, "Transverse Temperature Gradient Effect on Fin Efficiency for Micro-Channel Design," *Journal of Electronic Packaging* 123, no. 4 (December, 2001): 344-350.

[12] A. Husain and Kwang-Yong Kim, "Shape Optimization of Micro-Channel Heat Sink for Micro-Electronic Cooling," *Components and Packaging Technologies, IEEE Transactions on* 31, no. 2 (2008): 322-330.

[13] Sung Jin Kim, "Methods for Thermal Optimization of Microchannel Heat Sinks," *Heat Transfer Engineering* 25, no. 1 (2004): 37.

[14] Baodong Shao et. al., "Application of thermal resistance network model in optimization design of micro-channel cooling heat sink," *International Journal of Numerical Methods for Heat & Fluid Flow* 19, no. 3/4 (2009): 535-545.

[15] Koyuncuoğlu, A., Okutucu, T. and Külah, H., "A CMOS Compatible Metal-Polymer Microchannel Heat Sink for Monolithic Chip Cooling Applications", Proceedings of the 14th International Heat Transfer Conference, IHTC14, August 13th 2010, Washington, DC, USA, IHTC14-232128.

[16] Satish Kandlikar et.al., *Heat Transfer and Fluid Flow in Minichannels and Microchannels*, illustrated edition. (Elsevier Science, 2005).

[17] Satish Kandlikar ve William Grande, "Evolution of microchannel flow passages – Thermohydraulic performance and fabrication technology," Proceedings, https://ritdml.rit.edu/handle/1850/7459.

[18] Andrei G. Fedorov ve Raymond Viskanta, "Three-dimensional conjugate heat transfer in the microchannel heat sink for electronic packaging," *International Journal of Heat and Mass Transfer* 43, no. 3 (February 2000): 399-415.

[19] S. Garimella, Dong Liu, ve Poh-Seng Lee, "Investigation of heat transfer in rectangular microchannels," *Research Publications* (January 31, 2005), http://docs.lib.purdue.edu/coolingpubs/7.

[20] Phillips, R. J., "Forced convection, liquid cooled, microchannel heat sinks", MS Thesis, Department of Mechanical Engineering, Massachusetts Institute of Technology, Cambridge, MA, 1987.

[21] Frank P. Incropera, *Fundamentals of Heat and Mass Transfer 6th Edition*, 6th ed. (Wiley, 2006).

[22] Wibulswas, P., "Laminar flow heat transfer in non-circular ducts", PhD Thesis, London, UK, London University, 1966

[23] A. Bejan, *Convection heat transfer*, 1984.(Wiley, 2004)

[24] Hong-Sen Kou, Ji-Jen Lee, ve Chih-Wei Chen, "Optimum thermal performance of microchannel heat sink by adjusting channel width and height," *International Communications in Heat and Mass Transfer* 35, no. 5 (May 2008): 577-582.

[25] Intel Core i7-900 Desktop Processor Extreme Edition Series Data Sheet. (July 2010).(Volume 1, Data Sheet 1). Retrieved 30 July 2010 from http://download.intel.com/design/processor/datashts/323252.pdf

CURVE FIT EQUATIONS FOR POISEUILLE AND NUSSELT NUMBERS

Curve-fit equations for developed and developing region Poiseuille and Nusselt numbers are given in the Table A.1 [16].

Table A.1 Curve-fit equations for Table 2.3,Table 2.5 and Table 2.6, [16]

Equations	Constants					
	a	b	c	d	e	f
1	141.97	−7.0603	2603	1431.7	14364	−220.77
2	142.05	−5.4166	1481	1067.8	13177	−108.52
3	142.1	−7.3374	376.69	800.92	14010	−33.894
4	286.65	25.701	337.81	1091.5	26415	8.4098
5	8.2321	2.0263	1.2771	0.29805	2.2389	0.0065322
6	8.2313	1.9349	−2.295	0.92381	7.928	0.0033937
7	36.736	2254	17559	66172	555480	1212.6
8	30.354	1875.4	13842	154970	783440	−8015.1
9	31.297	2131.3	14867	144550	622440	−13297
10	28.315	3049	27038	472520	1783300	−35714
11	6.7702	−3.1702	0.4187	2.1555	2.76×10^{-6}	NA
12	9.1319	−3.7531	0.48222	2.5622	5.16×10^{-6}	NA

$$\text{Equations } 1-4 : y = \frac{a + c\,x^{0.5} + e\,x}{1 + b\,x^{0.5} + d\,x + f\,x^{1.5}},$$

$$\text{Equations } 5-10 : y = \frac{a + c\,x + e\,x^2}{1 + b\,x + d\,x^2 + f\,x^3},$$

Equations $11 - 12$: $y = a + b\,x + c\,(\ln x)^2 + d(\ln x) + e\,x^{-1.5}$

Equation variables:

Laminar flow Poiseuille number for hydrodynamically developing flow, Table 2.3

y – Poiseuille number

x – Equation 1 : $\alpha_c = 1.0$

  Equation 2 : $\alpha_c = 0.5$

  Equation 3 : $\alpha_c = 0.2$

  Equation 4 : $\alpha_c = 0.1$ or $\alpha_c = 10$

Fully Developed Nusselt Number for three-side heated channel, Table 2.5

y – Nusselt number

x – Equation 5 : α_c

Fully Developed Nusselt Number for four-side heated channel, Table 2.5

y – Nusselt number

x – Equation 6 : α_c

Nusselt numbers for developing region and four-side heated channels, Table 2.6

y – Nusselt number

x – Equation 7 : $\alpha_c = 0.1$

  Equation 8 : $\alpha_c = 0.25$

  Equation 9 : $\alpha_c = 0.333$

  Equation 10 : $\alpha_c = 0.5$

  Equation 11 : $\alpha_c = 1$

Equation 12 : $\alpha_c = 10$

APPENDIX B

REGRESSION ANALYSIS OF WATER'S THERMOPHYSICAL PROPERTIES

Thermophysical properties of water are estimated as a function of temperature with a five degree polynomial using the computer software Mathematica. Errors at data points are under two percent. The polynomials are used to calculate thermophysical properties of water in the range from 290 K to 400 K.

Thermal Conductivity of Water(W/m K):

$$k_{water}(T) =$$
$$13.489570412628389 - 0.18636302198442292T +$$
$$0.001038017908134152T^2 - 0.000002804982391186139T^3 +$$
$$3.706103515056938 \times 10^{-9}T^4 - 1.923479859228344 \times 10^{-12}T^5$$

Dynamic Viscosity of Water ($N\,s/m^2$):

$$\mu_{water}(T) = 0.5025102704691259 - 0.0067156991966355805T$$
$$+ 0.00003616010169715 62T^2 - 9.78237312448091 \times 10^{-8}T^3$$
$$+ 1.327768486642027 \times 10^{-10}T^4 - 7.226550132002678$$
$$\times 10^{-14}T^5$$

Density of Water (kg/m^3):

$$\rho_{water}(T) = -4639.664006710693 + 79.58248159743773T$$
$$- 0.44916444564265906T^2 + 0.0012732825012659163T^3$$
$$- 0.00000181621635360001T^4 + 1.036645857487733$$
$$\times 10^{-9}T^5$$

Specific Heat of Water (J/kg K):

$$C_{p,water}(T) = 50409.971627447245 - 648.975194675759T$$
$$+ 3.6460031073150465T^2 - 0.01024489159460627T^3$$
$$+ 0.000014382294907486088T^4 - 8.050626987741287$$
$$\times 10^{-9}T^5$$

Prandtl Number of Water

$$Pr_{water} = 4115.117399556474 - 55.07719160243998T$$
$$+ 0.29673949038943886T^2 - 0.00080293193912015027^3$$
$$+ 0.0000010898660926341537^4 - 5.931787174938298$$
$$\times 10^{-10}T^5$$

Vertical Axis: Thermal Conductivity of Water(W/m K)

Horizontal Axis: Temperature of Water (K)
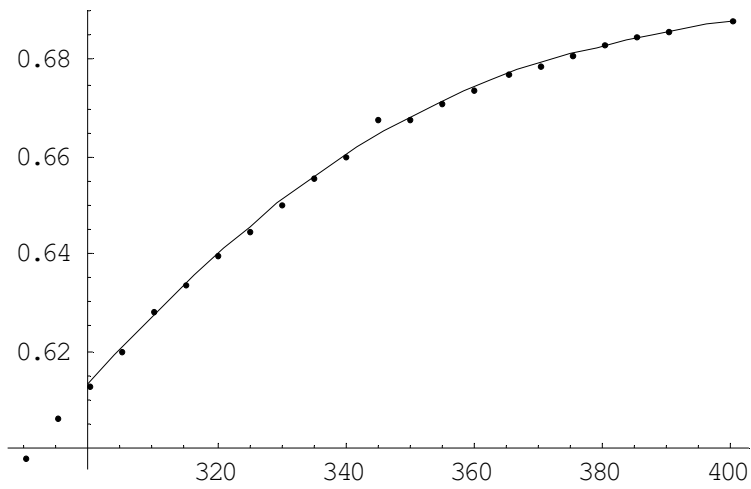
Figure B.1 Function obtained from regression analysis and specific data points for thermal conductivity of water

Vertical Axis: Dynamic Viscosity of Water (N s/m^2)

Horizontal Axis: Temperature of Water (K)
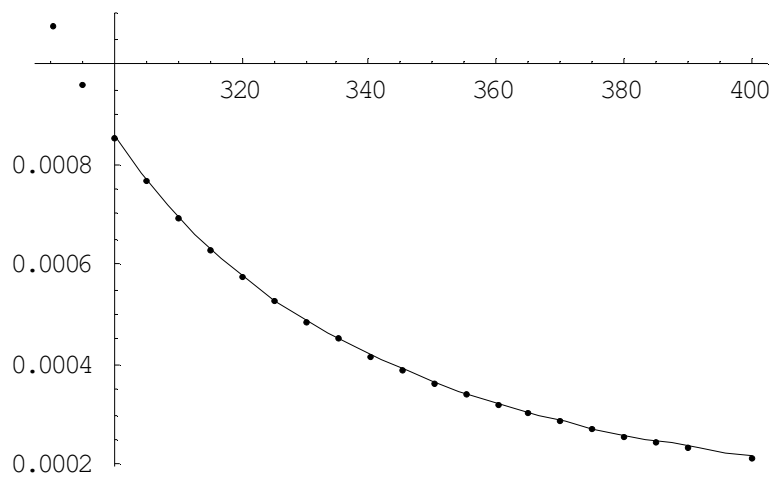
Figure B.2 Function obtained from regression analysis and specific data points for dynamic viscosity of water

Vertical Axis: Density of Water (kg/m^3)

Horizontal Axis: Temperature of Water (K)
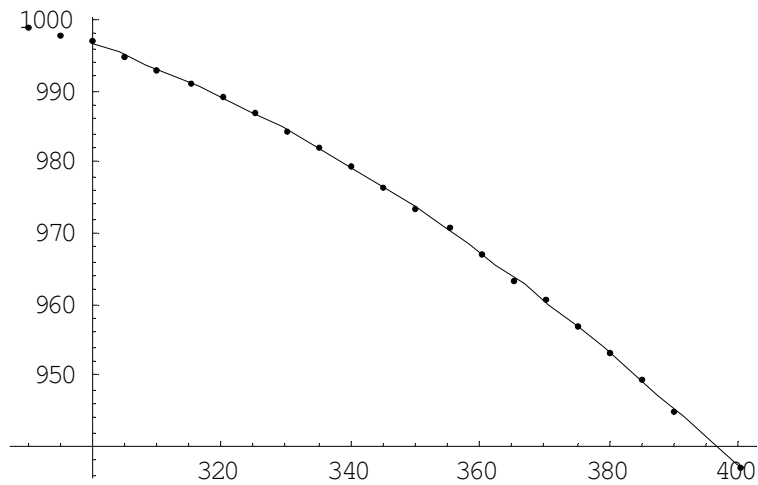
Figure B.3 Function obtained from regression analysis and specific data points for density of water

Vertical Axis: Specific Heat of Water $(J/Kg\ K)$

Horizontal Axis: Temperature of Water (K)
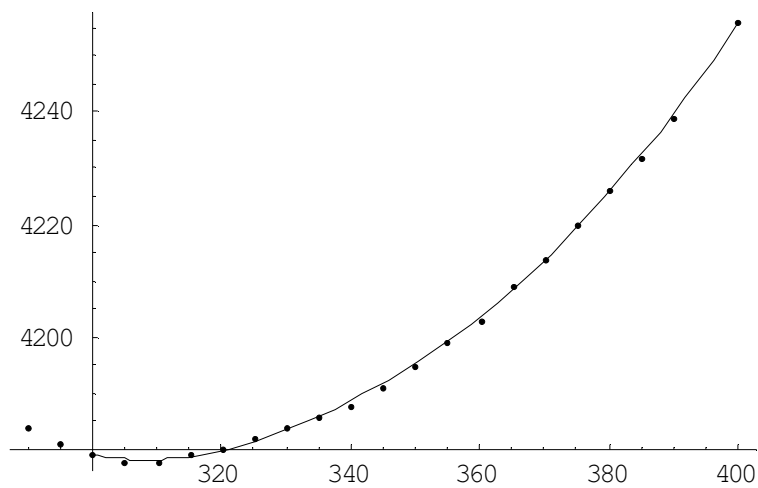
Figure B.4 Function obtained from regression analysis and specific data points for specific heat of water

Vertical Axis: Prandtl Number of Water

Horizontal Axis: Temperature of Water (K)
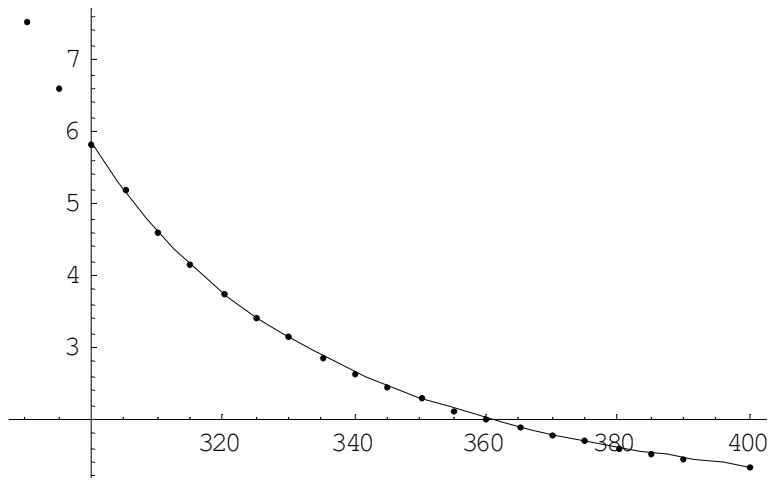
Figure B.5 Function obtained from regression analysis and specific data points for

Prandtl number of water

SAMPLE ANALYTICAL CALCULATIONS

For silicon fin structure with 300 μm height, 0.35 W pumping power, a sample calculation is conducted.

The fixed parameters of the electronic device and the heat sink are listed in the Tables C.1 and C.2 respectively.

Table C.1 Heat load and main dimensions of the electronic device

Heat Load	130 W
Heat Flux	47.74 W/cm^2
Total Channel Length	1.891 cm
Total Channel Width	1.44 cm

Table C.2 Substrate thickness and channel height

Layer	Thickness
Silicon Substrate	100 μm
Silicon Fins (Height)	300 μm

Firstly, a pressure drop value that corresponds to 0.35 W pumping power is entered. In the optimization code, this value is corrected based on the result given

117

by the computer code and an exact value is obtained at the end of a few iterations. Similar iterations are also performed for the fluid outlet temperature.

Thermal conductivity of silicon is taken as 143.09 W/m K. [21]

Fluid properties are calculated as explained in APPENDIX B and are given in Table C.3. Fluid inlet temperature is taken as 300 K.

Table C.3 Thermophysical properties of water

Density (kg/m^3)	995.9260
Thermal Conductivity $(W/m\ K)$	0.6164
Specific Heat $(J/kg\ K)$	4178.4
Dynamic Viscosity $(kg/m\ s)$	$818.67 \times 10^{*6}$
Prandtl Number	5.5442

The pressure drop is found iteratively as $\Delta P = 47000$ Pa.

The upper and lower bounds for the design variables are given below. Taking the step size as 1 µm, starting from the lower bounds of the design variables, the thermal resistances are calculated at all data points. Then, the minimum resistance is determined.

$$20 \times 10^{-6}\ m < w_c < 400 \times 10^{-6} m$$

$$10 \times 10^{-6}\ m < w_w < 60 \times 10^{-6} m$$

The channel dimensions that yield the minimum resistance are,

$$w_c = 109\ \text{µm}$$

$$w_w = 16\ \text{µm}$$

The optimum dimensions are normally found at the very end of the calculations but are listed here in the sample calculations.

$$\alpha_c = \frac{w_c}{H_c} = 0.3633$$

$$D_h = \frac{4 \times H_c \times w_c}{2 \times (w_c + H_c)} = 159.9 \; \mu\text{m}$$

$$\Delta P = 47000 \; \text{Pa} = \frac{2 f \rho \, u_m{}^2 L}{D_h}$$

In order to find the friction factor and the mean velocity, the Poiseuille number should be known.

Assuming that the flow is hydrodynamically fully developed

$$Po = f * Re$$

$$= 24 * \left(1 - 1.3553\alpha_c + 1.94677 \, \alpha_c{}^2 - 1.7012 \, \alpha_c{}^3 + 0.9564 \, \alpha_c{}^4 - 0.2537 \, \alpha_c{}^5\right)$$
$$= 16.98$$

$$u_m = \frac{\Delta P \, D_h^2}{2 \, Po \, \mu \, L} = 2.2857 \; \frac{\text{m}}{\text{s}}$$

$$x_{fd,h} = Re \, D_h = 0.071 \; \text{m}$$

The entrance length is greater than the channel length, so the flow is in the developing region. Therefore, the fully developed assumption is not valid and the *Po* number should be calculated again based on the entrance region correlations listed in Table 2.3

$$x^+ = \frac{L}{x_{fd,h}} = 0.266$$

The Poiseuille number for the developing region is found to be 19.42, and

The *Re*, u_m and x^+ are recalculated as

$$u_m = \frac{\Delta P \, D_h^2}{2 \, Po \, \mu \, L} = 1.99 \frac{m}{s}$$

$$\text{Re} = \frac{\rho \, u_m D_h}{\mu} = \frac{u_m D_h}{\nu} = 388$$

$$x^+ = \frac{L}{\text{Re } D_h} = 0.3042$$

In order to get the heat transfer coefficient, Nu number should be known.

$$x_{fd,t} = 0.1 \, Re \, Pr D_h$$

$$x^* = \frac{L}{Re \, Pr D_h} = \frac{0.01891}{388 \times 5.5442 \times 159.9 \times 10^{-6} \text{ m}} = 0.0548 < 0.1$$

As the dimensionless length is less than 0.1, the flow is in thermally developing region. That is why the Nu number is calculated as explained in title 2.5.2 and by the help of Table 2.6.

Regarding the dimensionless length and the aspect ratio of the channel, the Nusselt number is found as 5.86.

$$h = \frac{Nu \, k}{D_h} = 22598 \, \frac{W}{m^2 \, K}$$

Using model 4, the total thermal resistance may be calculated as follows:

$$m = \sqrt{\frac{2 \, h}{k_s \, w_w}}$$

$$\eta = \frac{Tanh(m * H_c)}{(m * H_c)}$$

$$S = \frac{h \, L}{\rho \, C_p \, u_m (w_c/2)}$$

$$A = \frac{H_c}{L}$$

$$R_{substrate} = \frac{t_{silicon}}{k_s \, W}$$

$$R_{total,model4} = R_{substrate}$$

$$+ \frac{2\eta\alpha_c}{2\eta\alpha_c + 1} \frac{(w_c + w_w)}{2\,h\,H_c} \left[mH_c \frac{Cosh(mH_c)}{Sinh(mH_c)} + S + \left(\frac{SA}{mH_c} \right)^2 \right] \frac{1}{LW}$$

$$= 0.0681\ \frac{°C}{W}.$$

APPENDIX D

DETAILED OPTIMIZATION RESULTS

Table D.1 Optimization results for 300 μm channel height, 0.35 W pumping power and silicon fin structure

	Model 1	Model 2	Model 3	Model 4
Channel Height (μm)	300	300	300	300
Channel Length (cm)	1.891	1.891	1.891	1.891
Channel Width (cm)	1.44	1.44	1.44	1.44
Q_{load} (W/cm^2)	47.74	47.74	47.74	47.74
Pressure Drop (Pa)	45500	45500	47000	47000
Aspect Ratio	0.39	0.39	0.37	0.36
Reynolds Number	425	425	403	389
Nusselt Number	5.96	5.96	5.90	5.86
Thermal Dimensionless Entry Length, L^*	0.0479	0.0479	0.0523	0.0549
Optimum w_C (μm)	116	116	111	109
Optimum w_W (μm)	18	18	19	16
$R_{min}(°C/W)$, T_{max} (°C)	0.076, 36.9	0.076, 36.9	0.0695, 36	0.0681, 35.8
u_m (m/s)	2.09	2.09	2.04	2.00
Pump power (W)	0.356	0.356	0.354	0.354
Poiseuille Number	19.64	19.64	19.51	19.42
Hydrodynamic Dimensionless Entry Length, L^+	0.266	0.266	0.2898	0.3043
T_{outlet} (K)	303.99	303.99	304.15	304.15
Thermal Entry Length (mm)	39.5	39.5	36.2	34.4
Hydrodynamic Entry Length (mm)	71.1	71.1	65.2	62.1

Table D.2 Optimization results for 400 μm channel height, 0.35 W pumping power and silicon fin structure

	Model 1	Model 2	Model 3	Model 4
Channel Height (μm)	400	400	400	400
Channel Length (cm)	1.891	1.891	1.891	1.891
Channel Width (cm)	1.44	1.44	1.44	1.44
Q_{load} (W/cm^2)	47.74	47.74	47.74	47.74
Pressure Drop (Pa)	39850	39850	41500	45000
Aspect Ratio	0.27	0.27	0.26	0.23
Reynolds Number	382	382	374	289
Nusselt Number	6.31	6.31	6.32	6.54
Thermal Dimensionless Entry Length, L^*	0.0518	0.0518	0.0541	0.0795
Optimum w_C (μm)	109	109	106	91
Optimum w_W (μm)	22	22	25	16
$R_{min}(°C/W)$, T_{max} (°C)	0.0658, 35.5	0.0658, 35.5	0.0617, 35	0.0572, 34.4
u_m (m/s)	1.84	1.84	1.84	1.60
Pump power (W)	0.352	0.352	0.357	0.353
Poiseuille Number	20.35	20.35	20.30	19.89
Hydrodynamic Dimensionless Entry Length, L^+	0.2891	0.289	0.3018	0.4418
T_{outlet} (K)	303.5341	303.534	303.6345	303.9776
Thermal Entry Length (mm)	36.5	36.5	34.9	23.7
Hydrodynamic Entry Length (mm)	65.4	65.4	62.7	42.8

Table D.3 Optimization results for 500 µm channel height, 0.35 W pumping power and silicon fin structure

	Model 1	Model 2	Model 3	Model 4
Channel Height (µm)	500	500	500	500
Channel Length (cm)	1.891	1.891	1.891	1.891
Channel Width (cm)	1.44	1.44	1.44	1.44
Q_{load} (W/cm^2)	47.74	47.74	47.74	47.74
Pressure Drop (Pa)	36600	36600	37500	37500
Aspect Ratio	0.21	0.21	0.21	0.20
Reynolds Number	341	340	349	326
Nusselt Number	7.06	7.06	7.08	7.12
Thermal Dimensionless Entry Length, L^*	0.058	0.058	0.0567	0.0622
Optimum w_C (µm)	103	103	103	100
Optimum w_W (µm)	24	24	24	22
$R_{min}(°C/W)$, T_{max} (°C)	0.0579, 34.5	0.0579, 34.5	0.056, 34.2	0.053, 33.9
u_m (m/s)	1.65	1.65	1.69	1.62
Pump power (W)	0.354	0.354	0.351	0.359
Poiseuille Number	20.64	20.64	20.69	20.56
Hydrodynamic Dimensionless Entry Length, L^+	0.3251	0.3251	0.3174	0.3484
T_{outlet} (K)	303.23	303.23	303.33	303.26
Thermal Entry Length (mm)	32.6	32.6	33.3	30.4
Hydrodynamic Entry Length (mm)	58.2	58.2	59.6	54.3

Table D.4 Optimization results for 300 µm channel height, 0.088 W pumping power and silicon fin structure

	Model 1	Model 2	Model 3	Model 4
Channel Height (µm)	300	300	300	300
Channel Length (cm)	1.891	1.891	1.891	1.891
Channel Width (cm)	1.44	1.44	1.44	1.44
Q_{load} (W/cm^2)	47.74	47.74	47.74	47.74
Pressure Drop (Pa)	17900	17900	18500	18500
Aspect Ratio	0.50	0.50	0.47	0.46
Reynolds Number	318	318	300	289
Nusselt Number	5.64	5.64	5.61	5.58
Thermal Dimensionless Entry Length, L^*	0.0552	0.0552	0.0605	0.0639
Optimum w_C (µm)	149	149	142	139
Optimum w_W (µm)	18	18	18	15
$R_{min}(°C/W)$, T_{max} (°C)	0.1111, 41.4	0.1111, 41.4	0.0985, 39.8	0.097, 39.6
u_m (m/s)	1.28	1.28	1.25	1.22
Pump power (W)	0.089	0.089	0.089	0.088
Poiseuille Number	18.25	18.25	18.19	18.13
Hydrodynamic Dimensionless Entry Length, L^+	0.2986	0.2986	0.3265	0.3445
T_{outlet} (K)	306.31	306.31	306.52	306.57
Thermal Entry Length (mm)	34.3	34.3	31.3	29.6
Hydrodynamic Entry Length (mm)	63.3	63.3	57.9	54.9

Table D.5 Optimization results for 400 μm channel height, 0.088 W pumping power and silicon fin structure

	Model 1	Model 2	Model 3	Model 4
Channel Height (μm)	400	400	400	400
Channel Length (cm)	1.891	1.891	1.891	1.891
Channel Width (cm)	1.44	1.44	1.44	1.44
Q_{load} (W/cm^2)	47.74	47.74	47.74	47.74
Pressure Drop (Pa)	14850	14850	15300	15300
Aspect Ratio	0.38	0.38	0.36	0.36
Reynolds Number	324	324	309	296
Nusselt Number	5.96	5.96	5.90	5.86
Thermal Dimensionless Entry Length, L^*	0.0484	0.0484	0.0524	0.0555
Optimum w_C (μm)	152	152	146	143
Optimum w_W (μm)	24	24	25	21
$R_{min}(°C/W)$, T_{max} (°C)	0.0987, 39.8	0.0987, 39.8	0.0904, 38.7	0.0885, 38.5
u_m (m/s)	1.1949	1.1949	1.1702	1.1409
Pump power (W)	0.088	0.088	0.088	0.088
Poiseuille Number	19.71	19.71	19.58	19.49
Hydrodynamic Dimensionless Entry Length, L^+	0.265	0.265	0.2865	0.3028
T_{outlet} (K)	305.26	305.26	305.43	305.45
Thermal Entry Length (mm)	39.1	39.1	36.1	34.1
Hydrodynamic Entry Length (mm)	71.4	71.4	66.0	62.4

Table D.6 Optimization results for 500 μm channel height, 0.088 W pumping power
and silicon fin structure

	Model 1	Model 2	Model 3	Model 4
Channel Height (μm)	500	500	500	500
Channel Length (cm)	1.891	1.891	1.891	1.891
Channel Width (cm)	1.44	1.44	1.44	1.44
Q_{load} (W/cm^2)	47.74	47.74	47.74	47.74
Pressure Drop (Pa)	13600	13600	14100	14100
Aspect Ratio	0.28	0.28	0.28	0.27
Reynolds Number	290	290	283	266
Nusselt Number	6.22	6.22	6.22	6.21
Thermal Dimensionless Entry Length, L^*	0.0535	0.0535	0.0562	0.0613
Optimum w_C (μm)	142	142	138	134
Optimum w_W (μm)	27	27	31	24
$R_{min}(°C/W)$, T_{max} (°C)	0.0876, 38.3	0.0876, 38.3	0.0818, 37.6	0.0792, 37.3
u_m (m/s)	1.07	1.07	1.07	1.02
Pump power (W)	0.088	0.088	0.088	0.088
Poiseuille Number	20.20	20.20	20.15	20.02
Hydrodynamic Dimensionless Entry Length, L^+	0.2945	0.2946	0.3088	0.3365
T_{outlet} (K)	304.82	304.82	304.98	304.99
Thermal Entry Length (mm)	35.3	35.3	33.6	30.8
Hydrodynamic Entry Length (mm)	64.2	64.2	61.2	56.2

Table D.7 Optimization results for 70 μm channel height, 0.35 W pumping power and copper fin structure

	Model 1	Model 2	Model 3	Model 4
Channel Height (μm)	70	70	70	70
Channel Length (cm)	1.891	1.891	1.891	1.891
Channel Width (cm)	1.44	1.44	1.44	1.44
Q_{load} (W/cm^2)	47.74	47.74	47.74	47.74
Pressure Drop (Pa)	172000	172000	170000	170000
Aspect Ratio	1	1	1	1
Reynolds Number	199.6047	199.6047	197.2219	197.23
Nusselt Number	3.6398	3.6398	3.6375	3.6376
Thermal Dimensionless Entry Length, L^*	0.2758	0.2758	0.2791	0.2791
Optimum w_C (μm)	70	70	70	70
Optimum w_W (μm)	2	2	1	1
$R_{min}(°C/W)$, T_{max} (°C)	0.1677, 48.8	0.1677, 48.8	0.1253, 46.8	0.1338, 44.4
u_m (m/s)	2.10	2.10	2.08	2.08
Pump power (W)	0.355	0.355	0.351	0.351
Poiseuille Number	14.44	14.44	14.44	14.44
Hydrodynamic Dimensionless Entry Length, L^+	1.3534	1.3534	1.3697	1.3696
T_{outlet} (K)	315.18	315.18	315.15	315.15
Thermal Entry Length (mm)	6.9	6.9	6.8	6.8
Hydrodynamic Entry Length (mm)	14	14	13.8	13.8

Table D.8 Optimization results for 300 μm channel height, 0.35 W pumping power and copper fin structure

	Model 1	Model 2	Model 3	Model 4
Channel Height (μm)	300	300	300	300
Channel Length (cm)	1.891	1.891	1.891	1.891
Channel Width (cm)	1.44	1.44	1.44	1.44
Q_{load} (W/cm^2)	47.74	47.74	47.74	47.74
Pressure Drop (Pa)	44000	44000	45000	45000
Aspect Ratio	0.39	0.39	0.38	0.37
Reynolds Number	412	412	400	387
Nusselt Number	5.93	5.93	5.90	5.86
Thermal Dimensionless Entry Length, L^*	0.0493	0.0493	0.0518	0.0543
Optimum w_C (μm)	116	116	113	111
Optimum w_W (μm)	11	11	12	10
$R_{min}(°C/W)$, T_{max} (°C)	0.0755, 36.8	0.0755, 36.8	0.0694, 36	0.0779, 37.1
u_m (m/s)	2.03	2.03	2.01	1.96
Pump power (W)	0.353	0.353	0.353	0.35
Poiseuille Number	19.54	19.54	19.47	19.39
Hydrodynamic Dimensionless Entry Length, L^+	0.2742	0.2742	0.2877	0.3016
T_{outlet} (K)	303.9	303.9	303.9	304.01
Thermal Entry Length (mm)	38.4	38.4	36.5	34.8
Hydrodynamic Entry Length (mm)	69	69	65.7	62.7

Table D.9 Optimization results for 70 μm channel height, 0.088 W pumping power and copper fin structure with no lower limit for w_w

	Model 1	Model 2	Model 3	Model 4
Channel Height (μm)	70	70	70	70
Channel Length (cm)	1.891	1.891	1.891	1.891
Channel Width (cm)	1.44	1.44	1.44	1.44
Q_{load} (W/cm^2)	47.74	47.74	47.74	47.74
Pressure Drop (Pa)	80500	80500	80100	80100
Aspect Ratio	1	1	1	1
Reynolds Number	118	119	118	117
Nusselt Number	3.53	3.53	3.53	3.53
Thermal Dimensionless Entry Length, L^*	0.5313	0.53	0.5338	0.5349
Optimum w_C (μm)	70	70	70	70
Optimum w_W (μm)	1.2	1.2	0.2	0.1
$R_{min}(°C/W)$, T_{max} (°C)	0.273, 62.5	0.2722, 62.4	0.1819, 50.6	0.1759, 49.9
u_m (m/s)	1.11	1.11	1.10	1.10
Pump power (W)	0.088	0.089	0.089	0.089
Poiseuille Number	14.44	14.43	14.44	14.44
Hydrodynamic Dimensionless Entry Length, L^+	2.2888	2.2764	2.2979	2.3089
T_{outlet} (K)	328.48	328.48	328.29	328.32
Thermal Entry Length (mm)	3.6	3.6	3.5	35.3
Hydrodynamic Entry Length (mm)	8.3	8.3	8.2	8.2

Table D.10 Optimization results for 70 μm channel height, 0.088 W pumping power and copper fin structure with lower limit 10 μm for w_w

	Model 1	Model 2	Model 3	Model 4
Channel Height (μm)	70	70	70	70
Channel Length (cm)	1.891	1.891	1.891	1.891
Channel Width (cm)	1.44	1.44	1.44	1.44
Q_{load} (W/cm^2)	47.74	47.74	47.74	47.74
Pressure Drop (Pa)	66400	66400	68500	68500
Aspect Ratio	4.4	4.4	3.66	3.66
Reynolds Number	228	228	214	214
Nusselt Number	3.14	3.14	3.15	3.15
Thermal Dimensionless Entry Length, L^*	0.1612	0.1612	0.1795	0.1795
Optimum w_C (μm)	308	308	256	256
Optimum w_W (μm)	10	10	10	10
$R_{min}(°C/W)$, T_{max} (°C)	0.3404, 71.2	0.3404, 71.2	0.212, 54.6	0.221, 55.7
u_m (m/s)	1.37	1.37	1.32	1.32
Pump power (W)	0.089	0.089	0.088	0.088
Poiseuille Number	24.54	24.54	24.50	24.50
Hydrodynamic Dimensionless Entry Length, L^+	0.728	0.728	0.8033	0.8033
T_{outlet} (K)	323.46	323.46	324.40	324.40
Thermal Entry Length (mm)	11.8	11.7	10.5	10.5
Hydrodynamic Entry Length (mm)	26	26	23.5	23.5

Table D.11 Optimization results for 300 µm channel height, 0.088 W pumping power and copper fin structure

	Model 1	Model 2	Model 3	Model 4
Channel Height (µm)	300	300	300	300
Channel Length (cm)	1.891	1.891	1.891	1.891
Channel Width (cm)	1.44	1.44	1.44	1.44
Q_{load} (W/cm^2)	47.74	47.74	47.74	47.74
Pressure Drop (Pa)	17500	17500	18000	18000
Aspect Ratio	0.5	0.5	0.48	0.47
Reynolds Number	311	311	296	293
Nusselt Number	5.62	5.62	5.6	5.59
Thermal Dimensionless Entry Length, L^*	0.0563	0.0563	0.0609	0.062
Optimum w_C (µm)	149	149	143	142
Optimum w_W (µm)	11.3	11.3	11	10
$R_{min}(°C/W)$, T_{max} (°C)	0.1092, 41.2	0.1092, 41.2	0.0974, 39.7	0.1058, 40.7
u_m (m/s)	1.26	1.26	1.23	1.22
Pump power (W)	0.088	0.088	0.089	0.089
Poiseuille Number	18.18	18.18	18.13	18.11
Hydrodynamic Dimensionless Entry Length, L^+	0.305	0.305	0.3293	0.3351
T_{outlet} (K)	306.18	306.18	306.33	306.35
Thermal Entry Length (mm)	33.6	33.6	31	30.5
Hydrodynamic Entry Length (mm)	62	62	57.4	56.4